REPORT DOCUMENTATION PAGE

Dist: A

Form Approved
OMB No. 0704-0188

1. AGENCY USE ONLY (Leave blank)	2. REPORT DATE	3. REPORT TYPE AND DATES COVERED
	26 October 1994	Final Technical Report

4. TITLE AND SUBTITLE
(U) Molecular Mixing in Shear Layers Forced by 2-D and 3-D Disturbances

5. FUNDING NUMBERS
PE-61102F
PR-2307
SA-BS
G-AFOSR-91-0314

2307/BS

6. AUTHOR(S)
Manoochehr M. Koochesfahani

7. PERFORMING ORGANIZATION NAME(S) AND ADDRESS(ES)
Michigan State University
East Lansing, MI 48824

8. PERFORMING ORGANIZATION REPORT NUMBER
AFOSR-TR- 95 0057

9. SPONSORING / MONITORING AGENCY NAME(S) AND ADDRESS(ES)
AFOSR/NA
110 Duncan Avenue, Suite B115
Bolling AFB, DC 20332-0001

NA

10. SPONSORING / MONITORING AGENCY REPORT NUMBER
AFOSR-
91-0314

11. SUPPLEMENTARY NOTES

12a. DISTRIBUTION / AVAILABILITY STATEMENT
Approved for public release; distribution is unlimited

12b. DISTRIBUTION CODE
A

13. ABSTRACT (Maximum 200 words)

Experiments on 2-D forcing of shear layers were completed. Analysis of data from two different forcing techniques have revealed that much of the global aspects of the scalar mixing field appear to exhibit a universal behavior in terms of the non-dimensional downstream distance $x^* = x\lambda f/U_c$, where $\lambda = (U_1 - U_2)/(U_1 + U_2)$ and $U_c = (U_1 + U_2)/2$. This universal behavior suggests that the total amount of mixing per unit width of the layer is enhanced in regions where $x^* > 1.5$. Work on 3-D forcing and combined 2-D/3-D forcing has lead to new findings. Results show that high amplitude 2-D forcing of a low Reynolds number wake can lead to a dramatic increase in mixing due to 3-D interaction of the vorticity field with the test section side walls. The possible application of this finding to mixing enhancement at higher Reynolds numbers is being investigated. Experiments on shear layers forced by a localized 3-D perturbation at the splitter plate along with 2-D forcing have shown that it is possible to significantly alter not only the predominant mixed-fluid composition but also the actual pdf structure (e.g. "non-marching" and "marching" behavior). Preliminary results suggest that the behavior of the span-averaged total mixing is similar to the case of purely 2-D forcing.

14. SUBJECT TERMS	15. NUMBER OF PAGES
Turbulent Mixing, Forced Shear Layers, Forced Wakes	152
	16. PRICE CODE

17. SECURITY CLASSIFICATION OF REPORT	18. SECURITY CLASSIFICATION OF THIS PAGE	19. SECURITY CLASSIFICATION OF ABSTRACT	20. LIMITATION OF ABSTRACT
Unclassified	Unclassified	Unclassified	UL

Molecular Mixing in Shear Layers Forced by 2-D and 3-D Disturbances

Manoochehr M. Koochesfahani*

Department of Mechanical Engineering
Michigan State University
East Lansing, Michigan 48824

Air Force Office of Scientific Research
Grant No. AFOSR-91-0314
Final Technical Report

26-October-1994

* Associate Professor; Principal Investigator.

1. Introduction

The objective of this research program is to determine how 2-D and 3-D disturbances affect the mixing of species in two-stream shear layers and wakes. The research is based on measurements of the mixing field in a gravity-driven liquid mixing layer facility. A major part of this effort involves the quantification of the mixing field by whole-field measurements using laser induced fluorescence (LIF) diagnostics. Mixing is to be quantified in terms of the concentration field of a passive scalar, using its probability density function (pdf) and the derived quantities based on the pdf. While the main goal here is to investigate basic fluid mechanical phenomena, it is expected that the knowledge gained will be useful in devising active and passive means to modify/control the mixing field in turbulent shear layers.

This final report provides a brief summary of the highlights of our results under this grant. Most of the results have been described in greater detail in previous annual reports [1-2] and conference presentations/papers [3-4]. An extensive study of the effects of 2-D forcing of shear layers by an oscillating airfoil was the subject of the recent M.S. thesis of Mr. Gregory Katch [5]; this work is attached in the Appendix.

It should be noted that the work carried out under this grant is being continued with the support of AFOSR Grant No. F49620-93-1-0282, which itself benefits from our novel diagnostics development under the companion AASERT grant (Grant No. F49620-92-J-0338). Accomplishments in the latter two research grants are described separately in their respective annual progress reports.

2. Summary of 2-D Forcing Results

Analysis and comparison of data from two sets of experiments corresponding to two different 2-D forcing schemes have lead to a unified picture of the effect 2-D forcing on the shear layer mixing field. In the original study [6], the shear layer was forced by oscillating the high-speed freestream speed. In the more recent experiments [3,5], 2-D perturbations were introduced into the shear layer by a 2-D oscillating airfoil placed downstream of the splitter plate tip. The angle of attack amplitude A and the frequency f were independently controlled. These experiments were more extensive in that a range of forcing amplitudes was considered and data were acquired at various downstream stations.

The growth rate characteristics of forced shear layers have been described in the past in terms of a non-dimensional downstream distance $x^* = x\lambda f/U_c$, where $\lambda = (U_1 - U_2)/(U_1 + U_2)$ and $U_c = (U_1 + U_2)/2$. The flow exhibits an enhanced growth

rate for $0 < x^* < 1$, the region $1 < x^* < 2$ refers to the "frequency-locked" region corresponding to the passage of a non-interacting array of vortices and a nearly constant shear layer thickness, and $x^* > 2$ describes the gradual relaxation to the growth characteristics of the unforced layer through various vortex interactions.

Our results indicate that much of the global behavior of the mixing field can also be described in terms of x^*. The details are included in the M.S. thesis attached in the Appendix. To highlight the role of x^*, the behavior of two particular aspects of mixing - the amount of mixed fluid in the center of the shear layer and the total amount of mixed fluid across the layer - are discussed below.

The maximum amount of mixed fluid is found in the middle of the shear layer and can be characterized in terms of the maximum value of total mixed-fluid probability $P_{m(max)}$. Figure 1 shows that the amount of mixed fluid in the middle of a forced layer decreases and reaches a minimum near $x^* = 1$. The total amount of mixed fluid integrated across the layer, quantified in terms of the mixed-fluid thickness δ_m, shows a significant increase. Owing to a comparable increase in the shear layer width δ_1, however, the fraction of the layer width occupied with mixed fluid (i.e. δ_m/δ_1) changes only modestly. These results are illustrated in Figure 2.

The main message from Figures 1 and 2 is that 2-D forcing of a shear layer does not necessarily lead to enhanced mixing. In fact, the region of enhanced mixing is defined in terms of x^*. In the range $x^* < 1.5$, the forced layer has less mixed fluid per unit width than the unforced case. The maximum amount of mixed fluid in the center of the layer, $P_{m(max)}$, and the total amount of mixed fluid per unit width δ_m/δ_1, reach a minimum at about $x^* = 1$. Figure 2 suggests that enhancement of δ_m/δ_1 occurs for $x^* > 1.5$ which can be achieved by either moving downstream (for a given forcing frequency), or by increasing the forcing frequency (for a fixed downstream station).

3. Summary of 3-D Forcing Results

Mixing in turbulent shear layers is closely tied to the generation of streamwise vorticity as part of the process leading to the much increased interfacial area as the flow becomes three-dimensional and turbulent. The investigation into 3-D forcing is motivated in part by our previous results that 2-D forcing alone may not be very effective for mixing enhancement and control. Our research to date has concentrated on two types of 3-D effects; those generated by an isolated spanwise disturbance element on the splitter plate and those that are induced by the side walls of the flow facility.

3.1 3-D Structure and Mixing of a Forced Wake inside a Confined Channel

The time evolution of the spanwise flow structure and the mixing field in a low Reynolds number wake (initial Re_θ = 100) were investigated. New information was obtained based on processing a large data set corresponding to the concentration field $\xi(x,y,z,t)$ at various downstream stations, x, over the cross-stream plane (i.e. in the y-z plane) as a function of time. The findings, described in more details previously [1,2,4], are summarized below.

High amplitude 2-D forcing of the low Reynolds number wake can lead to a dramatic increase in mixing. The streamwise vorticity in this flow is generated by the reorientation and stretching of the main 2-D spanwise vorticity as a result of the shear region in the side-wall boundary layer. The downstream evolution of the streamwise vorticity produces a region of enhanced mixing which is confined to the central portion of the test section span, with the regions near the side walls practically devoid of any mixed fluid. It is estimated that about 43% of the test section cross sectional area is occupied by mixed fluid at the farthest downstream measurement station. This represents an order of magnitude increase in mixing compared with the unforced case at the same downstream location. It can be envisioned that this type of mixing enhancement may play a role in an overall strategy for mixing control in confined mixing chambers. Of course, we still have to determine the range of flow Reynolds numbers that can benefit from the mixing enhancement mechanism identified here.

In trying to understand the complex 3-D structure of this flow, we have recently taken advantage of the flow periodicity in constructing the detailed "instantaneous" 3-D mixing field based on phase-averaged LIF images of the flow. A 3-D reconstruction of the flow structure using scientific visualization tools are being used to aid in the understanding of the flow topology near the wall. These developments, which started under this grant, were mostly carried out with support from grant F49620-93-1-0282. Therefore, this aspect of our progress will be more appropriately described in the annual report of the latter grant.

3.2 3-D Forcing of a Two-Stream Shear Layer at the Splitter Plate

Among the various types of splitter plate 3-D perturbation mechanisms investigated in the past, we decided to first investigate the effects on the mixing field generated by a single disturbance element. A cylindrical "peg" was placed on the splitter plate similar to that used by Lasheras, et al. [7] in a low Reynolds number shear layer. Mehta & Bell [8] had also used a similar device, but in a spanwise periodic arrangement. The peg had a diameter D = 7 mm, a height H = 3 mm, and was placed approximately 15 mm upstream

of the splitter plate tip at the mid-span location on the low-speed side of the splitter plate. Except for the addition of the peg, the flow conditions were the same as our previous 2-D forced shear layers ($U_1 \approx 40$ cm/s and $U_2 \approx 20$ cm/s). At these conditions, the height of the peg exceeded the momentum thickness of the boundary layer in which it was placed. In these experiments, the shear layer is forced simultaneously by both the streamwise vorticity due to the peg and 2-D perturbations by oscillating the high-speed freestream. Some details of the flow structure and mixing field have been previously reported [1,2]. Three particular findings constitute our main results and they are summarized below.

The addition of 3-D forcing causes a spanwise variation in the total amount of mixed fluid characterized by a mixed-fluid thickness variation $\delta_m(z)$ which has a higher than average value in the region near the mid-span location (i.e. the location of the 3-D perturbation source). The local shear layer thickness also varies in the spanwise direction and, in this case thickness, is defined by $\delta_1(z)$. The spanwise variation of the amount of mixed fluid per unit width of the layer, $\delta_m(z)/\delta_1(z)$, is shown in Figure 3 for various forcing frequencies. Note that the effect of the 3-D disturbance on the splitter plate does not remain localized; the entire span is affected. The well-defined spanwise wavy pattern is the signature of the counter-rotating streamwise vorticity introduced by the addition of 3-D forcing. As the forcing frequency increases, the mixed-fluid fraction, δ_m/δ_1, first decreases and then increases across the span. This trend is better seen when the span-averaged mixed-fluid fraction is plotted versus the forcing frequency f and the corresponding non-dimensional distance x^* (see Figure 4). We note that the span-averaged mixed-fluid fraction in this flow exhibits the same dependence on x^* as that in shear layers forced by purely 2-D disturbances. The highest value of mixed-fluid fraction (30% over unforced) occurs at the highest forcing frequency of $f = 16$ Hz which corresponds to the largest x^* we have studied to date.

The presence of strong three-dimensionality in the case of $f = 16$ Hz leads to unique new phenomena which are revealed when the spanwise variation of the pdf of the concentration field is considered. The contour plots of the transverse (y) distribution of the pdf's at three spanwise (z) locations are shown in Figure 5. The most striking feature is that the pdf's near the center-span ($z = 0$), where the 3-D disturbance source is located, are non-uniform across the layer (i.e. have a "marching" behavior). By contrast, the pdf's at off-center span locations ($z = \pm 12$ mm) exhibit uniformity, i.e. a "non-marching" behavior. These different pdf structures are apparently determined by the relative significance of 2-D and 3-D structures in the transport and mixing of species, a finding also supported by recent computations [9,10].

The overall (span-averaged) pdf of concentration field for the highest forcing frequency displays an interesting new feature for this flow; see Figure 6. At lower

frequencies, the predominant mixed-fluid concentration does not vary much as a result of forcing in agreement with previous findings [3,5,6]. At f = 16 Hz, however, there is a significant shift in the predominant mixed-fluid composition to lower values of concentration. This is the largest modification of the mixed fluid composition we have obtained to date. We do not currently have data at this forcing frequency for a shear layer perturbed by purely 2-D disturbances. Therefore, we cannot yet tell whether the observed composition shift is a purely 2-D effect or a combined 2-D/3-D effect. Work in progress to resolve this issue.

4. Work in Progress

The efforts in 3-D forcing constitute the main aspect of our continuing work. We are applying scientific visualization methods to our volumetric data sets in order to understand the influence of forcing on the flow structure and mixing field. Forcing affects both the spanwise and streamwise structure of the flow. It is not surprising, therefore, that we are finding it is essential that the flow structure be viewed in 3D space to reveal the intricate interplay between streamwise and spanwise structures.

The results discussed above were obtained in our small shear layer facility where the flow Reynolds number, $Re = \Delta U \delta_1 / \nu$, is limited to about 8,000. Many of the new findings we have reported need to be investigated at higher Reynolds numbers. A new larger shear layer facility capable of Reynolds numbers at least an order of magnitude higher than the present was designed. The original plans for performing experiments in this facility had to be postponed due to major delays in the delivery of the facility. The new facility has finally been delivered and we are in the process of bringing it on-line. The higher Reynolds number experiments will be carried out as part of the continuation grant F49620-93-1-0282.

5. References

1. Koochesfahani, M. M. [1992] "Molecular mixing in shear layers forced by 2-D and 3-D disturbances." Annual Technical Report, AFOSR Grant No. AFOSR-91-0314, 19-August-1992.
2. Koochesfahani, M. M. [1993] "Molecular mixing in shear layers forced by 2-D and 3-D disturbances." Annual Technical Report, AFOSR Grant No. AFOSR-91-0314, 19-August-1993.
3. Katch, G. J. and Koochesfahani, M. M. [1993] "Mixing of species in a two-stream shear layer forced by an oscillating airfoil," AIAA Paper 93-0444.
4. MacKinnon, C. G. and Koochesfahani, M. M. [1993] "Three-dimensional structure and mixing of a forced wake inside a confined channel," AIAA Paper 93-0658.
5. Katch, G. J. [1994] "Mixing of species in a two-stream shear layer forced by an oscillating airfoil," M.S. Thesis, Michigan State University.
6. Koochesfahani, M. M. and MacKinnon, C. G. [1991] "Influence of forcing on the composition of mixed fluid in a two-stream shear layer," *Phys. Fluids A.*, **3(5)**, pp. 1135-1142.
7. Lasheras, J. C., Cho, J. S. and Maxworthy, T. [1986] "On the origin and evolution of streamwise vortical structures in a plane, free shear layer," *J. Fluid Mech.*, **172**, pp. 231-258.
8. Mehta, R. D. and Bell, J. H. [1989] "An experimental study of forced streamwise vortical structures in a plane mixing layer," Presented at the *Australasian Fluid Mechanics Conference*, Melbourne, Australia, Dec. 11-15, 1989.
9. Rogers, M. M. and Moser, R. D. [1993] "Direct simulation of a self-similar turbulent mixing layer," Submitted to *Physics of Fluids A*, March 1, 1993.
10. Park, K-H., Metcalfe, R. W. and Hussain, F. [1993] "Role of coherent structures in an isothermally reacting mixing layer," Submitted to *Physics of Fluids A*, June, 1993.

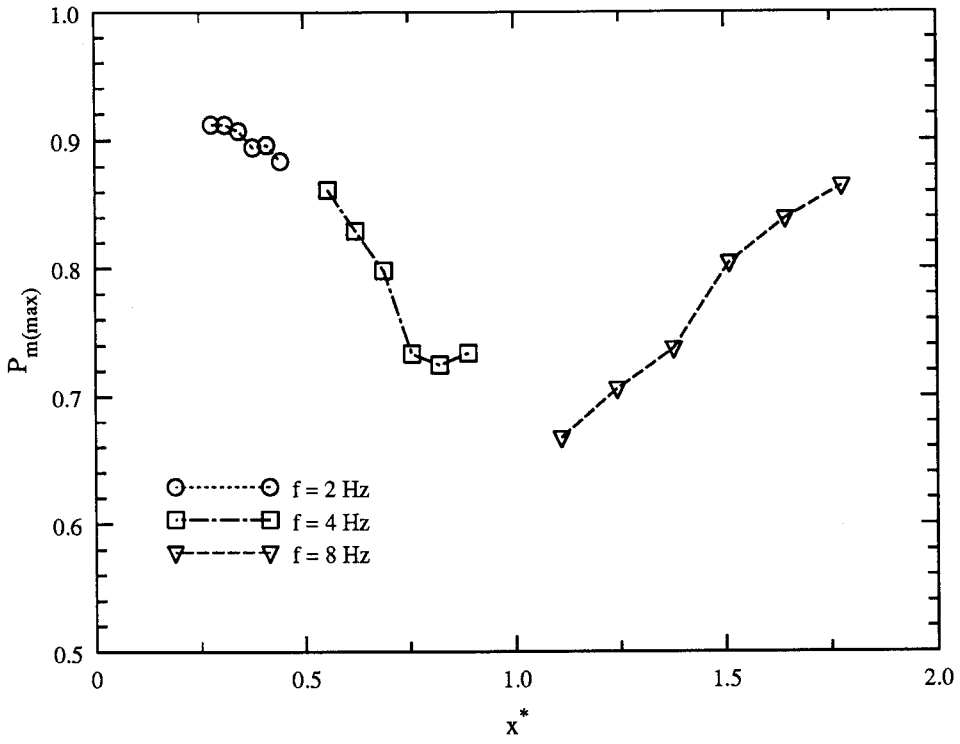

Figure 1. Amount of mixed fluid in the center of the forced shear layer versus x^*; forcing amplitude A = 4 deg.

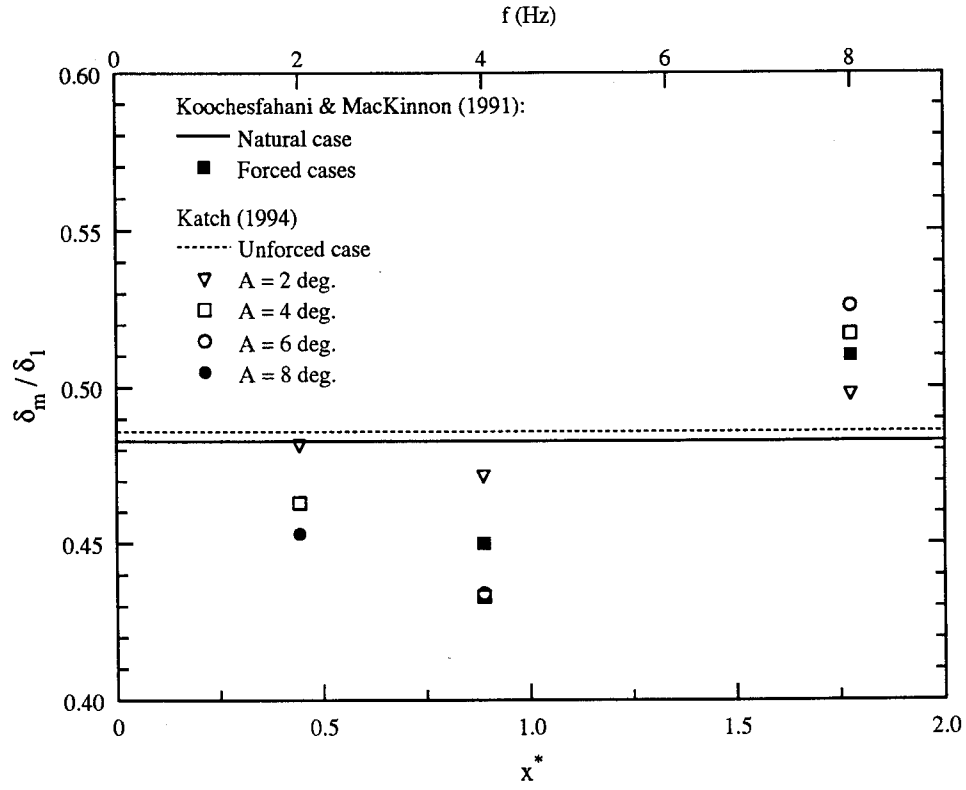

Figure 2. Mixed fluid fraction for various forcing conditions (x = 20 cm).

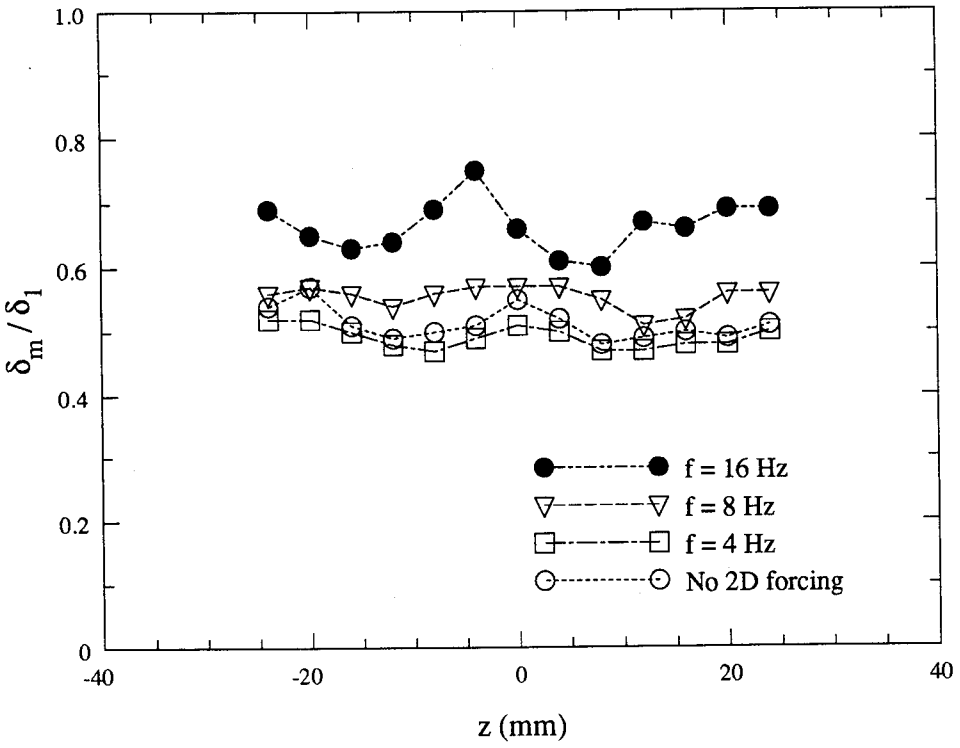

Figure 3. Spanwise distribution of mixed fluid fraction at x = 17 cm with 2-D and 3-D forcing.

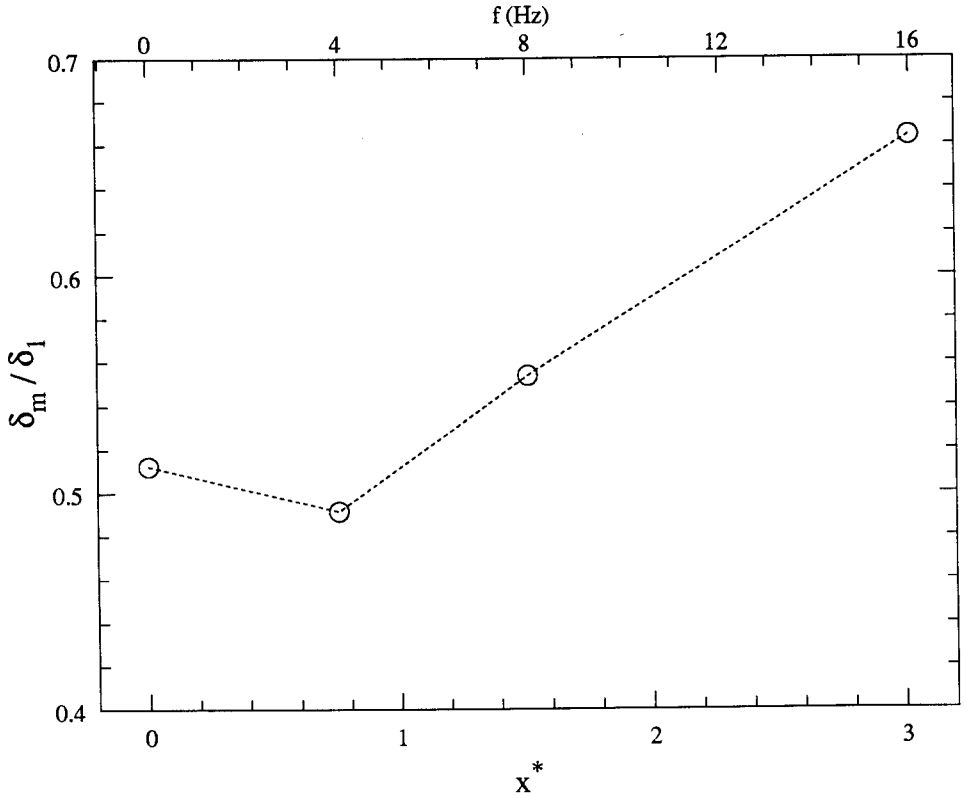

Figure 4. Variation of span-averaged mixed fluid fraction versus x^*.

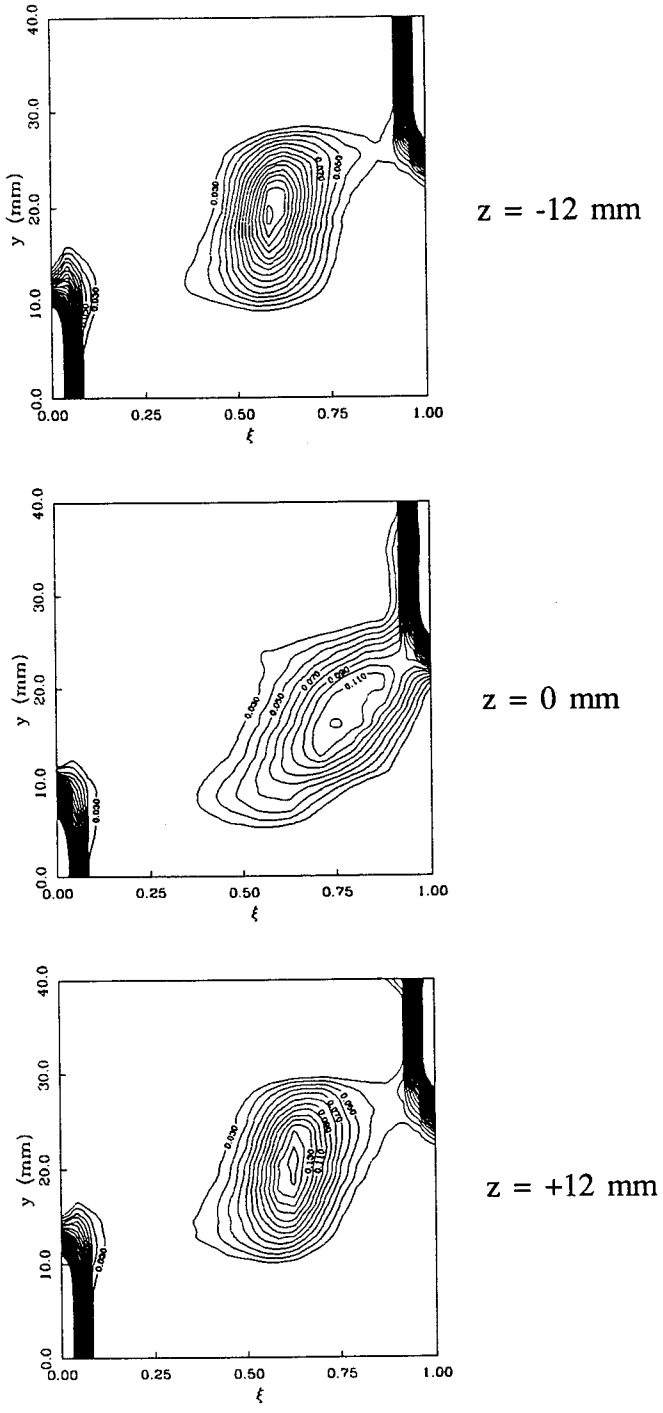

Figure 5. Contour plot of pdf $p(\xi,x,y,z)$ at x = 17 cm for different spanwise locations.

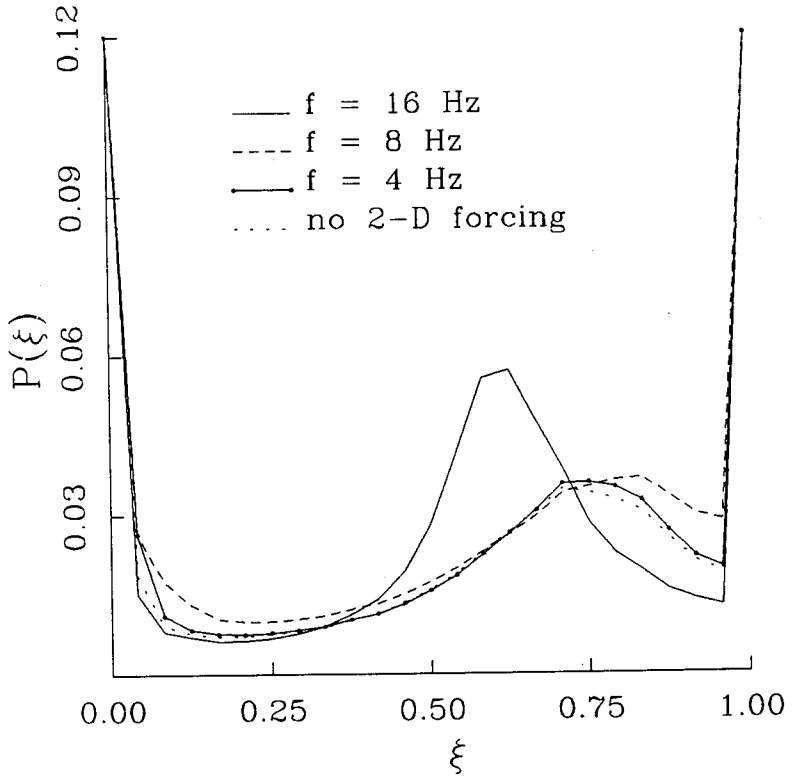

Figure 6 Span-averaged pdf's with 2-D and 3-D forcing at x = 17 cm.

APPENDIX

"Mixing of species in a two-stream shear layer
forced by an oscillating airfoil"

Katch, G. J. [1994] M.S. Thesis, Michigan State University

MIXING OF SPECIES IN A TWO-STREAM SHEAR LAYER FORCED BY AN OSCILLATING AIRFOIL

By

Gregory James Katch

A THESIS

Submitted to
Michigan State University
in partial fulfillment of the requirements
for the degree of

MASTER OF SCIENCE

Department of Mechanical Engineering

1994

ABSTRACT

MIXING OF SPECIES IN A TWO-STREAM SHEAR LAYER
FORCED BY AN OSCILLATING AIRFOIL

By

Gregory James Katch

The modifications to the structure and the mixing field in a shear layer forced by an oscillating airfoil were documented over a range of frequencies, amplitudes and streamwise locations using laser induced fluorescence in the passive scalar mode. The shear layer structure and growth were observed to conform to the well-established behavior of forced shear layers. Results on the mixing field show a variation in the amount of mixed fluid in the central portion of the forced shear layer with increasing downstream distance and forcing frequency, an increase in the width of the region occupied by mixed fluid and an increase in the total amount of mixed fluid in the layer. Only for the highest forcing frequency examined in this study was there an increase in the fraction of the layer occupied by mixed fluid when compared to the unforced layer. These results are consistent with those from a shear layer forced by a different method (oscillating one freestream). Attempts were made to describe the downstream evolution of the forced mixing layer in terms of a universal non-dimensional curve. The predominate mixed fluid concentration in the forced shear layer showed similar behavior to the layer forced by oscillating one freestream.

to my parents James and Barbara

ACKNOWLEDGMENTS

I am grateful to my advisor, Dr. Manooch Koochesfahani, for the opportunity to learn from his example as an outstanding scientist and educator. Additional thanks goes to C. G. M^{ac}Kinnon for all of his instruction and patience. I would also like to thank Dr. J. F. Foss and Dr. M. Zhuang for their review of this work. Finally, I would like to thank my family for their support and encouragement throughout the pursuit of this degree.

This work was supported by the Air Force Office of Scientific Research Grant No. AFOSR-87-0332 and AFOSR-91-0314.

TABLE OF CONTENTS

LIST OF TABLES

LIST OF FIGURES

LIST OF SYMBOLS

Symbol	Description
A	amplitude of oscillation
b	airfoil span
$\overline{c_p}(y)$	average product concentration
C	airfoil chord
C_d	instantaneous dye concentration
C_{d_o}	freestream dye concentration
D	coefficient of mass diffusivity
f	forcing frequency
f_0	natural shear layer roll up frequency
h	half height of the test section
I	raw instantaneous intensity
I_{cal}	intensity in the calibration image
I_{corr}	corrected instantaneous intensity
I_{corr_o}	corrected freestream dye intensity
$p(\xi, y)$	probability density function of ξ at y

$p_0(y)$	probability of pure low-speed fluid at y
$p_1(y)$	probability of pure high-speed fluid at y
$p_m(y)$	probability of mixed fluid at y
$(p_m)_{\max}$	maximum value of the $p_m(y)$ curve
$P(\xi)$	average probability density function of ξ
r	velocity ratio, U_1 / U_2
Re_{δ_1}	Reynolds number, $\Delta U \delta_1 / \nu$
Re'	unit Reynolds number $\Delta U / \nu$
Sc	Schmidt number, ν/D
Δt	time between fields
ΔU	velocity difference, $U_1 - U_2$
U_1	high-speed velocity
U_2	low-speed velocity
U_c	convection speed, average speed, $(U_1 + U_2)/2$
v_1	high-speed fluid volume
v_2	low-speed fluid volume
x	streamwise coordinate
x^*	nondimensional streamwise parameter, $\lambda x f / U_c$
y	vertical coordinate

Greek symbols

α	absorption coefficient
δ_1	shear layer 1% thickness

δ_m	mixed fluid thickness
δ_{vis}	shear layer visual thickness
δ_{p_2}	chemical product thickness
ε	uncertainty in ξ
ε_0	dye molar absorption coefficient
θ	momentum thickness
θ_ξ	concentration thickness
λ	growth rate parameter, $(U_1 - U_2) / (U_1 + U_2)$
λ_D	diffusion scale
λ_K	Kolmogorov scale, $\delta_1 Re^{-3/4}$
ν	kinematic viscosity
ξ	concentration
$\bar{\xi}$	average concentration

Chapter 1

INTRODUCTION

The shear layer has been the subject of a large number of studies over the past few decades. One reason for the great interest in this flow is the common occurrence of shear layers in both naturally occurring phenomena and in industrial processes. Some familiar examples of shear layers are the wind blowing over a body of water, the injection of fuel into a combustor and the separated flow over an airfoil. A shear layer is generated by allowing two parallel streams of fluid moving at different speeds (initially separated by a thin interface) to come together. The flow formed as a result of the two fluids merging is the shear layer. A schematic of the geometry of a plane shear layer is shown in Figure 1.

Consider modelling the combustor as a plane shear layer, where one fluid is the fuel and the other fluid is the oxidizer. If, for example, mixing of the fuel and oxidizer in the combustor could be optimized, less unburned fuel would be exhausted from the combustor, resulting in a more efficient combustion process. Like the combustor, many other industrial applications would benefit from a more detailed understanding of shear layer dynamics and the mixing process in turbulent shear layers.

Previous studies on shear layers have examined many different aspects of natural and forced shear layers. In the following sections the behavior of the natural layer, the

forced layer and mixing in the shear layer will be discussed as related to this study.

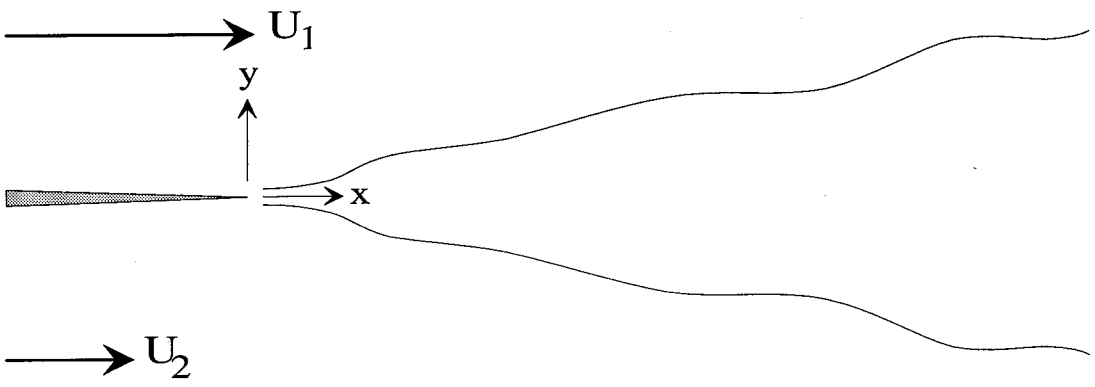

Figure 1. Schematic of the plane shear layer.

1.1 The natural shear layer

It was first noted by Brown and Roshko (1971, 1974) that in addition to the numerous small scales, large scale structures were a prominent feature of the natural shear layer over a wide range of Reynolds numbers. Dimotakis and Brown (1976) showed that the large scale structures seen by Brown and Roshko persist at Reynolds numbers up to 3×10^6, based on high speed velocity and downstream distance. It was also noted that the shear layer dynamics were governed by a global feedback mechanism. This feedback mechanism suggests that the initiation of the layer at the splitter plate tip is coupled to the large scale structures located far downstream.

Growth of the natural shear layer was observed to occur as the result of the amalgamation of neighboring large scale structures by Winant and Browand (1974). This process, resulting in a single larger structure, termed *pairing*, results (on average) in the

linear growth of the natural layer.

Many experimentalists have observed large scale, two-dimensional structures in the natural shear layer, e.g. Browand and Weidman (1976) and Wygnanski, Oster, Fiedler and Dziomba (1979). It was Miksad (1972), however, who first observed a weaker longitudinal (streamwise) vortex structure in the (low Reynolds number) natural shear layer. Later, Konrad (1976) also saw these streamwise structures at much higher Reynolds numbers, and concluded that the transition to turbulence occurred as a result of the formation of this secondary flow structure. Breidenthal (1978, 1981) also observed the streamwise structures and suggested that this structure was, in fact, pairs of counter rotating vortices.

1.2 The forced shear layer

Forcing refers to the application of a periodic disturbance to a shear layer in an attempt to modify the behavior of the layer by exciting the natural instabilities of the flow. Much work has been done on understanding forced shear layers and many different methods of forcing have been used. Some of the various forcing methods previously used include: oscillating one or both of the freestream speeds, Ho and Huang (1982), Roberts and Roshko (1985) and Koochesfahani and M^{ac}Kinnon (1991), oscillating the splitter plate tip, Oster and Wygnanski (1982), forcing by acoustical methods, Fiedler *et al.* (1981) and Zaman and Hussain (1981), spanwise heating on the surface of the splitter plate, Nyggard and Glezer (1991), and by oscillating an airfoil downstream of the splitter plate, Koochesfahani and Dimotakis (1989).

Perhaps the most important observation of forced shear layers is the control over

the growth rate and the structure of the shear layer by external forcing. It was reported by Oster and Wygnanski (1982) and Ho and Huang (1982) among others, that low amplitude two-dimensional periodic forcing can be used, to some extent, to control the growth and structure of the shear layer. The effect of forcing on the growth of the shear layer is demonstrated in Figure 2, reproduced from Browand and Ho (1983). In this Figure shear layer growth is quantified by the local momentum thickness of the shear

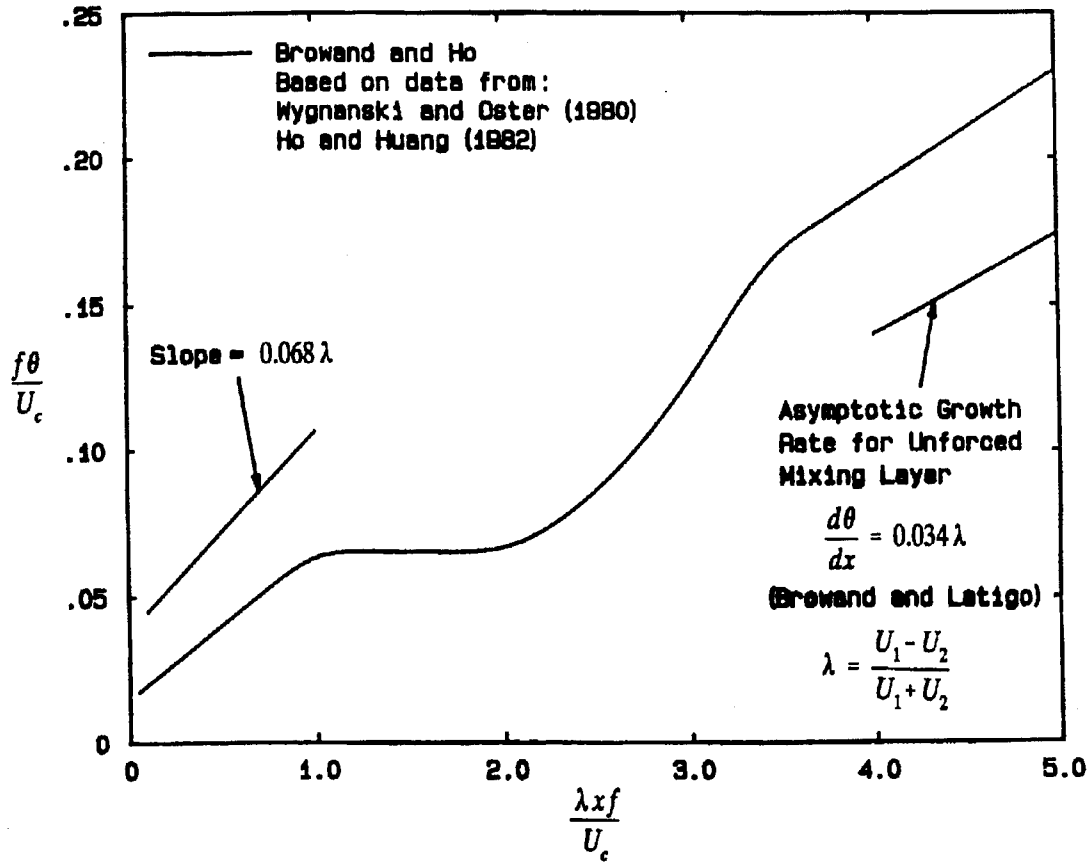

Figure 2. Effect of forcing on the shear layer growth, reprinted from Browand and Ho (1983).

layer as defined by

$$\theta = \int_{-\infty}^{+\infty} \frac{(U_1-U)(U-U_2)}{(U_1-U_2)^2}\, dy.$$

In this figure the independent axis is the Wygnanski-Oster parameter, $x^* = x\lambda f/U_c$, where x is the distance from the splitter plate tip, $\lambda = (U_1-U_2)/(U_1+U_2)$ is the shear layer growth rate parameter, f is the forcing frequency and $U_c = (U_1+U_2)/2$. This parameter is used to define three distinct regions of the evolution of the forced shear layer.

The first region, called *the enhanced growth region*, $x^* < 1$, exhibits enhanced growth rates up to twice that of the natural shear layer. The next region, *the frequency locked region*, $1 < x^* < 2$, shows reduced growth rates when compared to the natural layer. In this region the structures are observed to be equally spaced, and have passage frequency equal to the forcing frequency. In the third region, $x^* > 2$, the growth rate relaxes to the natural growth rate.

1.3 Mixing in the shear layer

A majority of the experimental and computational studies to date have focused on the effects of forcing on the momentum transport properties of the shear layer such as the layer growth rate, the resulting velocity and vorticity fields and their fluctuating components and the Reynolds stresses. By contrast, there have been few detailed studies devoted specifically to the behavior of the scalar mixing field in forced shear layers. Throughout this work, mixing will refer to the mixing of species, the kind of mixing that

is necessary for chemical reaction and combustion.

Konrad (1976) and Breidenthal (1978, 1981) were among the first to consider molecular mixing in the shear layer. Konrad (1976) found in a non-reacting gaseous layer, a rapid increase in the amount of mixed fluid at some distance downstream of the splitter plate. The increase in mixing was attributed to increased interfacial area between the two fluids resulting from the development of small-scale motion which were generated during transition to turbulence. Breidenthal (1978, 1981) and Koochesfahani and Dimotakis (1986) also found this dramatic increase in mixing, in chemically reacting liquid layers, and referred to this as the mixing transition. The mixing transition is shown in Figure 3, reproduced from Roshko (1990). The velocity ratio $r = U_1/U_2$ in Figure 3 is 2.6.

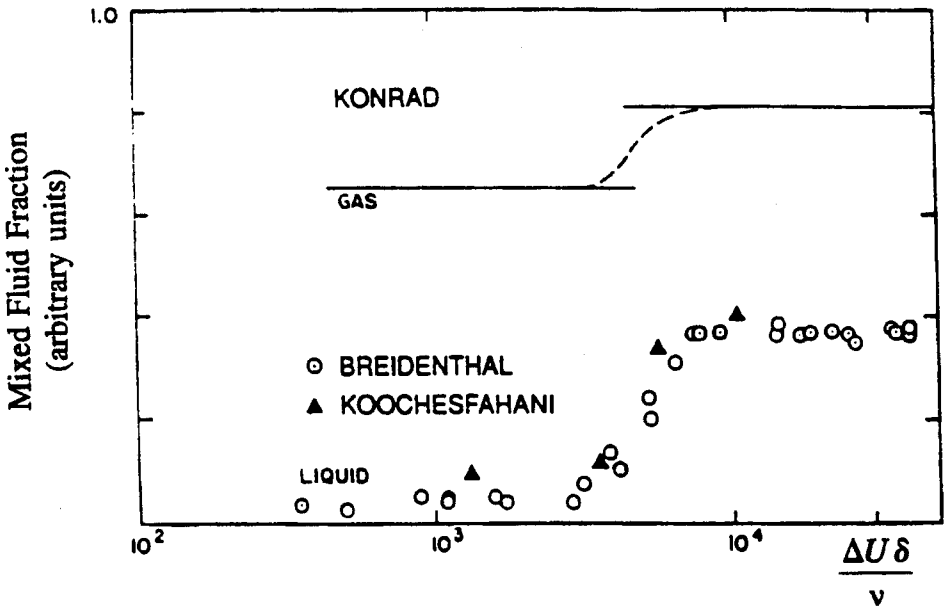

Figure 3. The mixing transition, reprinted from Roshko (1990).

The velocity ratio, $r = U_1/U_2$, has been shown to have an effect on the mixing transition, see Figure 4, reproduced from Breidenthal (1978). In Figure 4 the velocity ratio is defined as $r = U_2/U_1$, the inverse of the notation used in this work. In the current work the velocity ratio is $r = U_1/U_2 = 2$.

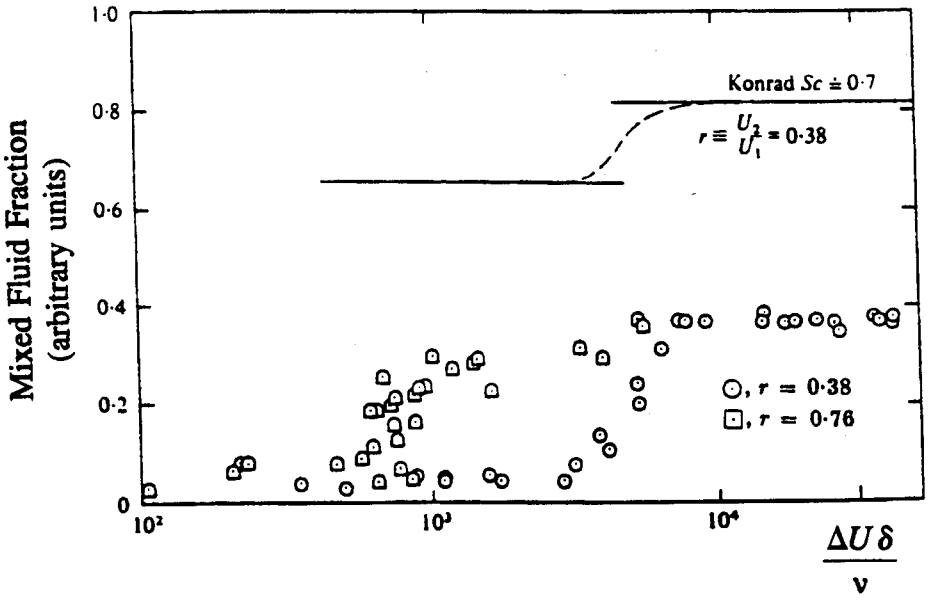

Figure 4. Effect of the velocity ration on the mixing transition, reprinted from Breidenthal (1978).

Roberts (1984, 1985) observed the amount of chemical product in a liquid shear layer using chemically reacting techniques. It was found that the effect of two-dimensional forcing can significantly alter the amount of chemical product in the layer. In pre-transitional flows there were large increases in the amount of chemical product in the frequency locked region. In post-transitional flows increases were observed only in the very early stages of the enhanced growth region. In the frequency locked region and

beyond there was actually less chemical product in the forced layer than in the natural layer. The technique of Laser Induced Fluorescence (LIF) introduced by Koochesfahani and Dimotakis (1986), was used to measure the chemical product in reacting flows and the composition of mixed fluid in non-reacting flows.

The effects of periodic oscillation of the high-speed freestream on the composition of mixed fluid in a non-reacting shear layer were reported by Koochesfahani and M^{ac}Kinnon (1991). It was found that while the total amount of mixed fluid integrated across the layer had increased, the amount of mixed fluid per unit width of the layer had, in fact, remained nearly constant. This suggests that the larger growth rate of a shear layer forced by a two-dimensional disturbance does not necessarily lead to a more efficient mixer. In this work efficiency, as related to the mixing of species in a shear layer, is defined as the amount of mixed fluid per unit width of the layer. It was also noted that forcing shifted the predominant mixed fluid concentration to higher values, i.e. larger proportion of high-speed to low-speed fluid.

1.4 Objectives

As stated earlier, there are many different ways to perturb a shear layer. All of the methods previously discussed impose disturbances on the shear layer by different mechanisms, each entering the flow in a different way. Surprisingly, the net result on the growth rate and structure of the shear layer in response to forcing is very similar for all methods. The goal of the present work is to investigate the influence of the forcing mechanism on the mixing of species in a two stream shear layer.

In an earlier investigation, the effects of the periodic oscillation of the high-speed

freestream on the composition of mixed fluid in a plane shear layer were reported by Koochesfahani and M^{ac}Kinnon (1991). The results from the oscillating freestream experiments are compared to a shear layer forced by oscillating an airfoil located downstream of the splitter plate tip. In addition to comparing the methods of forcing, the effect of the forcing amplitude and streamwise evolution on the total amount of mixed fluid in the layer, the amount of mixed fluid in the central portion of the layer and the composition of mixed fluid will also be examined.

Chapter 2

EXPERIMENTAL FACILITY AND INSTRUMENTATION

All of the data presented in this work were acquired over a two day period, in two sets of experiments. Each of the two experiments consisted of ten forcing conditions and covered a different streamwise view of the test section. In this chapter the shear layer facility, forcing mechanism and diagnostics are described.

2.1 Experimental facility

The experiments were performed in a gravity-driven water shear layer apparatus, a schematic of the facility is shown in Figure 5. For reference, the inside dimensions of the test section were 4 (height) x 8 (width) x 36 (length) cm. The system was fed from two 210 liter reservoirs, one for each the high-speed and low-speed sides of the shear layer. Water was pumped from the reservoirs to constant head tanks, located approximately eight feet above the test section. Flow through the test section was regulated by three valves; one valve in each of the supply lines upstream of the contraction, and a third valve downstream of the test section.

For these experiments the freestream velocities were set to U_1 = 40 cm/s and U_2 = 20 cm/s, yielding a velocity ratio of, r = 2. In this work the flow was examined over the range $12.5 < x < 20.0$ cm, corresponding to $0.28 < x^* < 1.78$. The Reynolds number,

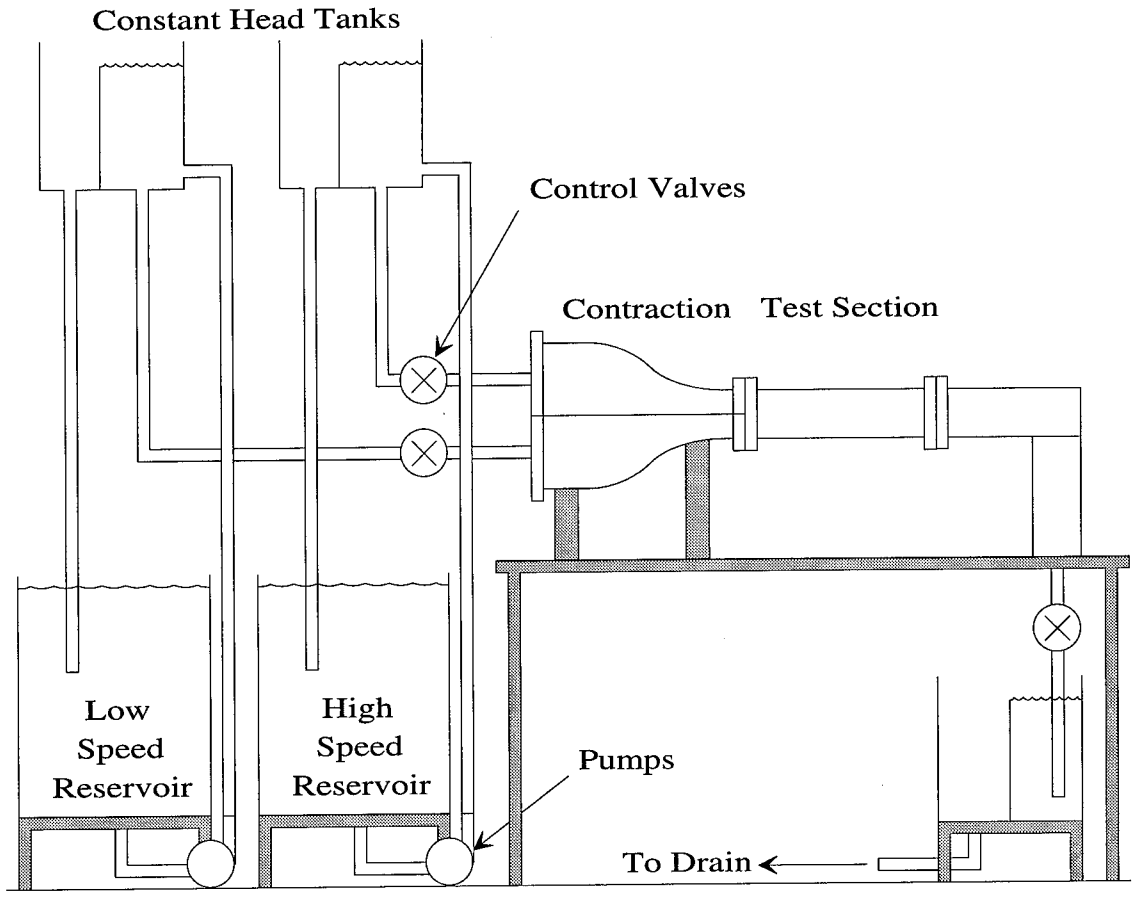

Figure 5. Schematic of the shear layer facility.

$Re_{\delta_1} = \Delta U\, \delta_1 / \nu$, based on velocity difference and shear layer width, ranges from 4400 < Re_{δ_1} < 6000. This range of Reynolds numbers corresponds to the later stages of the mixing transition, see Breidenthal (1981) and Figure 4. It is not clear however, if the presence of the airfoil affects the mixing transition. Due to the constraints of the flow facility, this is nearly the highest Reynolds number currently attainable. The natural shear layer roll up frequency f_o, at the splitter plate tip was approximately 27 Hz.

An important consideration to flow quality was the development of the boundary layer on both the upper and lower surfaces of the splitter plate. A series of screens and straws were used to create a uniform flow through the contraction. Additionally, extreme

care was taken during the filling process to expel all air from the system. Any air trapped under the splitter plate or in the straws may affect the boundary layer growth and the resulting shear layer.

2.2 Forcing mechanism

Perturbations were introduced into the shear layer by a 15% thick, 2-D airfoil of chord C = 2 cm, spanning the entire width of the test section b = 8 cm, oscillating sinusoidally in pitch about the quarter-chord with angle of attack amplitude A and frequency f. The airfoil was rotated about its quarter-chord point, located midway

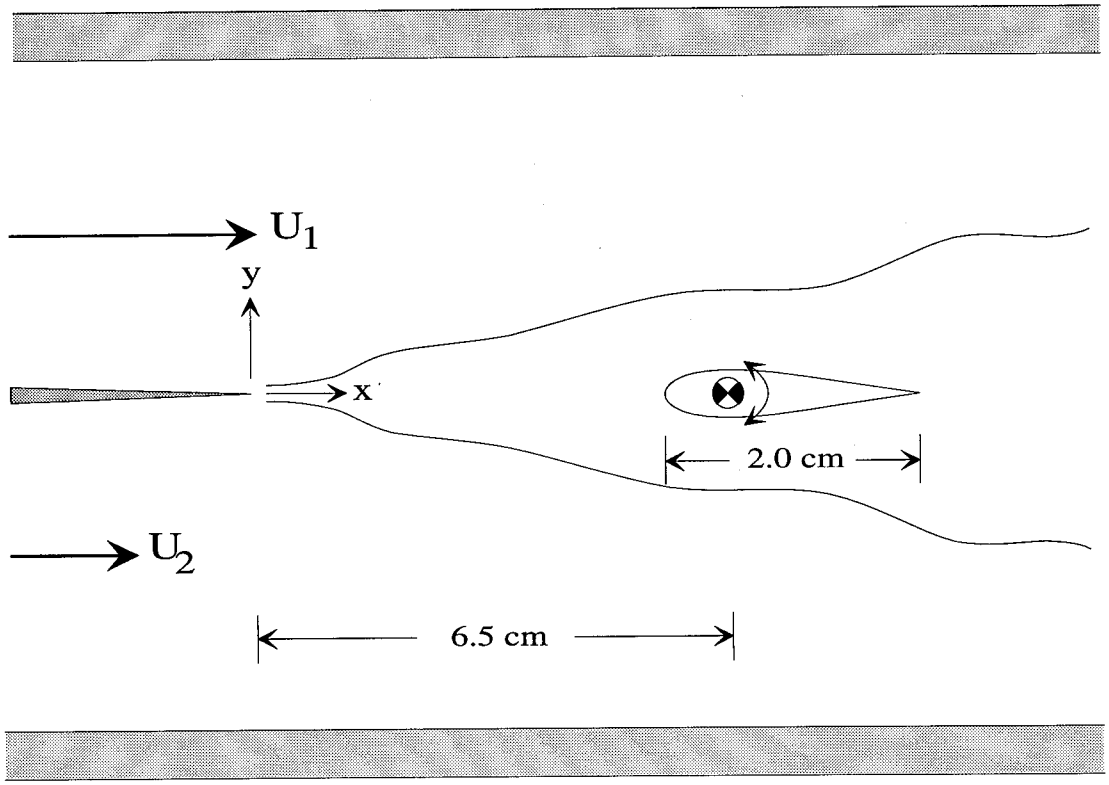

Figure 6. Schematic of the forcing arrangement.

between the upper and lower surfaces of the test section and 6.5 cm downstream of the splitter plate tip. A schematic of the forcing mechanism is shown in Figure 6. The placement of the airfoil was determined by the physical constraints of the airfoil assembly. Movement of the airfoil was achieved by an electro-magnetic coil vibrator (Vibrations Test Systems VG 100-8). To improve the sinusoidal motions of the airfoil a P-D feedback control system was used to match the airfoil position to a command input.

The angle of attack of the airfoil varied between -A and +A, with a mean angle of attack approximately zero. In this work an unforced case and nine forced cases were examined. In the unforced case the airfoil was stationery at zero degrees angle of attack. The forced cases included three frequencies at three amplitudes each; the combinations examined are shown in Table 1.

Table 1. Forcing frequency-amplitude combinations.

f (Hz)	A (degrees)
2	2, 4, 8
4	2, 4, 6
8	2, 4, 6

2.3 Diagnostics

The mixing field was measured using Laser Induced Fluorescence (LIF) in the passive scalar (non-reacting) mode. This technique utilizes a passive scalar containment, such as a fluorescent dye that is initially mixed with one of the freestream fluids. In this case the low-speed fluid was marked with the fluorescent dye disodium fluorescein. The

dye is then diluted as a result of mixing with fluid from the high-speed stream. By recording the fluorescence intensity issuing from a sample volume as a function of time, a quantitative measurement of the dye concentration, and therefore the relative concentration of high-speed to low-speed fluid within the volume may be made. The instantaneous dye concentration C_d in the sample volume is defined by

$$C_d = C_{d_o} \frac{v_2}{v_1 + v_2},$$

where C_{d_o} is the freestream (low-speed) dye concentration, v_1 and v_2 are the volume of fluid from the high- and low-speed freestreams, respectively, within the sample volume. Throughout this work the concentration ξ will be normalized as

$$\xi = 1 - \frac{C_d}{C_{d_o}}.$$

In terms of the high-speed volume fraction, concentration may be written as

$$\xi = \frac{v_1}{(v_1 + v_2)}.$$

Therefore, pure fluid from the low- and high- speed sides have concentrations $\xi = 0$ and $\xi = 1$, respectively.

The LIF measurements were carried out over a plane defined by a laser sheet, approximately 0.5 mm thick, aligned along the flow direction at the shear layer mid-span location. The laser sheet was formed by passing a 3 watt beam from a Lexel model 95

argon-ion laser through a converging lens and a spherical lens, see the schematic of the optical setup in Figure 7. The fluorescence intensity was imaged onto an electronically shuttered CCD (NEC TI-24A) camera (512 x 480 pixels) operating at standard video rate

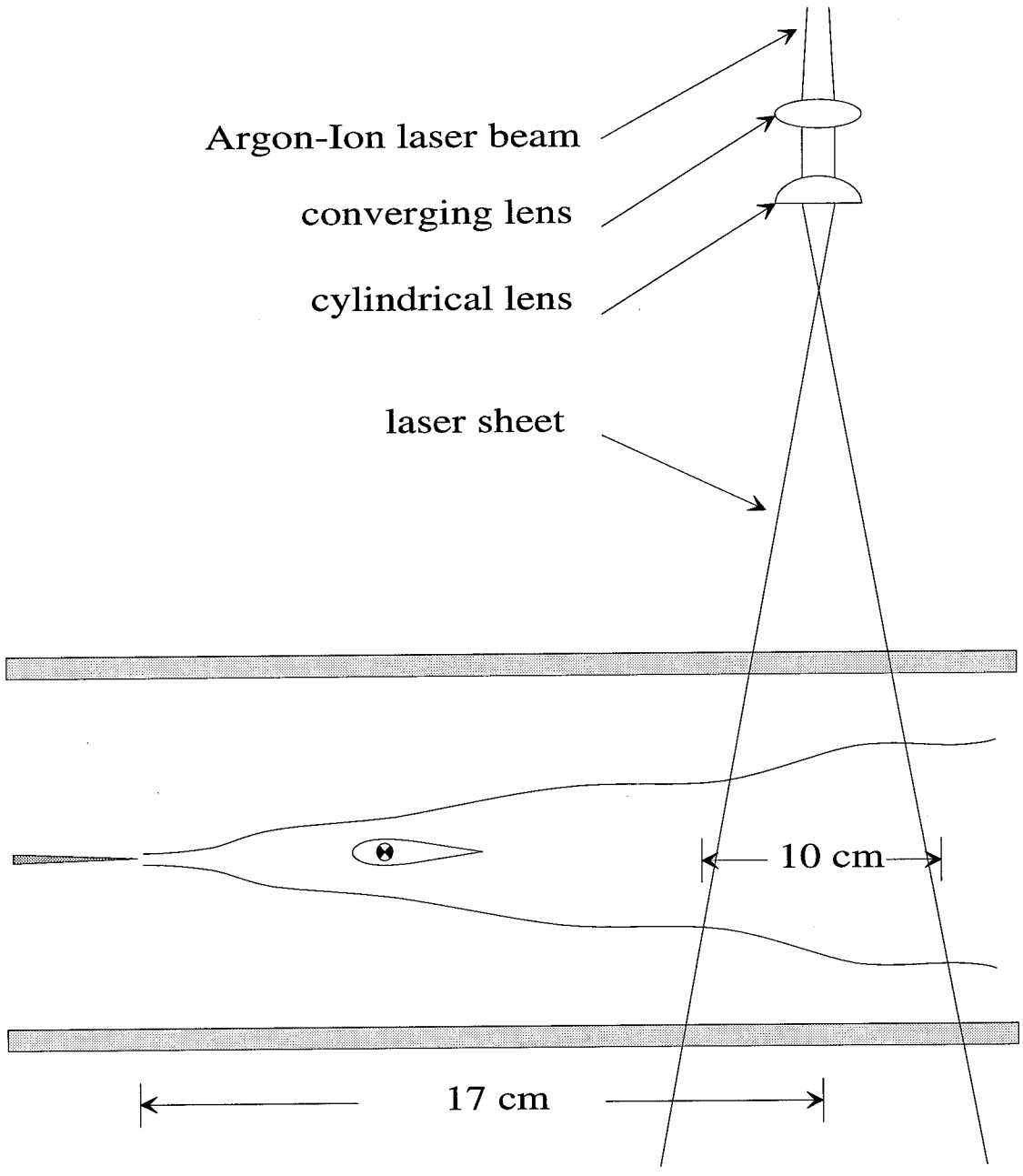

Figure 7. Schematic of the optical arrangement.

(30 frames/sec) with an exposure time of 2 msec. Images were then digitized to 8 bits and captured onto hard disk in real time by an image acquisition system (Recognition Concepts, Inc., TRAPIX-5500). For each of the ten forcing conditions, 256 consecutive LIF images (512 fields) were acquired, corresponding to 32, 64, and 128 large scale structures passing the field of view for forcing frequencies of $f = 2, 4, 8$ Hz, respectively.

The 4 cm test section height was imaged onto 200 of 480 vertical pixels; 512 pixels correspond to approximately 10 cm in the streamwise direction. The resulting resolution is approximately 200 x 200 μm. It should be noted that at this resolution the smallest expected diffusion (Batchelor) scales, λ_D, are not resolved. According to Miller and Dimotakis (1991), the smallest viscous scale, λ_v, and the Kolmogorov scale, $\lambda_K \approx \delta_1 Re^{-3/4}$, are related by $\lambda_v \sim 25\,\lambda_K$. The smallest diffusion scale λ_D is another factor of $Sc^{1/2}$ smaller than the smallest viscous scale, resulting in $\lambda_D \approx \lambda_K$ for water ($Sc \approx 600$). Over the range of parameters examined in this study the smallest diffusion scales, λ_D, are estimated to be about 41 μm, approximately 5 times smaller than the spatial resolution of the current memeasurement.

A curious limitation of this technique is that the measurements always over-estimate the amount of mixed fluid. Unmixed low- and high-speed fluids may simultaneously exist within the measurement resolution and appear as if they were actually mixed at that ratio. The results presented in this work are, therefore, not intended to provide an absolute measure of the extent of molecular mixing. The primary focus of these results is to characterize the *relative* changes in the mixing field in a forced layer compared to the unforced layer. Such comparisons are believed to be warranted since the resolution, compared to the smallest diffusion scale, is the same for all of the

measurements presented in this work.

2.4 Data reduction

The first, and perhaps the most time consuming step in the data reduction process, is the normalization of the images. The images were first processed to remove the Gaussian distribution of the laser sheet and nonuniform pixel response of the CCD camera. A calibration was performed at the start of the experiment to capture these effects. During the calibration the test section was flooded with low-speed fluid mixed with the dye, images were recorded and then averaged to produce a calibration image. The nonuniformities in the pre-processed images were then removed on a pixel by pixel basis according to

$$I_{corr} = \frac{I}{I_{cal}},$$

where I_{corr} is the corrected intensity, I is the instantaneous image intensity and I_{cal} is the intensity from the calibration image. Concentration may then be computed as

$$\xi = 1 - \frac{I_{corr}}{I_{corr_o}},$$

where I_{corr_o} is the corrected freestream dye intensity. This expression is simply a conversion from the measured quantity, fluorescence intensity to dye concentration. The absorption coefficient $\alpha = \varepsilon_0 C_d$, where ε_0 is the dye molar absorption coefficient and C_d is the molar dye concentration, was measured by Koochesfahani (1984) to be 0.157 cm^{-1}

at a dye concentration of $C_d = 10^{-5}$M. Attenuation of the fluorescence intensity at a given depth y is then given by $I = I_0 e^{-\alpha y}$, where I_0 is the initial intensity. In the current work, the dye concentration is approximately 2.5×10^{-7}M; a factor of 40 smaller than in the work of Koochesfahani (1984). In the event that the test section is completely filled with dye, the worst possible case, the fluorescence intensity at the bottom of the test section would have been attenuated by only 1.6%. The effect of attenuation is much smaller than the overall signal-to-noise ratio of the experiment $\varepsilon = 4.5\%$.

From the normalized images the probability density function (pdf) of the concentration field can be constructed at any of the measurement points in the x-y plane. The pdf of concentration ξ as a function of position y in the layer, written $p(\xi, y)$, was computed at six different streamwise locations. The pdf $p(\xi, y)$ is the basis for all of the computed quantities in this study. The ideal pdf would have delta functions at ξ = 0 and 1 representing pure fluid from the low- and high-speed freestreams, respectively. In practice, the delta functions have a finite width ε which is the result of the overall signal-to-noise ratio of the experiment. In this work $\varepsilon = 0.045$, therefore concentrations in the range $0 \le \xi < \varepsilon$ and $1\text{-}\varepsilon < \xi \le 1$ are considered to be pure unmixed fluid from the low- and high-speed freestreams, respectively. Likewise, concentrations within the range $\varepsilon < \xi < 1\text{-}\varepsilon$ are considered mixed fluid.

The first quantity computed from $p(\xi, y)$ is the average concentration $\overline{\xi}$ which is found by integrating over all concentrations at a given position, as defined by

$$\overline{\xi}(y) = \int_0^1 \xi \, p(\xi, y) \, d\xi.$$

To characterize the effect of forcing on the mixing field the probability of occurrence of unmixed fluid from either the low- or high-speed freestreams can be computed by

$$p_0(y) = \int_0^{\varepsilon} p(\xi, y)\, d\xi,$$

$$p_1(y) = \int_{1-\varepsilon}^{1} p(\xi, y)\, d\xi.$$

Similarly, the probability of occurrence of mixed fluid is computed by integrating over the range of concentrations defining mixed fluid as given by

$$p_m(y) = \int_{\varepsilon}^{1-\varepsilon} p(\xi, y)\, d\xi.$$

It should be noted that p_m is the probability of occurrence of mixed fluid of *all* concentrations; a value of less than one implies the presence of unmixed fluid.

The shear layer width δ_1 may be computed based on the total mixed fluid probability curve at a given downstream location. The local width is defined in a manner similar to boundary layer thickness. Recall, the boundary layer thickness is the height above a surface where the local velocity is 99% of the free stream velocity. The shear layer width δ_1 is similarly defined as the distance between the two points where the probability of mixed fluid is 1% of the maximum value of $p_m(y)$. Koochesfahani and Dimotakis (1986) reported that the visual width of the shear layer δ_{vis} is approximately equal to δ_1.

A measure of the total amount of mixed fluid (at all concentrations) in the layer,

the mixed fluid thickness, is defined by

$$\delta_m = \int_{-h}^{+h} \int_{\varepsilon}^{1-\varepsilon} p(\xi, y)\, d\xi\, dy = \int_{-h}^{+h} p_m(y)\, dy.$$

Note that the mixed fluid thickness is simply the area under the total mixed fluid probability curve. The quantity δ_m/δ_1, termed the mixed fluid fraction, is used to quantify the amount of mixed fluid per unit width of the shear layer.

It has been shown by Koochesfahani and M^{ac}Kinnon (1991) that the distribution of the mixed fluid composition is nearly invariant across the entire width of the layer, and therefore may be characterized by an average pdf. The average pdf is defined by

$$P(\xi) = \frac{1}{2h} \int_{-h}^{+h} p(\xi, y)\, dy,$$

where h is the test section half width.

A common measure of shear layer growth is the momentum thickness defined by

$$\theta = \int_{-\infty}^{+\infty} \frac{(U_1 - U)(U - U_2)}{(U_1 - U_2)^2}\, dy.$$

In this work no velocity measurements were made, therefore the momentum thickness cannot be calculated. Another integral thickness, called the concentration thickness, may be defined in a manner analogous to the momentum thickness, based on the average concentration, defined as

$$\theta_\xi = \int_{-\infty}^{+\infty} \frac{\left(\overline{\xi}_1 - \overline{\xi}\right)\left(\overline{\xi} - \overline{\xi}_2\right)}{\left(\overline{\xi}_1 - \overline{\xi}_2\right)^2} dy.$$

Recall that the subscripts 1 and 2 in the above equation refer to the average concentration of the high- and low-speed freestreams, respectively. The average concentration of the high-speed freestream $\overline{\xi}_1 = 1$ and for the low-speed freestream $\overline{\xi}_2 = 0$. The concentration thickness is then reduced to

$$\theta_\xi = \int_{-\infty}^{+\infty} \left(1 - \overline{\xi}\right)\overline{\xi}\, dy.$$

The relationship between the shear layer width δ_1 and the concentration thickness θ_ξ will be examined in section 3.4.

Chapter 3

RESULTS AND DISCUSSION

3.1 Flow visualization results

Figures 8 - 12 illustrate the influence of the forcing frequency and amplitude on the structure and growth of the shear layer. In all of the images the flow is from right to left with the high-speed stream on top. The time between images Δt is 1/30 sec, (every other field) with time increasing from top to bottom. Each image, composed of 90,000 pixels (450 in x and 200 in y), spans the entire height of the test section and the range $12 < x < 22$ cm (right to left). After processing, the images were pseudo-colored to simulate a chemical reaction. Pure fluid from either of the freestreams was assigned to black. Fluid composed of mainly low-speed fluid, $\xi \approx \varepsilon$, were assigned shades of blue; likewise nearly pure high-speed fluid, $\xi \approx 1\text{-}\varepsilon$, were colored shades of red (recall pure low-speed fluid has concentration $0 \leq \xi \leq \varepsilon$, high-speed fluid $1\text{-}\varepsilon \leq \xi \leq 1$).

Two different time series of images from the unforced layer are presented in Figure 8. These clearly show the random nature of the unforced layer. In Figure 8 (a) a fairly well defined large structure may be seen passing the field of view, while some time later in Figure 8 (b), there are no well defined large structures apparent. It should be noted that the unforced shear layer described here is not the same as the natural layer

due to the presence of the airfoil. Differences between the unforced and natural shear layers will be discussed in Section 3.6.

Figures 9 - 12 display the effect of the forcing amplitude A on the structure and growth of the shear layer forced at f = 2, 4 and 8 Hz, respectively. For the case forced at f = 2 Hz, A = 2°, see Figure 9 (a), there is very little if any visible effect on the structure and growth rate of the layer, when compared to the unforced case. With increasing amplitude, Figures 9 (b) and (c), the layer growth rate increases resulting in larger vortical structures and shear layer width at a given downstream location x. As a result of the larger layer width mixed-fluid can also be seen over a larger portion of the test section. Quantitative descriptions of the shear layer width and the amount of mixed fluid will be given in section 3.3. There are some periodic structures in the flow, however they are not very well defined. The location where the structures are fully formed is the center of the frequency locked region, x^* = 1.5; for f = 2 Hz this corresponds to $x \approx 68$ cm, which lies well beyond the end of the test section. See section 1.2 for description of the nondimensional streamwise coordinate x^*. Moving farther downstream, if possible, would not allow the structures to further develop because of the limiting height of the test section. The lower wall of the test section may be seen to influence the structures in Figure 9 (c). In the images, the nondimensional streamwise coordinate spans the range, $0.26 < x^* < 0.52$, which lies well within the enhanced growth region.

In Figure 10 the structure of the shear layer is shown as a function of the forcing amplitude A when forced at f = 4 Hz. At this frequency the nondimensional streamwise coordinate spans the end of the enhanced growth rate region, $0.52 < x^* < 1.02$. Again,

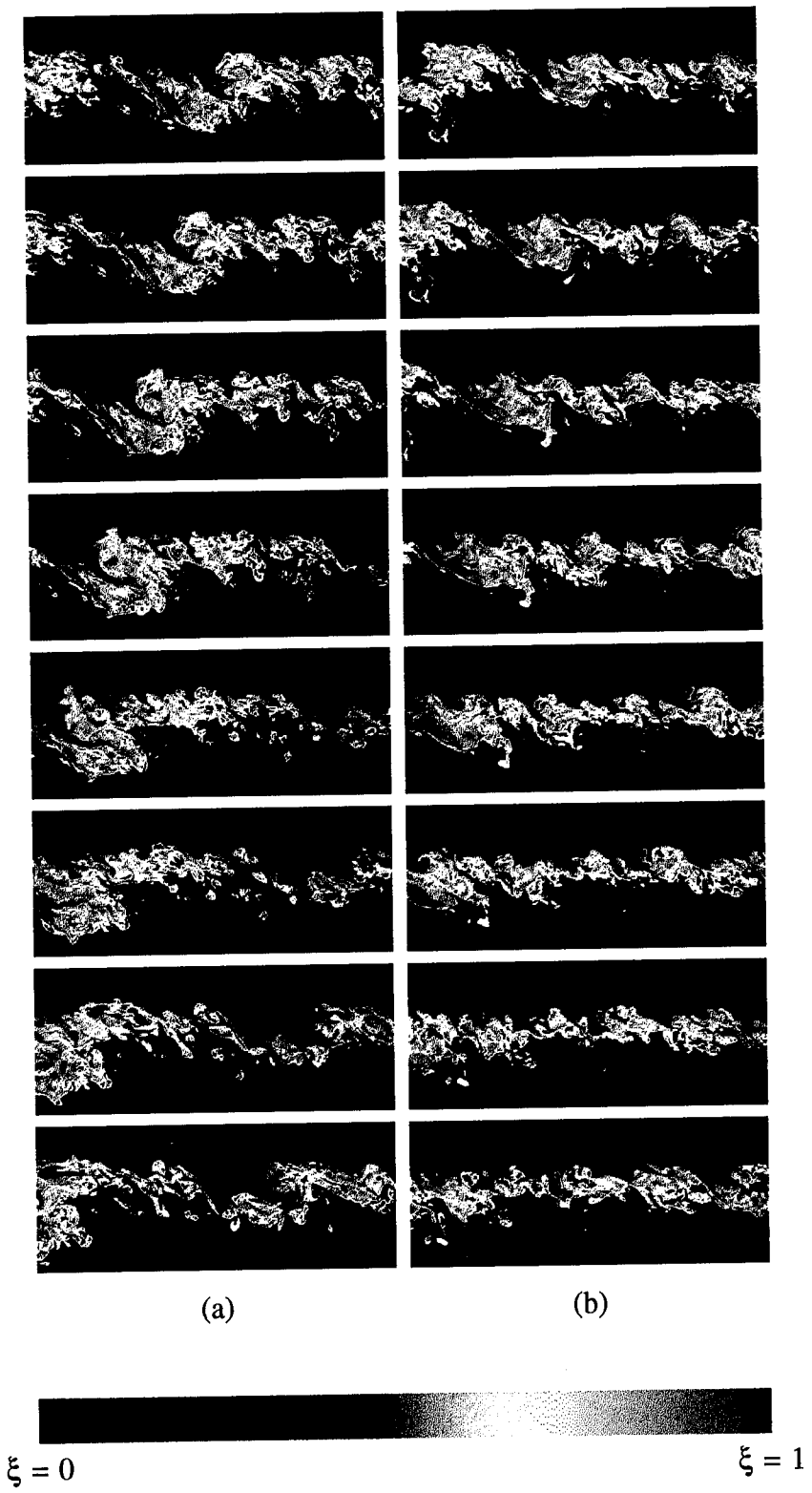

Figure 8. Time series of the unforced shear layer, (a) and (b) are not consecutive in time, flow is from right to left, $\Delta t = 1/30$ sec.

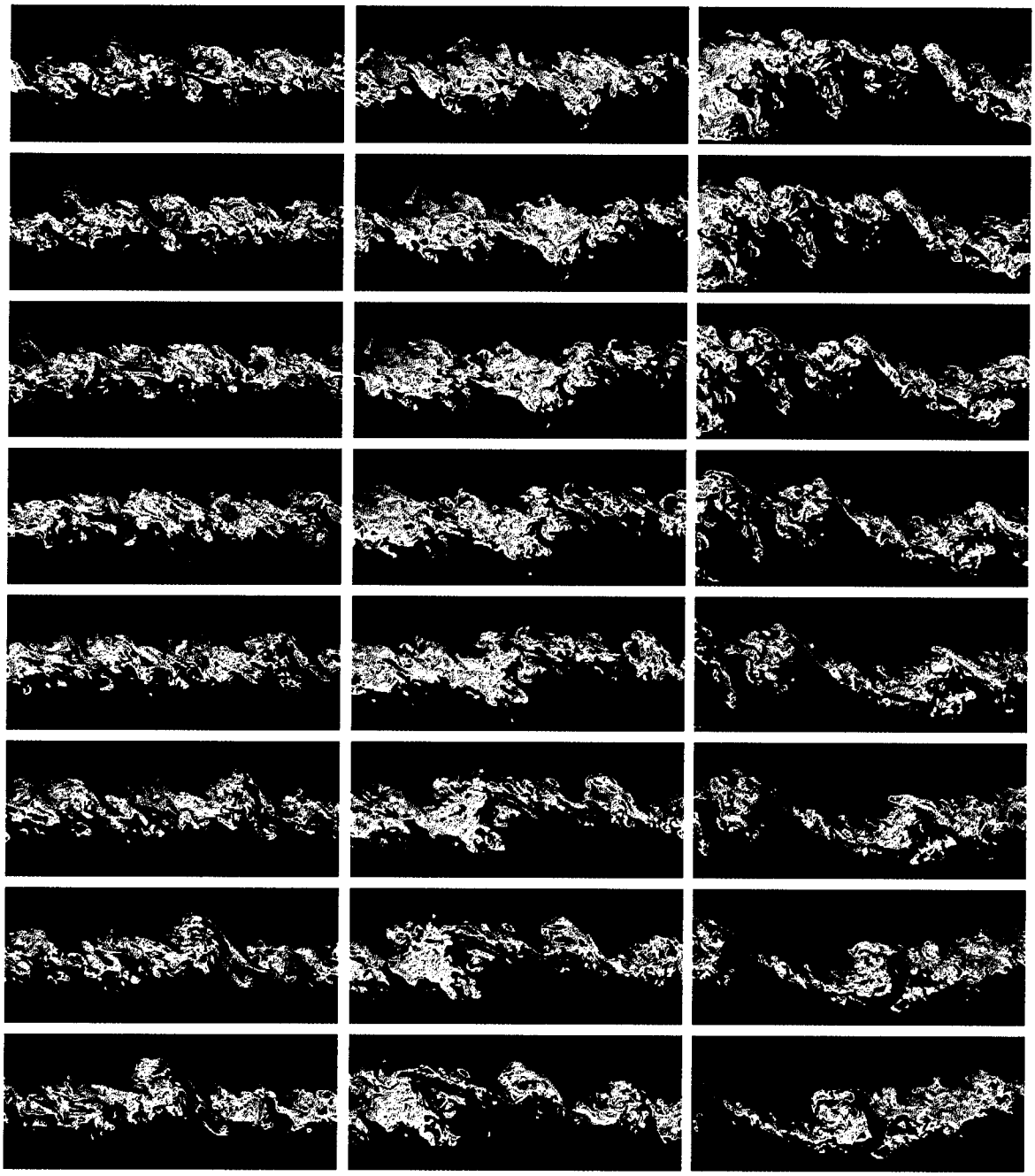

(a) $A = 2°$ (b) $A = 4°$ (c) $A = 8°$

$\xi = 0$ $\xi = 1$

Figure 9. Effect of the forcing amplitude on the structure of the shear layer forced at $f = 2$ Hz, flow is from right to left, $\Delta t = 1/30$ sec.

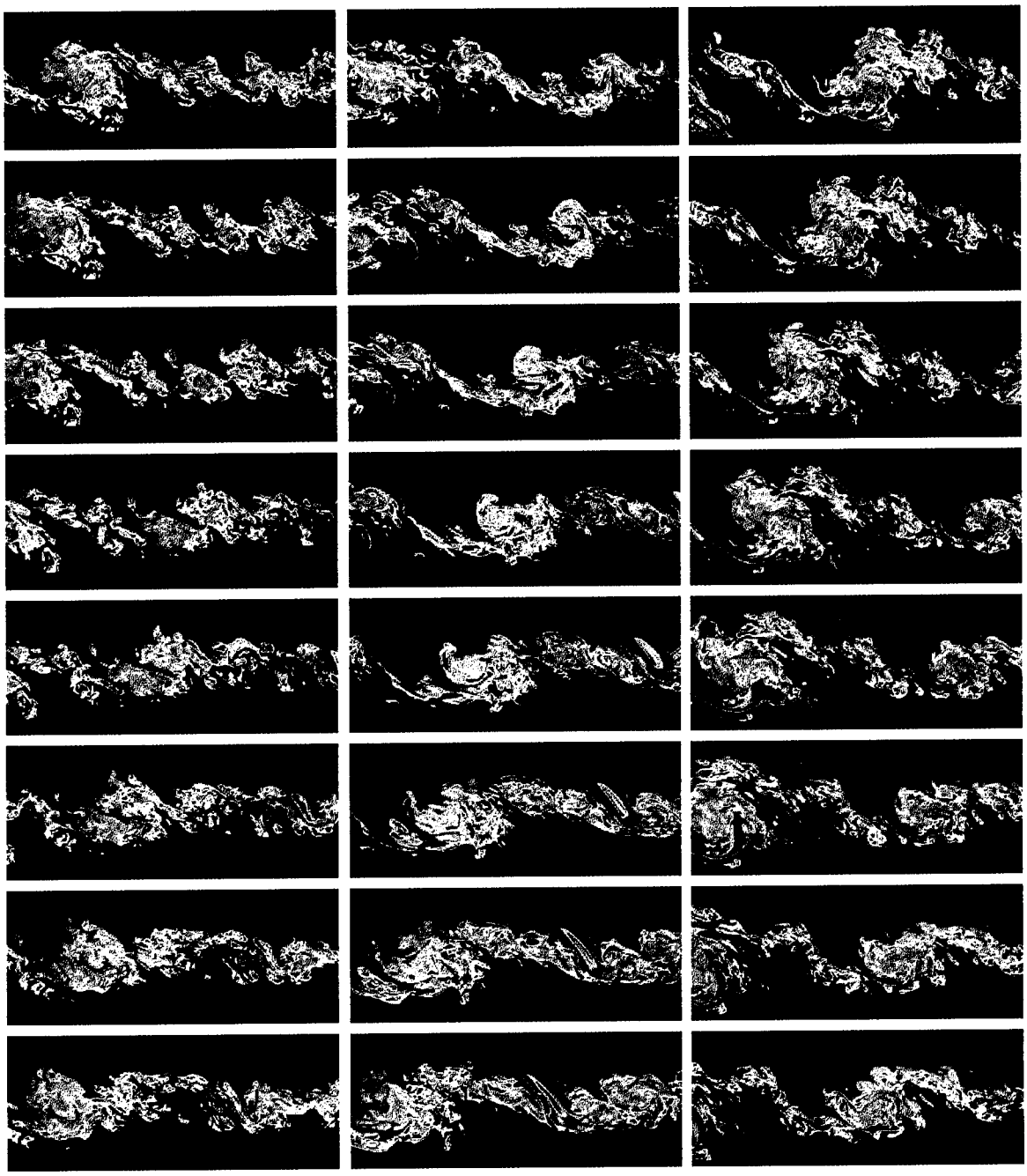

(a) $A = 2°$ (b) $A = 4°$ (c) $A = 6°$

$\xi = 0$ $\xi = 1$

Figure 10. Effect of the forcing amplitude on the structure of the shear layer forced at $f = 4$ Hz, flow is from right to left, $\Delta t = 1/30$ sec.

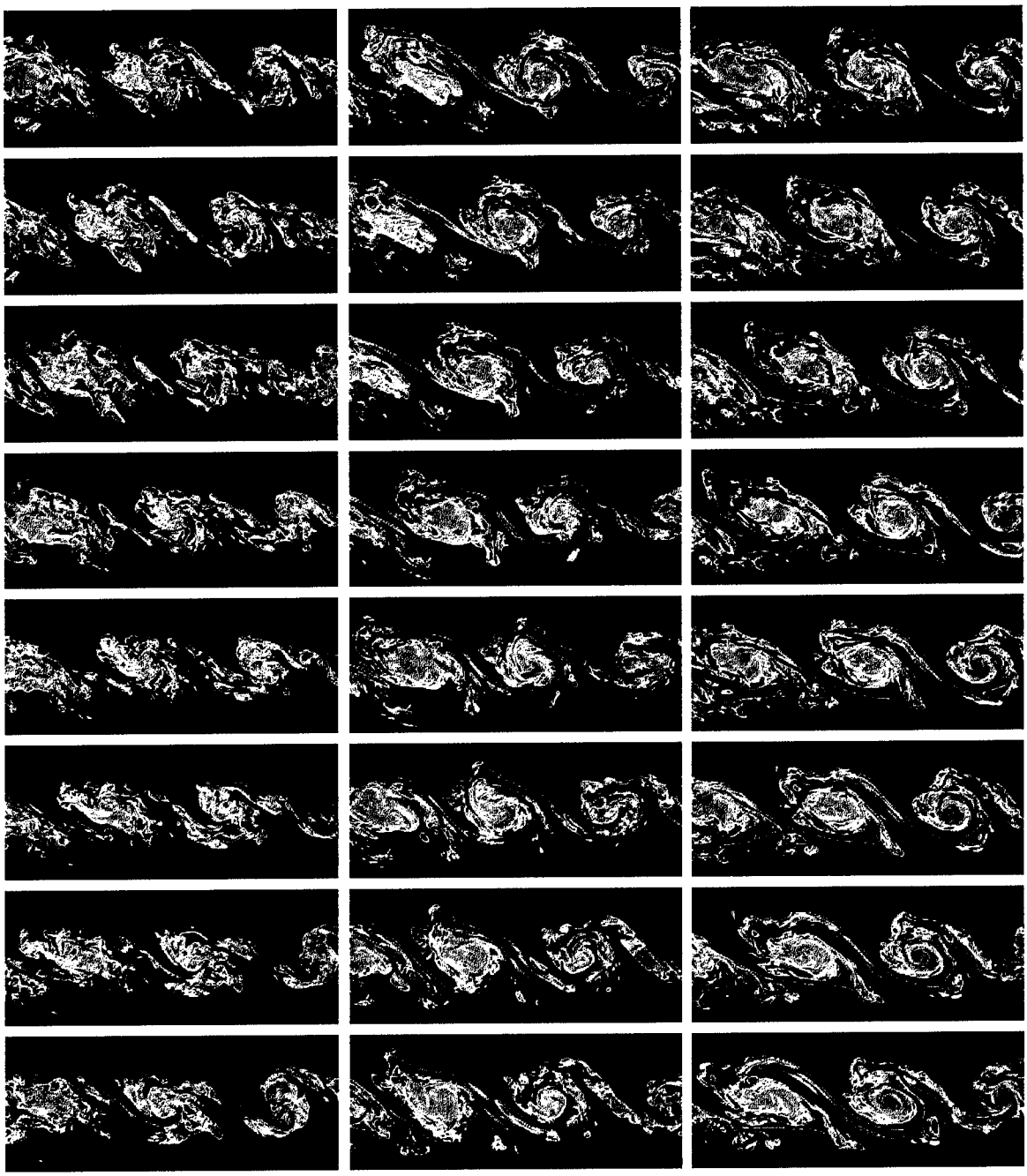

(a) $A = 2°$ (b) $A = 4°$ (c) $A = 6°$

$\xi = 0$ $\xi = 1$

Figure 11. Effect of the forcing amplitude on the structure of the shear layer forced at $f = 8$ Hz, flow is from right to left, $\Delta t = 1/30$ sec.

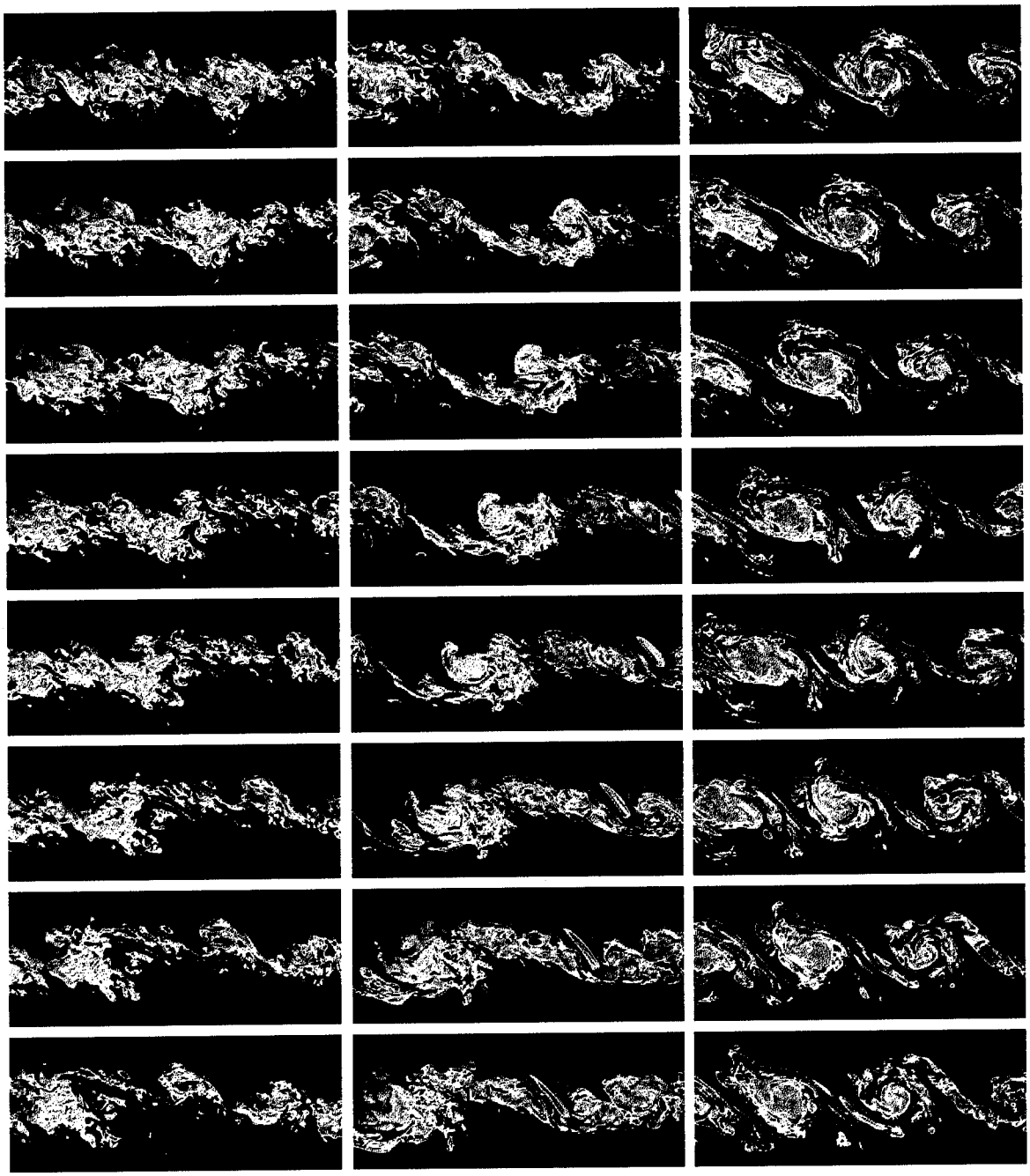

(a) f = 2 Hz (b) f = 4 Hz (c) f = 8 Hz

$\xi = 0$ $\xi = 1$

Figure 12. Effect of the forcing frequency on the structure of the shear layer forced at $A = 4°$, flow is from right to left, Δt = 1/30 sec.

it may be seen that as the amplitude increases the layer growth rate and the amount of mixed fluid within the layer also increases. In this case the structures are more well defined than the case forced at 2 Hz. At the largest amplitude the structures are, again, approaching the width of the test section.

The cases forced at f = 8 Hz, shown in Figure 11, span the frequency locked region ($1.04 < x^* < 2.04$) characterized by an array of non-interacting, equally spaced vortices and reduced growth rate. Even at the smallest amplitude $A = 2°$, the structures are very well defined. As in the previous cases, the effect of amplitude is shown to result in an increase in the layer width and the amount of mixed fluid within the layer. In all of these cases, the increase in shear layer growth rate, in response to low frequency forcing (relative to the natural frequency, f_0 = 27 Hz), culminating in the formation of large vortical structures is consistent with previous shear layer studies eg. Fiedler *et al.* (1981), Oster and Wygnanski (1982), Ho and Huang (1982), Koochesfahani and Dimotakis (1989). For completeness, Figure 12 is included to show the effect of the *forcing frequency* on the structure of the shear layer when forced at a *fixed amplitude* of $A = 4°$. Note as the frequency is increased, the excursions of low-speed fluid to the upper side, and high-speed fluid to the lower side of the shear layer becomes deeper. This excursion of fluid is often referred to as an entrainment tongue.

3.2 Transverse profiles of $\bar{\xi}$, p_m, p_0 and p_1

The quantities computed from the probability density function of the high-speed fluid volume fraction $p(\xi, y)$ are presented in this section. The plots are divided into two sections. The first section will present the evolution of the various computed quantities

as a function of streamwise location x, at a fixed forcing frequency and amplitude. The second will show the amplitude dependence at a fixed downstream location x. Data were computed at 6 uniformly spaced streamwise locations spanning the range $0.28 \leq x^* \leq 1.78$ ($12.5 \leq x \leq 20.0$ cm).

3.2.1 Streamwise dependence

Transverse profiles of the average concentration $\overline{\xi}$, the total mixed fluid probability $p_m(y)$ and unmixed fluid probabilities, $p_0(y)$ and $p_1(y)$ for the unforced shear layer are shown in Figure 13. In general, the results for the unforced layer are very similar in shape to the results of the natural layer reported by Koochesfahani and Dimotakis (1986) and Koochesfahani and M[ac]Kinnon (1991). As previously discussed, differences in the shear layer width and the amount of mixed fluid between the unforced and natural layers will be quantified in section 3.6.

The most obvious feature of the unforced layer is the increase in the layer width with increasing downstream distance as seen in the total mixed fluid probability curves displayed in Figure 13 (b). Increasing shear layer width may also be inferred from outward movement of the probability of pure low- and high-speed curves, see Figure 13 (c) and (d). A feature unique to the unforced layer is the nearly constant value of the peak of the mixed fluid probability curve $(p_m)_{\max} \approx 0.95$ with increasing downstream distance. Recall that a value of p_m less than unity implies the presence of unmixed fluid; therefore roughly 5% of the fluid in the center of the unforced layer is unmixed. It will be shown later, that there can be a significant streamwise variation in $(p_m)_{\max}$ in the forced cases.

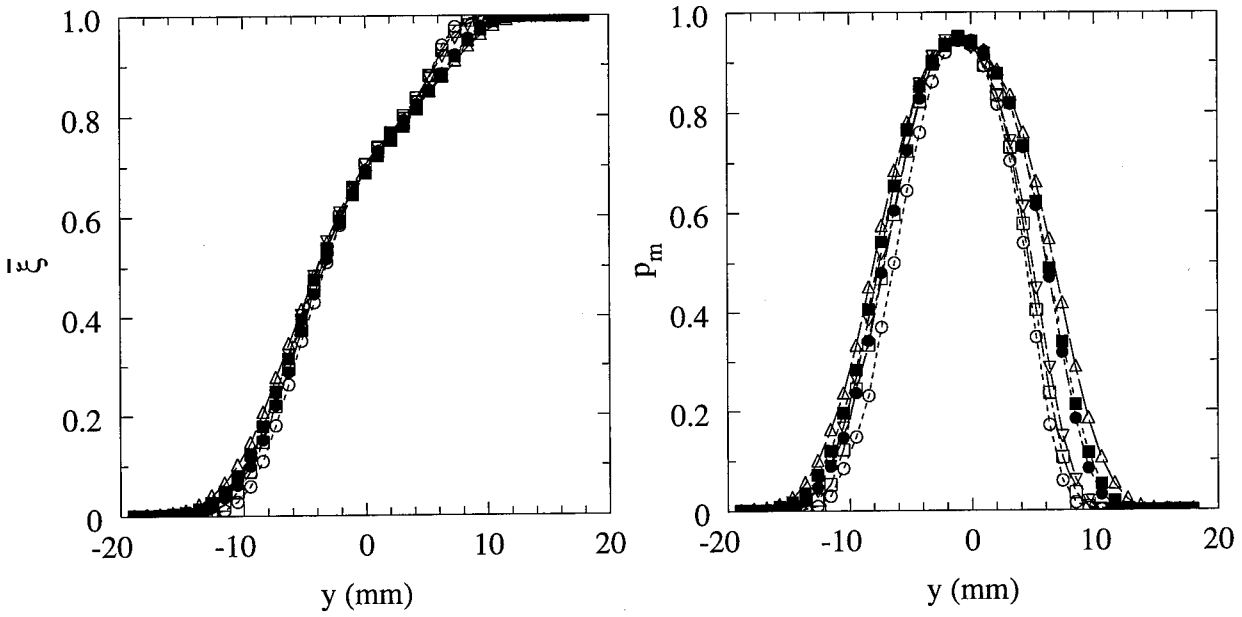

(a) Average concentration

(b) Total mixed fluid probability

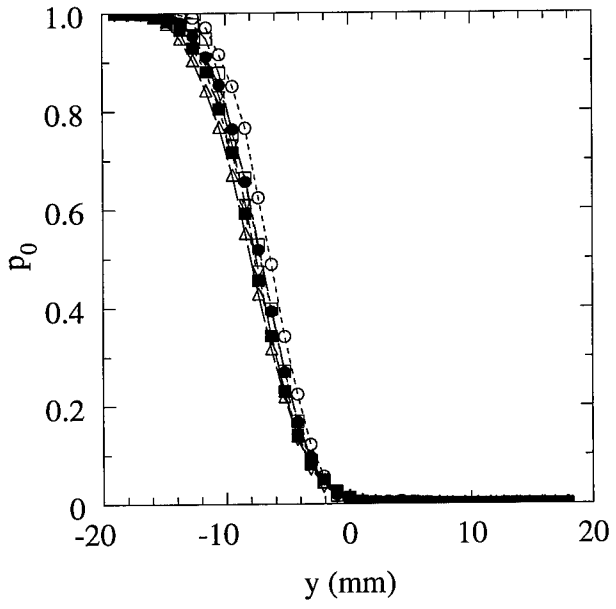

(c) Pure low-speed fluid probability

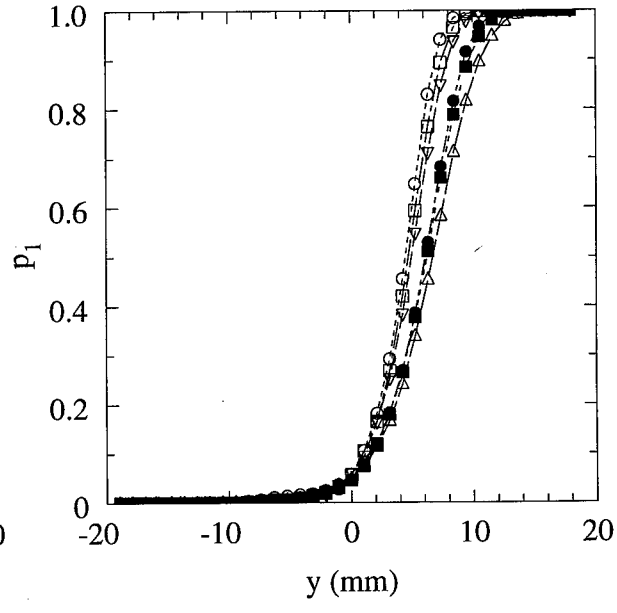

(d) Pure high-speed fluid probability

○ x = 12.5, □ x = 14.0, ▽ x = 15.5, ● x = 17.0, ■ x = 18.5, △ x = 20.0 cm

Figure 13. Transverse profiles for the unforced shear layer as a function of the downstream distance x.

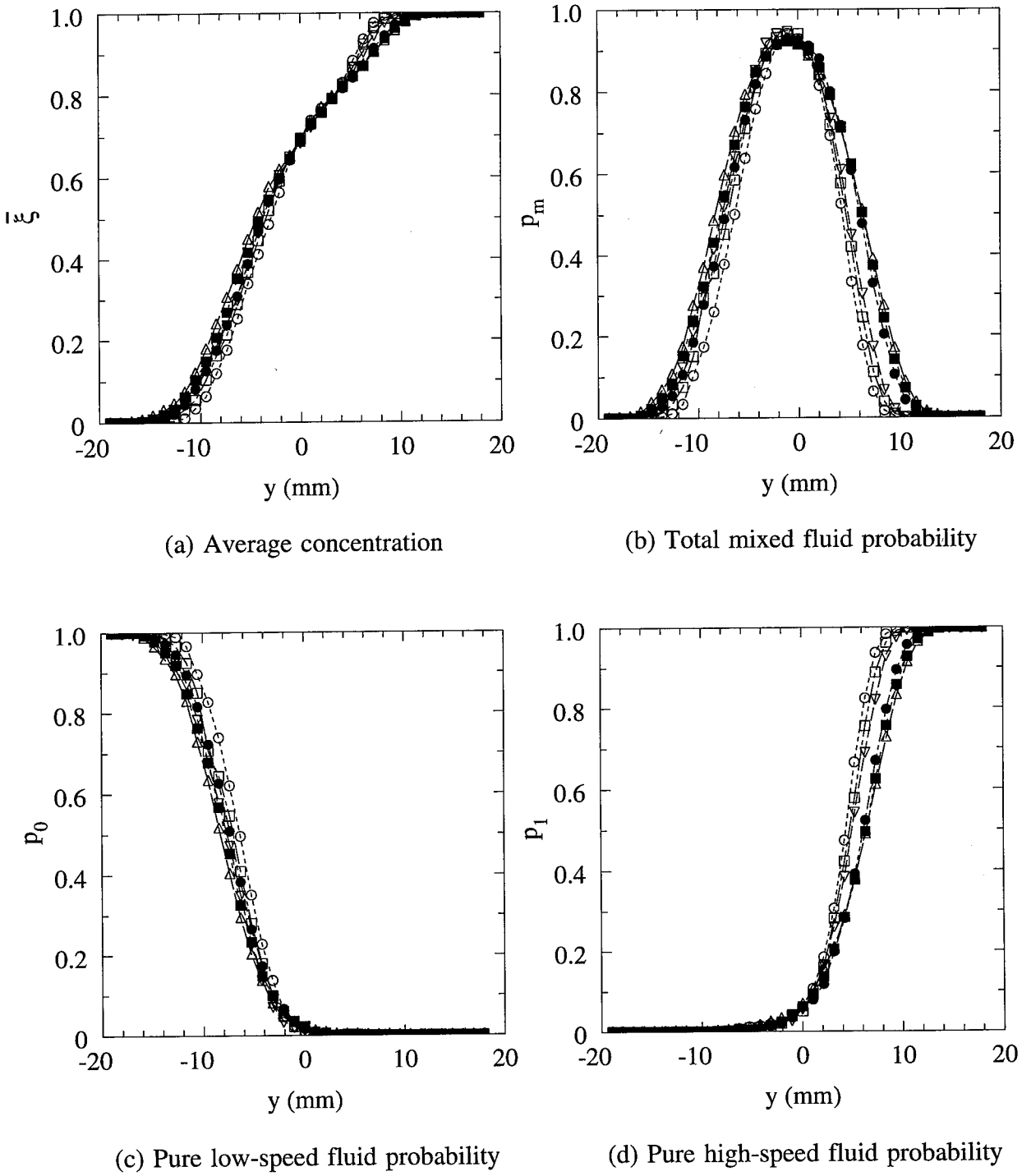

(a) Average concentration

(b) Total mixed fluid probability

(c) Pure low-speed fluid probability

(d) Pure high-speed fluid probability

○ $x^* = 0.28$, □ $x^* = 0.31$, ▽ $x^* = 0.34$, ● $x^* = 0.37$, ■ $x^* = 0.41$, △ $x^* = 0.44$

Figure 14. Transverse profiles for the shear layer forced at $f = 2$ Hz, $A = 2°$ as a function of the nondimensional downstream distance x^*.

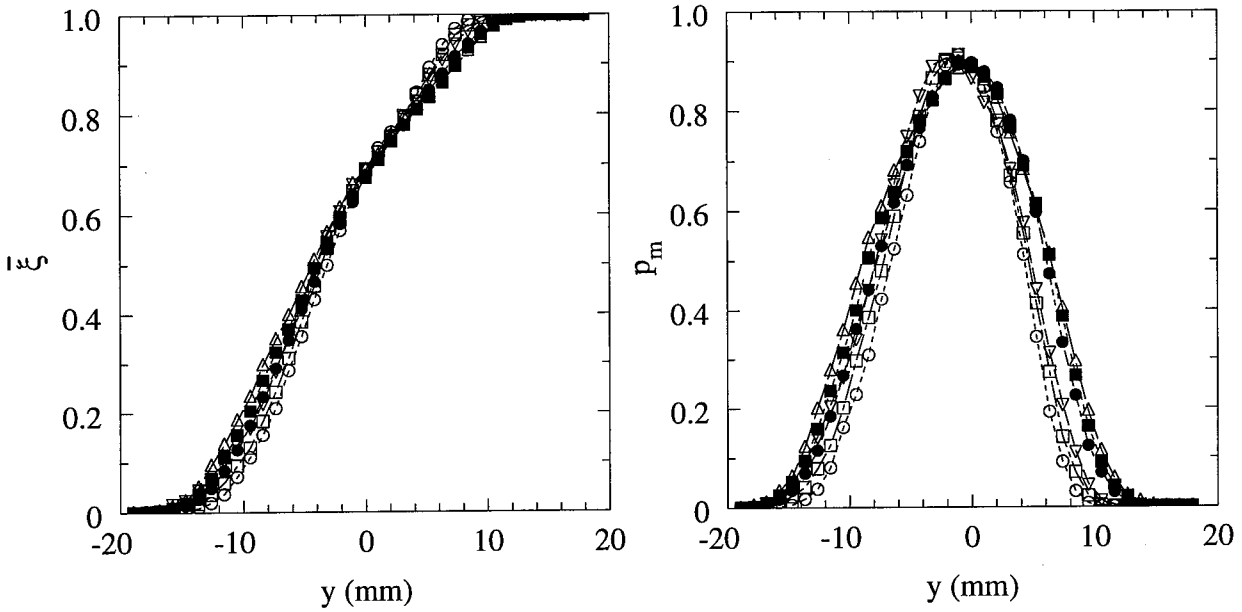

(a) Average concentration

(b) Total mixed fluid probability

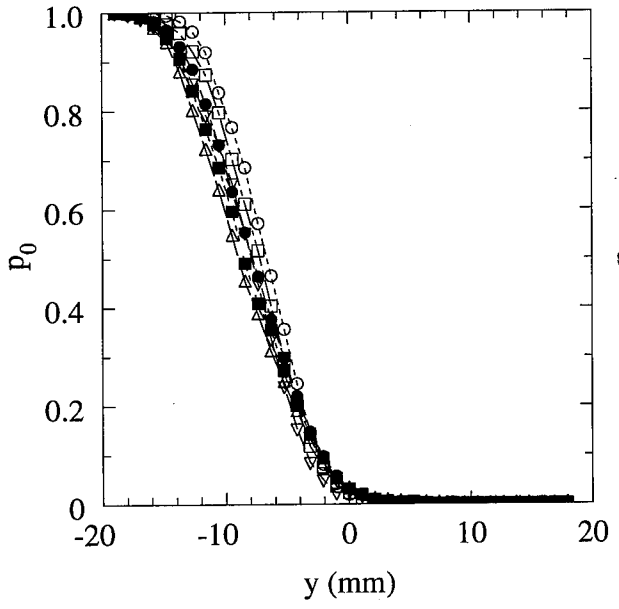

(c) Pure low-speed fluid probability

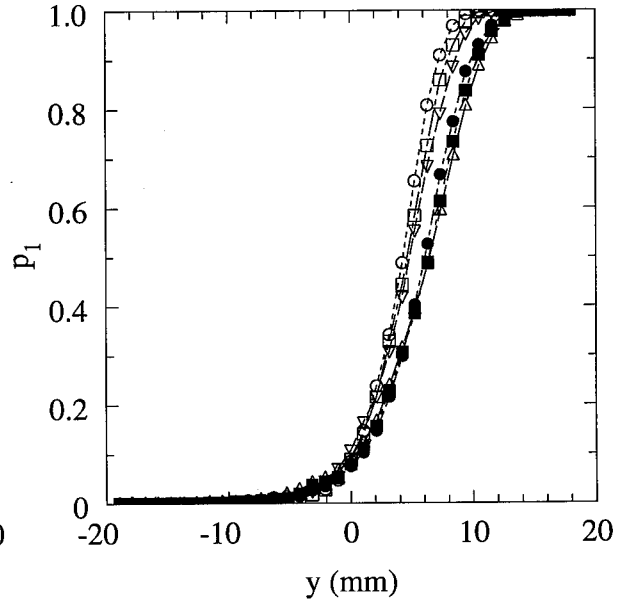

(d) Pure high-speed fluid probability

○ $x^* = 0.28$, □ $x^* = 0.31$, ▽ $x^* = 0.34$, ● $x^* = 0.37$, ■ $x^* = 0.41$, △ $x^* = 0.44$

Figure 15. Transverse profiles for the shear layer forced at $f = 2$ Hz, $A = 4°$ as a function of the nondimensional downstream distance x^*.

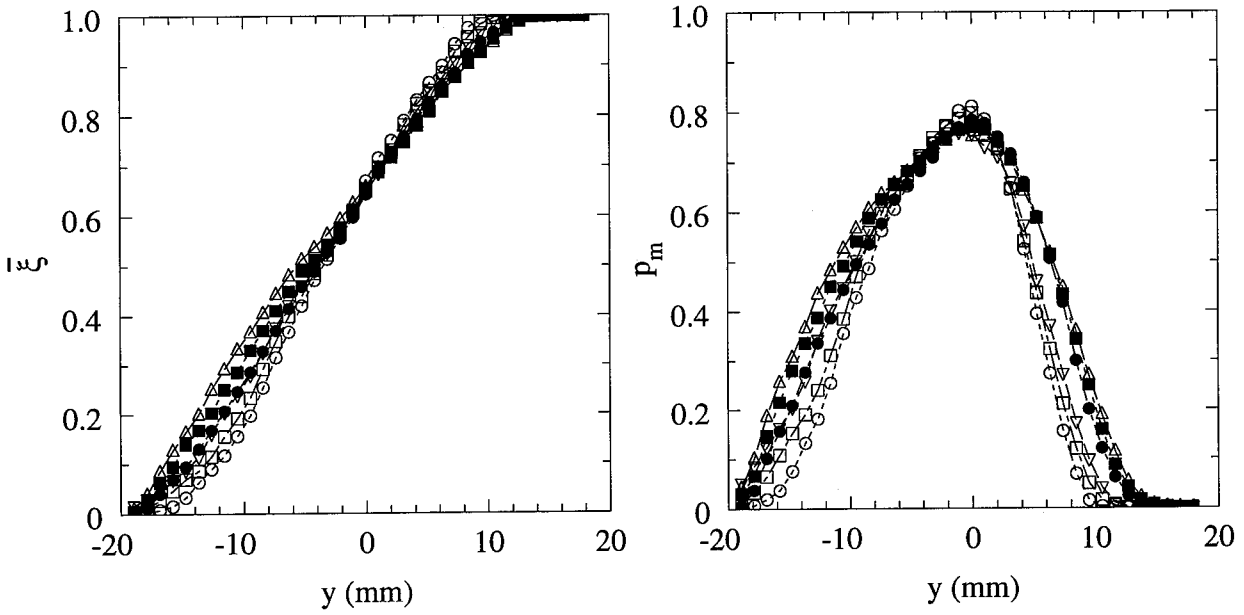

(a) Average concentration

(b) Total mixed fluid probability

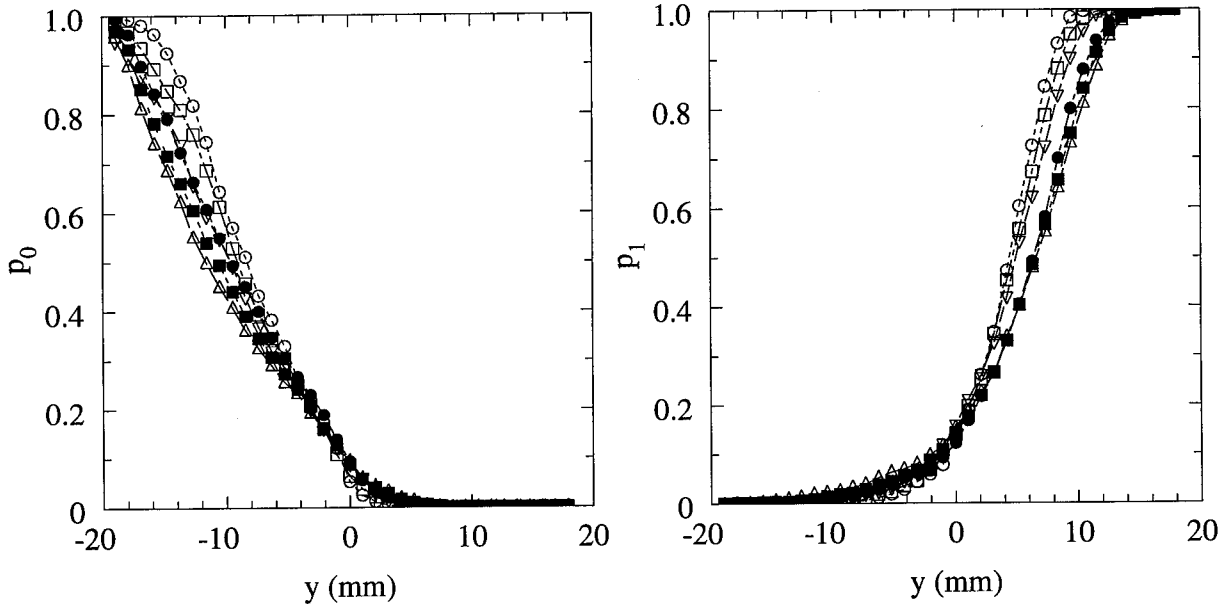

(c) Pure low-speed fluid probability

(d) Pure high-speed fluid probability

○ $x^* = 0.28$, □ $x^* = 0.31$, ▽ $x^* = 0.34$, ● $x^* = 0.37$, ■ $x^* = 0.41$, △ $x^* = 0.44$

Figure 16. Transverse profiles for the shear layer forced at $f = 2$ Hz, $A = 8°$ as a function of the nondimensional downstream distance x^*.

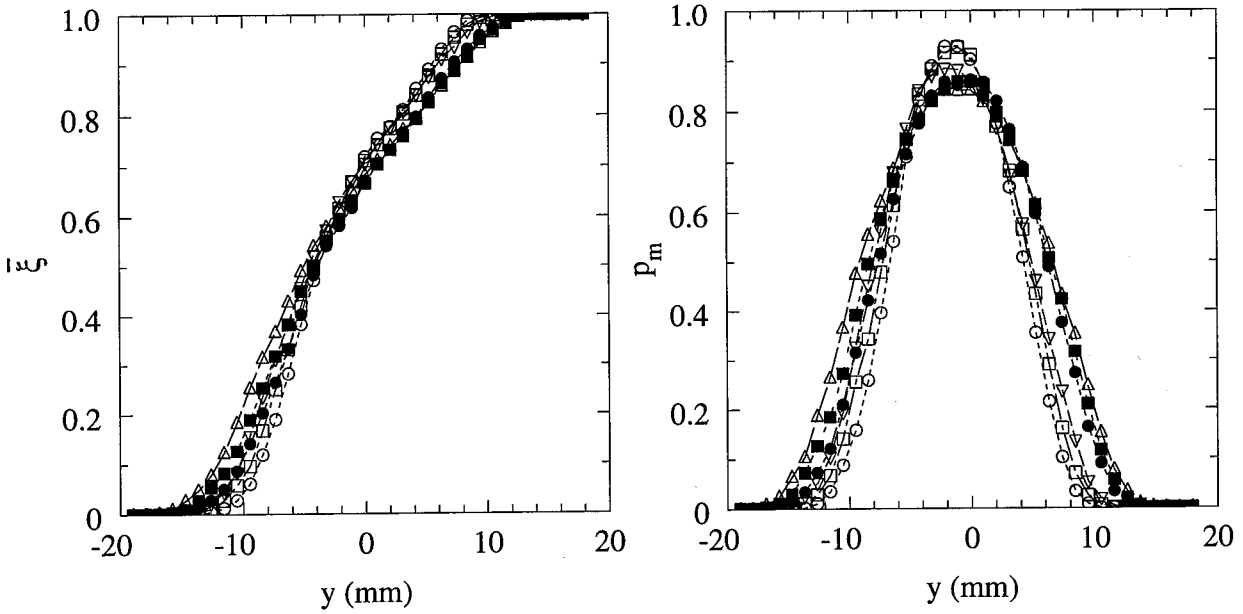

(a) Average concentration

(b) Total mixed fluid probability

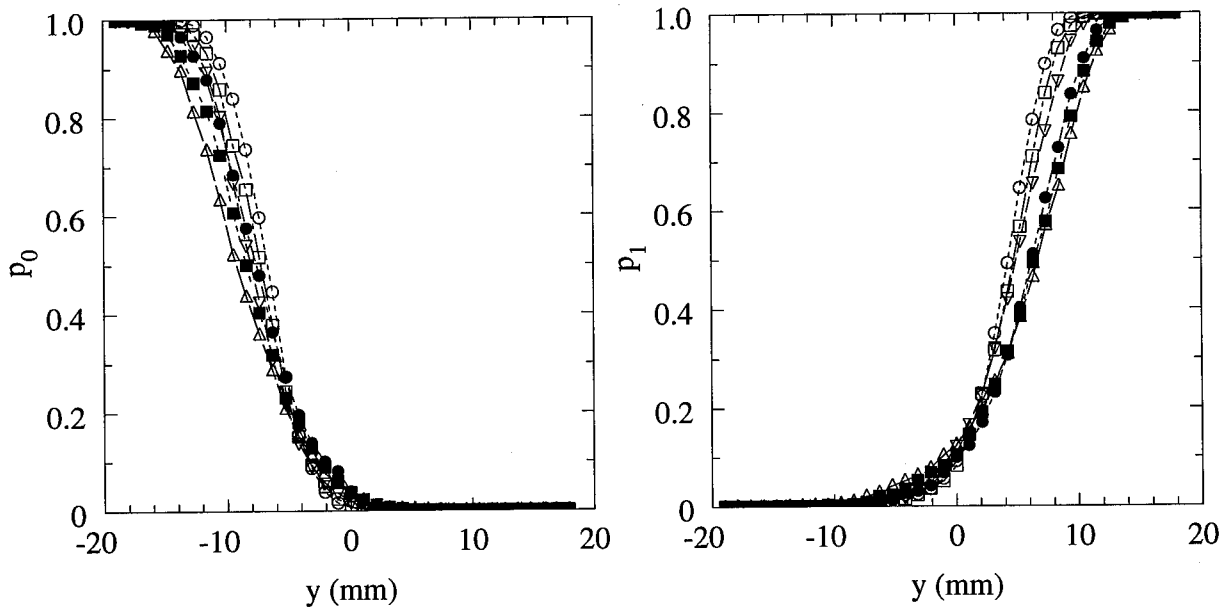

(c) Pure low-speed fluid probability

(d) Pure high-speed fluid probability

○ $x^* = 0.56$, □ $x^* = 0.62$, ▽ $x^* = 0.68$, ● $x^* = 0.75$, ■ $x^* = 0.82$, △ $x^* = 0.88$

Figure 17. Transverse profiles for the shear layer forced at $f = 4$ Hz, $A = 2°$ as a function of the nondimensional downstream distance x^*.

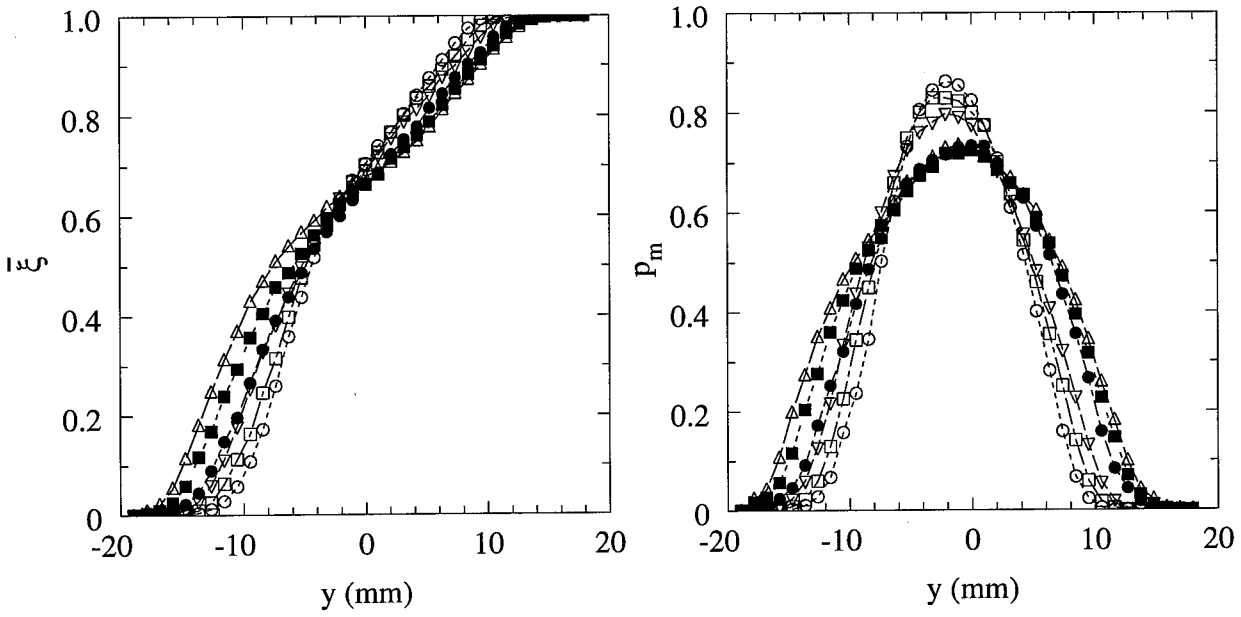

(a) Average concentration

(b) Total mixed fluid probability

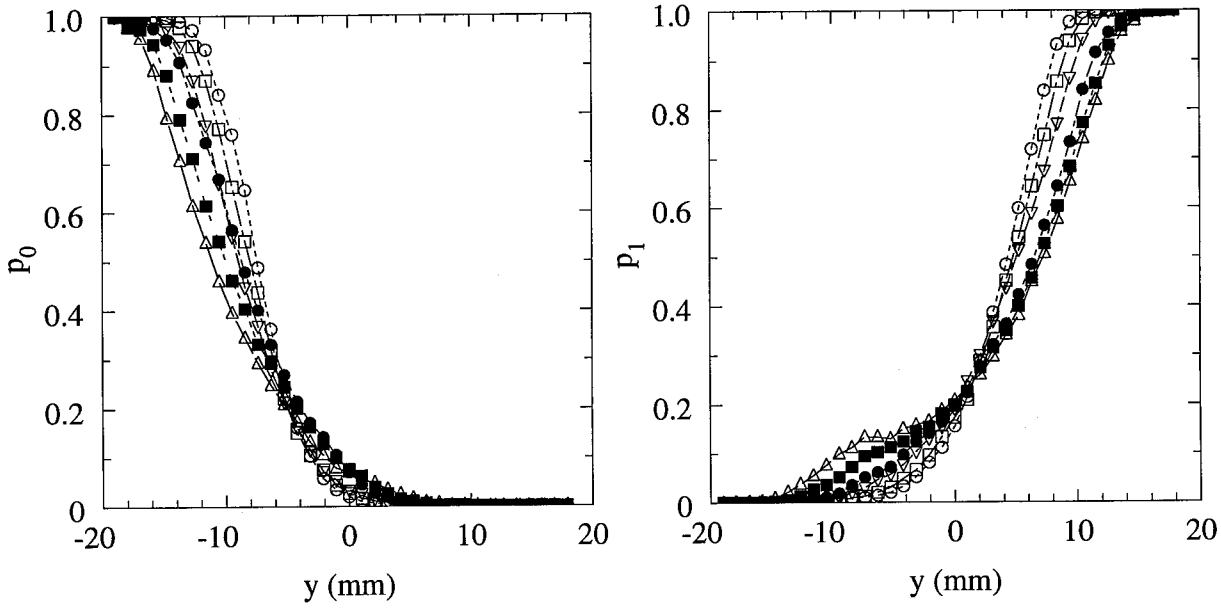

(c) Pure low-speed fluid probability

(d) Pure high-speed fluid probability

○ $x^* = 0.56$, □ $x^* = 0.62$, ▽ $x^* = 0.68$, ● $x^* = 0.75$, ■ $x^* = 0.82$, △ $x^* = 0.88$

Figure 18. Transverse profiles for the shear layer forced at $f = 4$ Hz, $A = 4°$ as a function of the nondimensional downstream distance x^*.

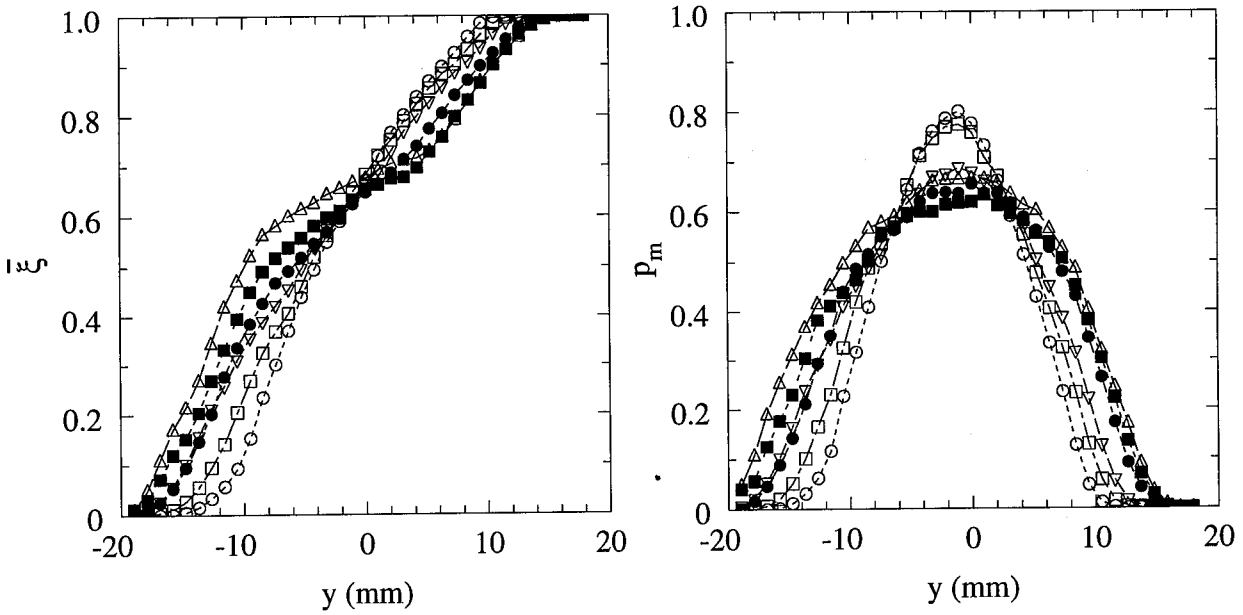

(a) Average concentration

(b) Total mixed fluid probability

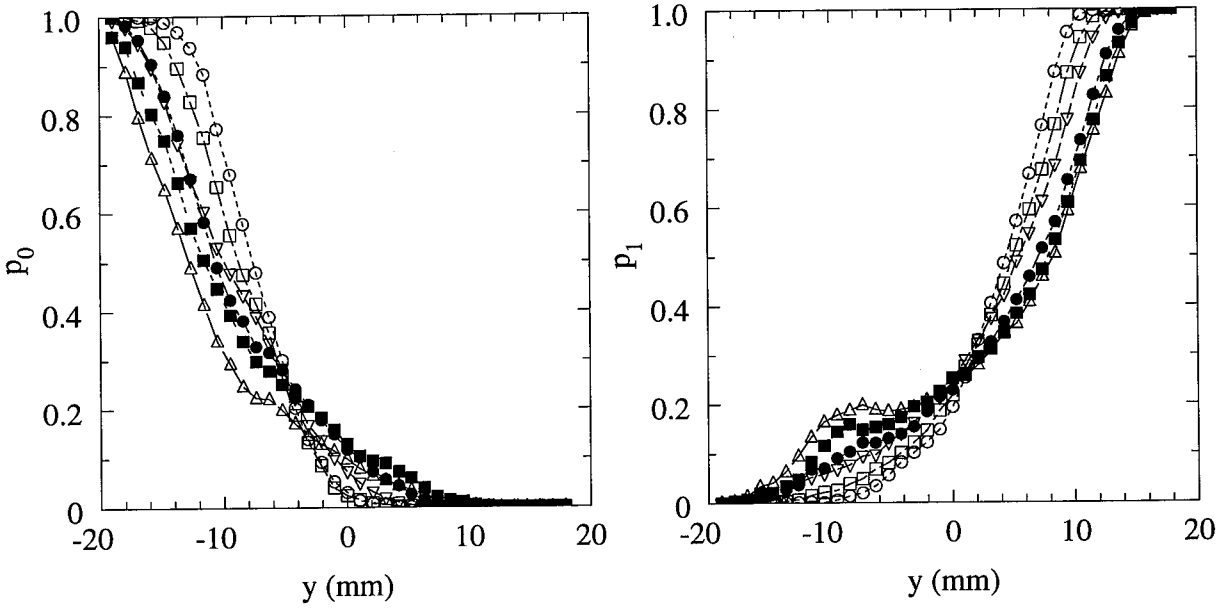

(c) Pure low-speed fluid probability

(d) Pure high-speed fluid probability

○ $x^* = 0.56$, □ $x^* = 0.62$, ▽ $x^* = 0.68$, ● $x^* = 0.75$, ■ $x^* = 0.82$, △ $x^* = 0.88$

Figure 19. Transverse profiles for the shear layer forced at $f = 4$ Hz, $A = 6°$ as a function of the nondimensional downstream distance x^*.

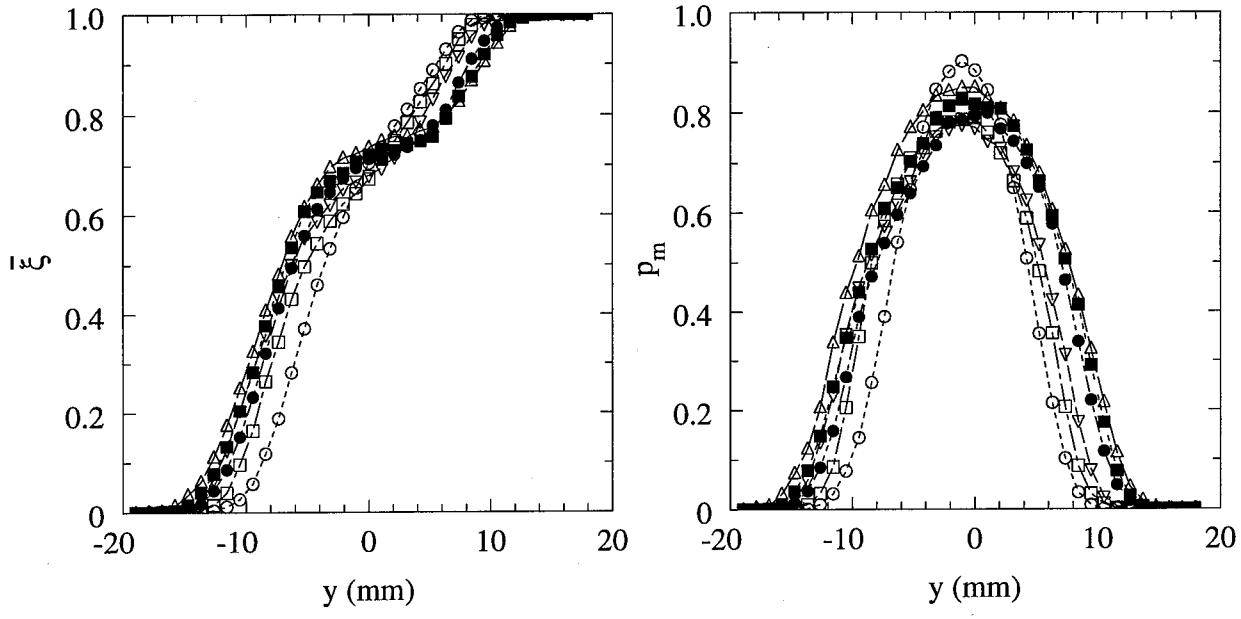

(a) Average concentration

(b) Total mixed fluid probability

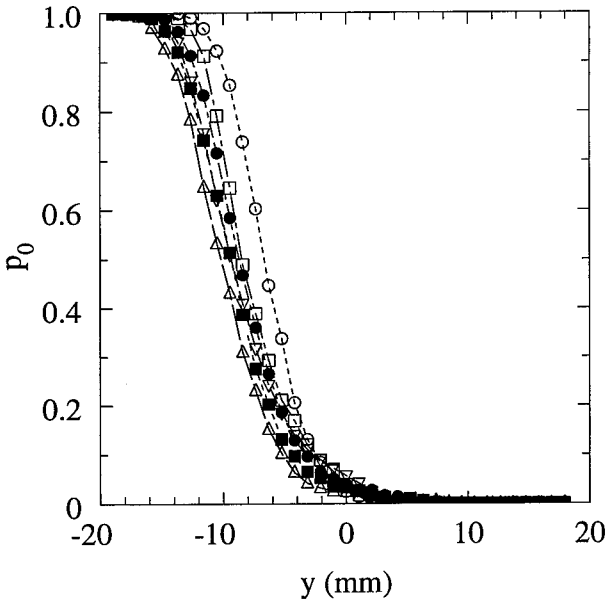

(c) Pure low-speed fluid probability

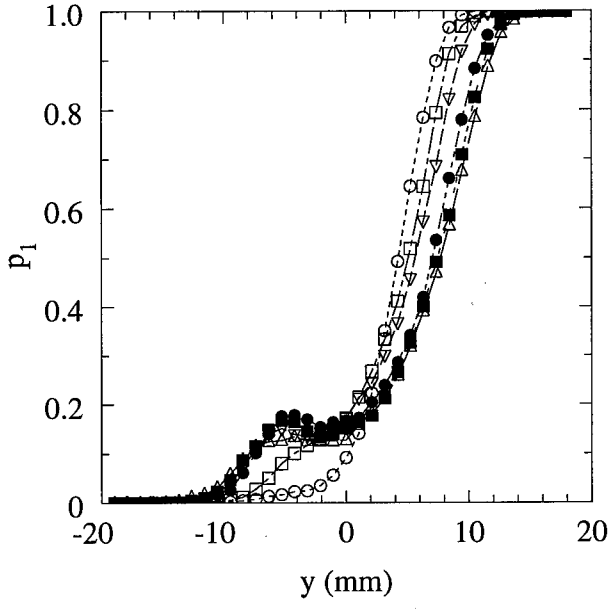

(d) Pure high-speed fluid probability

○ $x^* = 1.11$, □ $x^* = 1.24$, ▽ $x^* = 1.38$, ● $x^* = 1.51$, ■ $x^* = 1.64$, △ $x^* = 1.78$

Figure 20. Transverse profiles for the shear layer forced at f = 8 Hz, A = 2° as a function of the nondimensional downstream distance x^*.

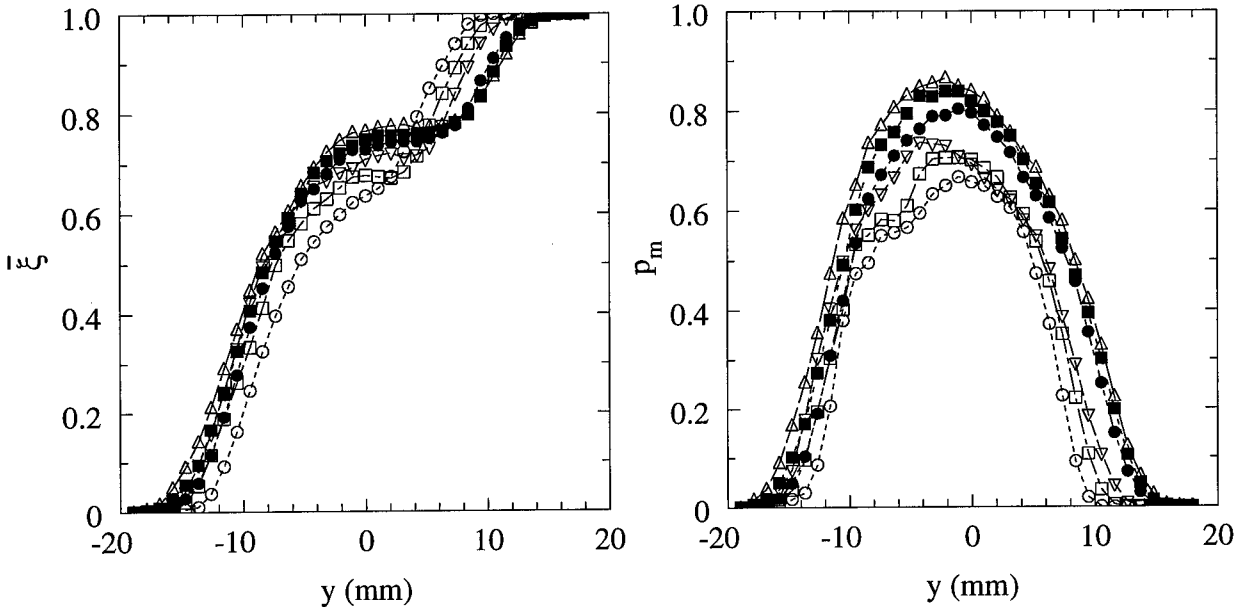

(a) Average concentration

(b) Total mixed fluid probability

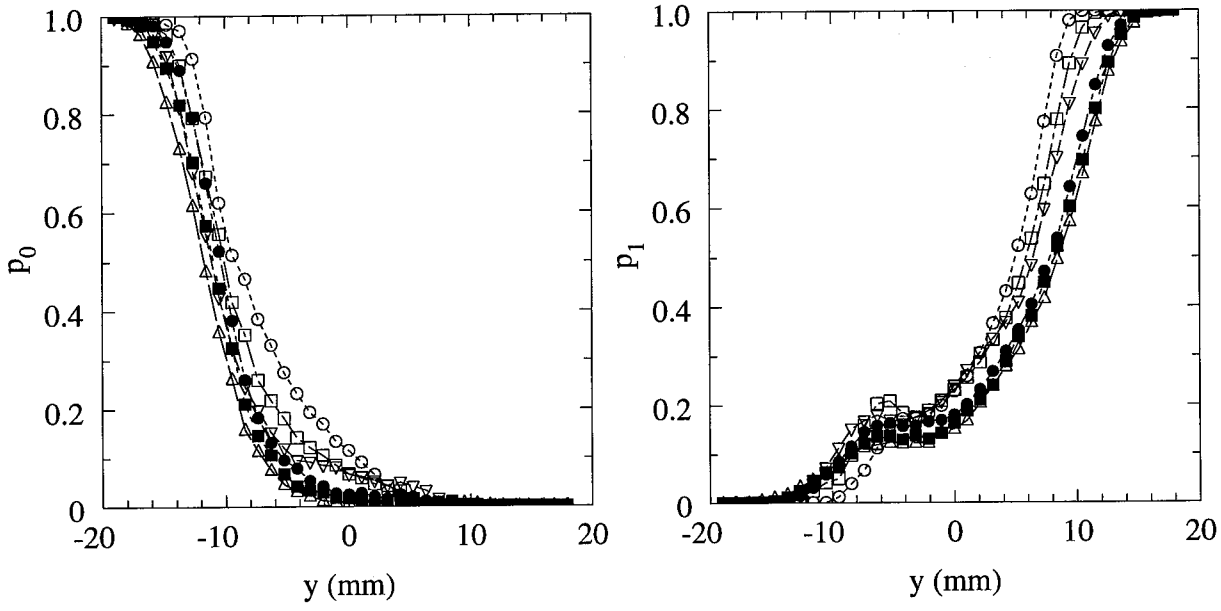

(c) Pure low-speed fluid probability

(d) Pure high-speed fluid probability

○ $x^* = 1.11$, □ $x^* = 1.24$, ▽ $x^* = 1.38$, ● $x^* = 1.51$, ■ $x^* = 1.64$, △ $x^* = 1.78$

Figure 21. Transverse profiles for the shear layer forced at $f = 8$ Hz, $A = 4°$ as a function of the nondimensional downstream distance x^*.

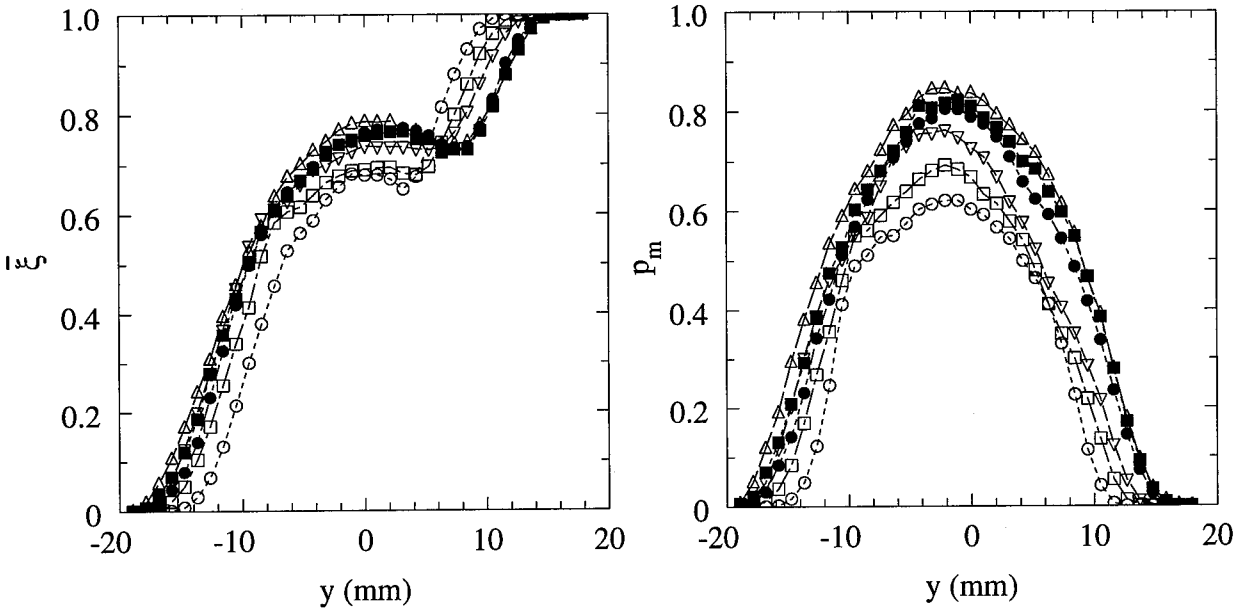

(a) Average concentration

(b) Total mixed fluid probability

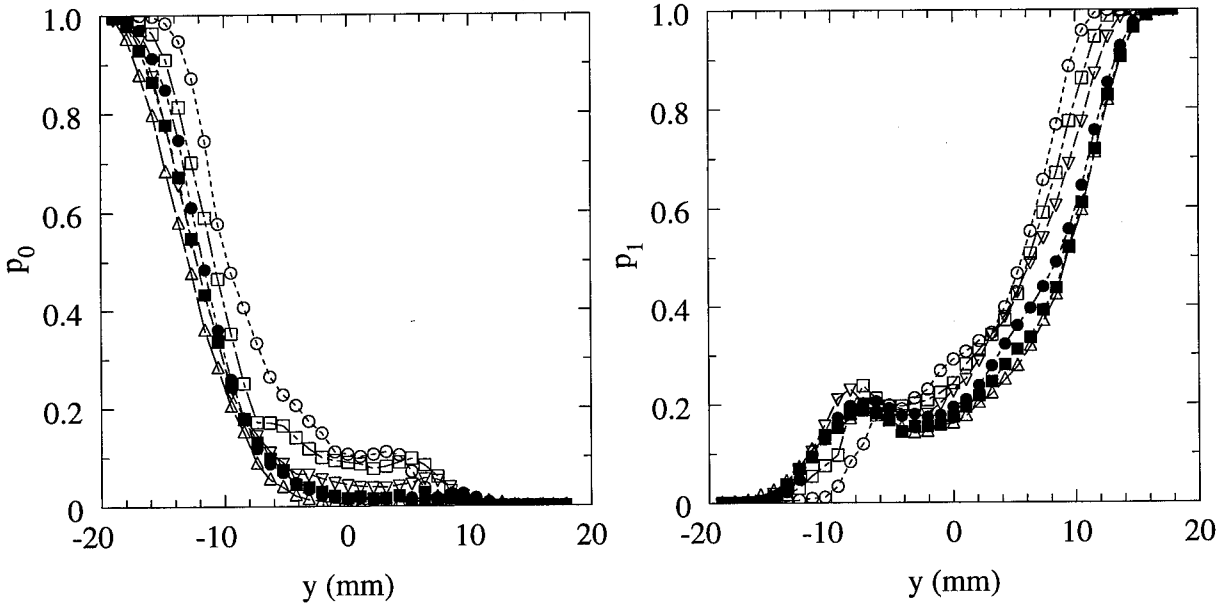

(c) Pure low-speed fluid probability

(d) Pure high-speed fluid probability

○ $x^* = 1.11$, □ $x^* = 1.24$, ▽ $x^* = 1.38$, ● $x^* = 1.51$, ■ $x^* = 1.64$, △ $x^* = 1.78$

Figure 21. Transverse profiles for the shear layer forced at $f = 8$ Hz, $A = 6°$ as a function of the nondimensional downstream distance x^*.

Results for the forced cases are displayed in Figures 14 - 22. A noteworthy feature of the forced shear layer is the severe distortion of the average concentration profiles $\overline{\xi}(y)$. The development of a 'flat region' in the center of the $\overline{\xi}(y)$ profile is characteristic of the passage of well mixed vortex cores, previously noted by Wygnanski, Oster and Fiedler (1979) and Koochesfahani and M^{ac}Kinnon (1991). This 'flat region' is seen developing in the cases forced at f = 4 Hz and is fully developed in the 8 Hz cases.

Similar to the unforced layer, the forced cases all show increasing shear layer width as downstream distance increases. Correspondingly, mixed fluid is found over a wider portion of the test section width. There is however, a reduction in the amount of mixed fluid $(p_m)_{\max}$ in the middle of the layer as the entrainment tongues become more prominent. For the cases forced at f = 2 Hz, there is a slight variation in $(p_m)_{\max}$ as a function of x, similar to the unforced layer. However, with increasing amplitude there is a noted decrease in $(p_m)_{\max}$, see Figures 14 - 16. When forced at f = 4 Hz, A = 2°, see Figure 17, there is a continual decrease in the amount of mixed fluid in the center of the layer. At the larger amplitudes A = 4° and 6° the amount of mixed fluid continually decreases except at x = 20.0 cm where a slight increase in $(p_m)_{\max}$ is noted, see Figures 18 and 19 (b). The cases forced at f = 8 Hz show markedly different behavior than the previous cases. When forced at f = 8 Hz, A = 2° $(p_m)_{\max}$ initially decreases then continually increases; while $(p_m)_{\max}$ continually increases at the higher amplitudes.

The reduction in the amount of mixed fluid in the central portion of the layer is accompanied by an increase in the amount of the unmixed fluid. In all forced cases there is more pure high-speed fluid than pure low-speed fluid in the center of the layer. This is most obvious in the cases forced at f = 4, 8 Hz, see Figures 17 - 22 (c) and (d). The

unequal amounts of unmixed fluid in the center of the layer are related to the inherent asymmetry of the shear layer.

It was previously noted in the flow visualization images of Figures 8 - 12 that some of the forced cases were influenced by the finite height of the test section. This is also seen in the total mixed fluid probability curves in Figures 16 (b) (f = 2 Hz, A = 8°) and 19 (b) (f = 4 Hz, A = 6°) as nonzero values of p_m at y = -20 cm.

3.2.2 Forcing amplitude dependence

In the previous section the streamwise dependence of two-dimensional forcing was noted for the various forcing conditions. In this section the dependence on the forcing amplitude will be shown at a fixed downstream location. In Figures 23 - 25, transverse profiles of the average concentration $\bar{\xi}$, the total mixed fluid probability $p_m(y)$ and unmixed fluid probabilities, $p_0(y)$ and $p_1(y)$ are shown as a function of the forcing amplitude at x = 20.0 cm. The unforced case is included for comparison. Figures for the remaining measurement locations are provided in Appendix A.

The 'flat region' of the average concentration profiles associated with the passage of well mixed vortex cores is not present in the 2 Hz cases because the vortices are not fully formed at this location. There is almost no difference in the average concentration profiles between the unforced case and the cases forced at amplitudes A = 2° and 4°, see Figure 22 (a). Well mixed vortex cores are associated with the well defined structures of the frequency locked region seen in the cases forced at f = 4 and 8 Hz. The developing 'flat region' may be seen in the 4 Hz cases and a very well defined 'flat region' is observed in the f = 8 Hz cases, see Figures 24 and 25 (a).

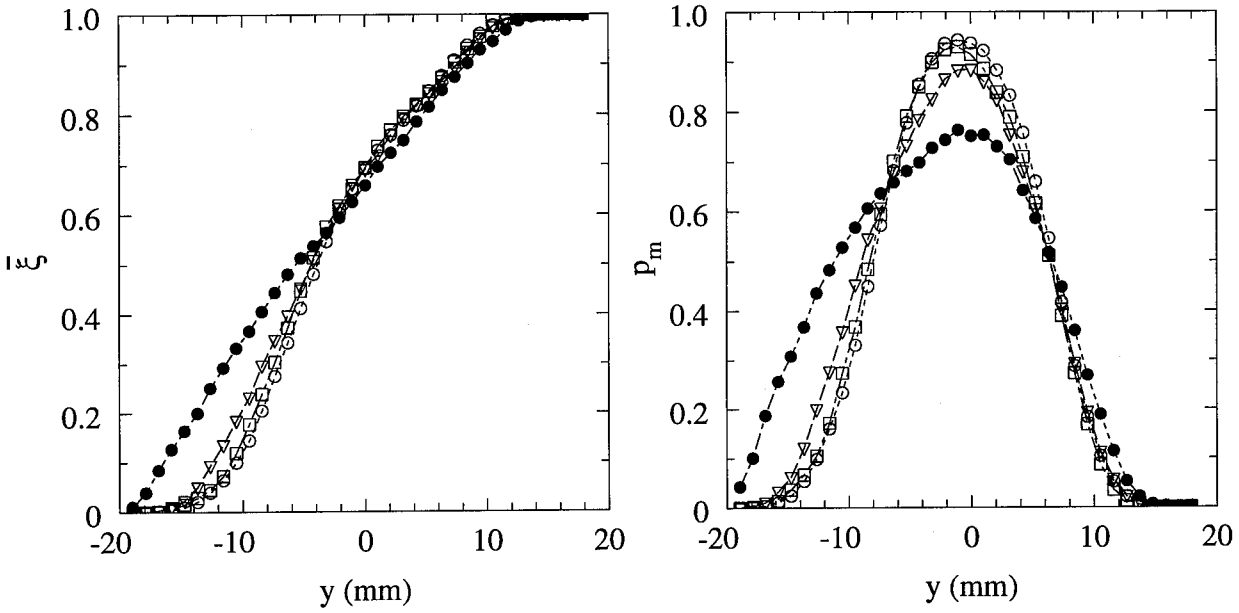

(a) Average concentration

(b) Total mixed fluid probability

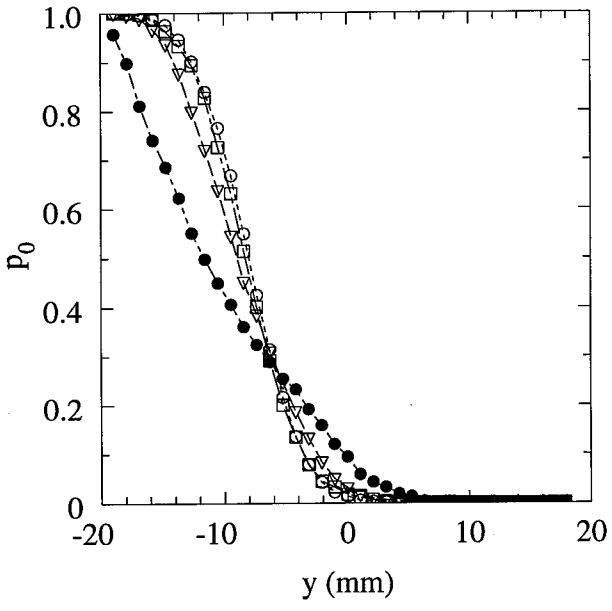

(c) Pure low-speed fluid probability

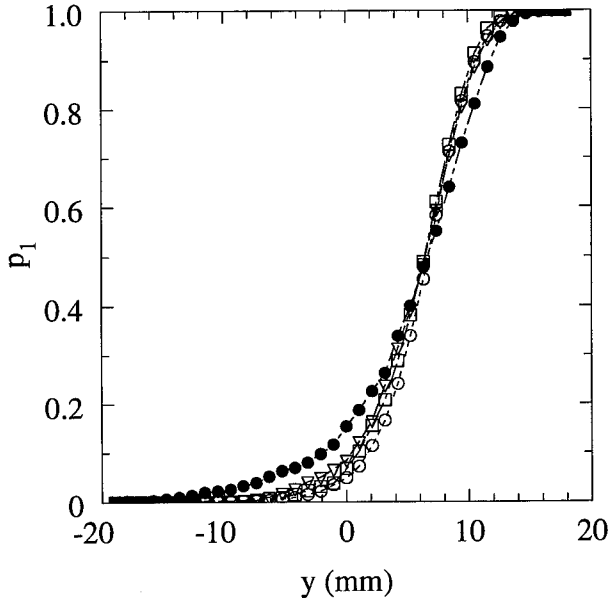

(d) Pure high-speed fluid probability

○ Unforced case, □ $A = 2°$, ▽ $A = 4°$, ● $A = 8°$

Figure 23. Transverse profiles for the shear layer forced at $f = 2$ Hz as a function of amplitude A, at $x^* = 0.44$ ($x = 20.0$ cm), compared to the unforced case.

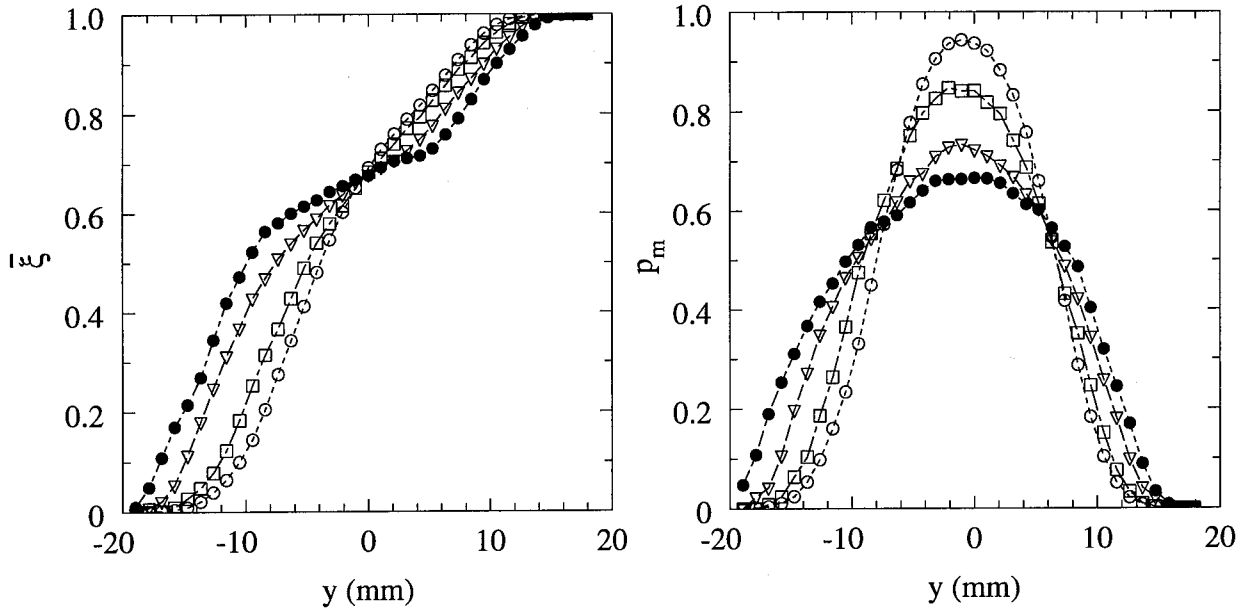

(a) Average concentration

(b) Total mixed fluid probability

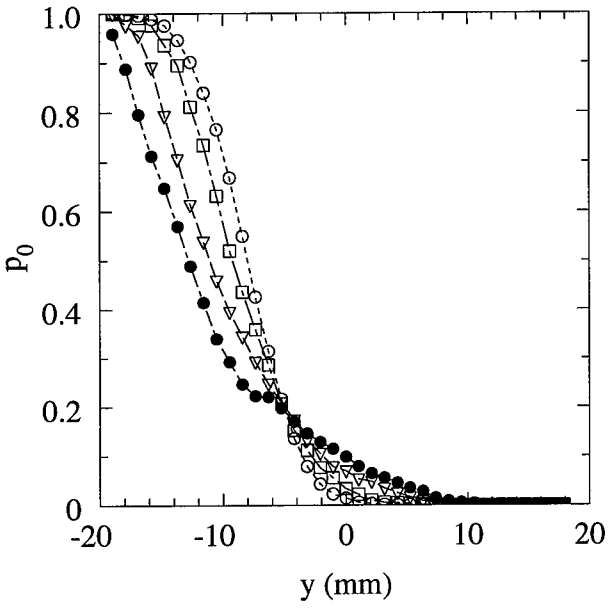

(c) Pure low-speed fluid probability

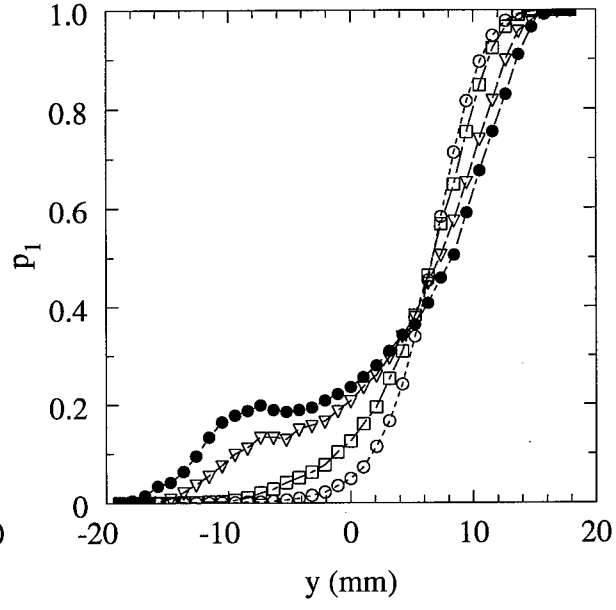

(d) Pure high-speed fluid probability

○ Unforced case, □ $A = 2°$, ▽ $A = 4°$, ● $A = 6°$

Figure 24. Transverse profiles for the shear layer forced at $f = 4$ Hz as a function of amplitude A, at $x^* = 0.88$ ($x = 20.0$ cm), compared to the unforced case.

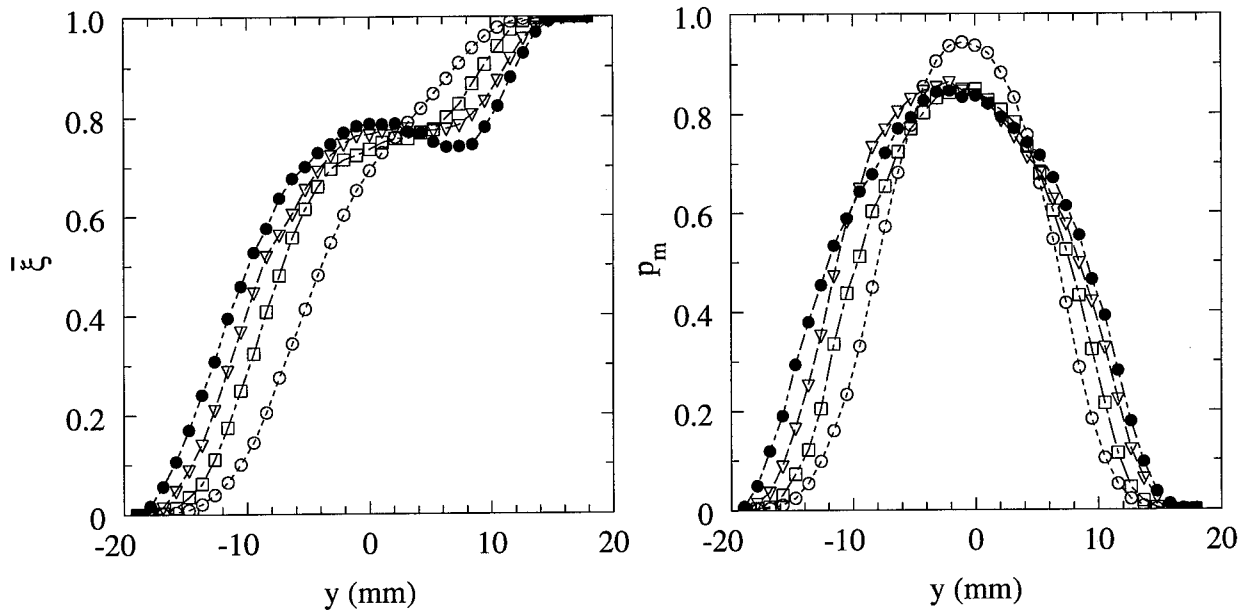

(a) Average concentration

(b) Total mixed fluid probability

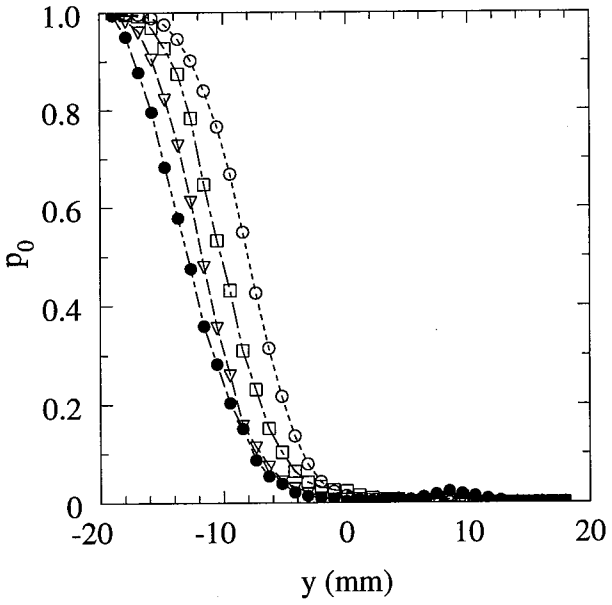

(c) Pure low-speed fluid probability

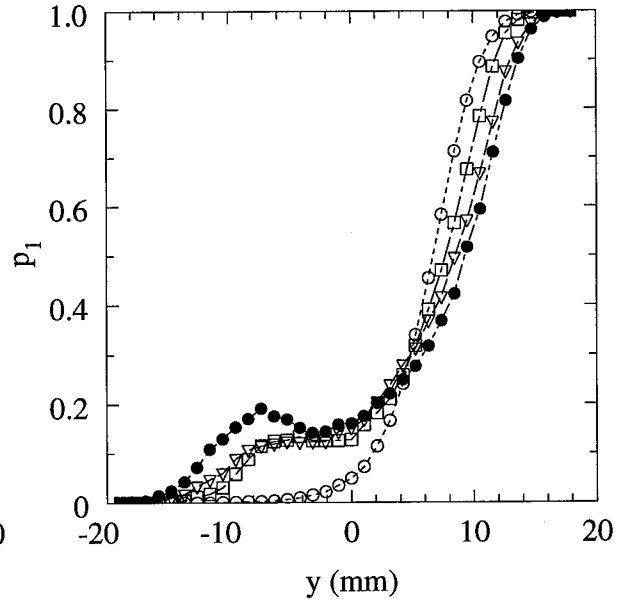

(d) Pure high-speed fluid probability

○ Unforced case, □ $A = 2°$, ▽ $A = 4°$, ● $A = 6°$

Figure 25. Transverse profiles for the shear layer forced at $f = 8$ Hz as a function of amplitude A, at $x^* = 1.78$ ($x = 20.0$ cm), compared to the unforced case.

In all of these cases, the width of the layer is larger than the unforced case and increases with increasing amplitude. In this sense the effect of the forcing amplitude on the shear layer width is similar to increasing the downstream distance. The cases forced at $f = 2$ and 4 Hz show a reduction in $(p_m)_{max}$ with increasing amplitude. Coinciding with the reduction in the amount of mixed fluid in the center of the layer there is an increase in the amounts of pure fluids from both streams. Note that there is in general significantly more high-speed fluid in the center and on the lower side than low-speed fluid in the center and on the upper side. Again, this is related to the inherent entrainment asymmetry of the shear layer. The cases forced at $f = 8$ Hz exhibit a similar behavior. Unlike the 2 and 4 Hz cases, however, there is no dramatic reduction in $(p_m)_{max}$ as a function of amplitude for the 8 Hz cases at this x. In this case, $(p_m)_{max}$ is nearly constant at this location (x = 20.0 cm). This is believed to be connected to the saturation of the large structures in the frequency locked region.

3.3 Streamwise variation of δ_1, δ_m, δ_m/δ_1 and $(p_m)_{max}$

The detailed profiles of the previous section can be used to compute the shear layer width δ_1 and other mixing quantities such as the mixed-fluid thickness δ_m, mixed fluid fraction δ_m/δ_1 and the amount of fluid in the center of the layer $(p_m)_{max}$. These results are discussed in this section.

In Figures 26 (a) - (c) the shear layer width δ_1, is plotted versus x as a function of amplitude for the forcing frequencies $f = 2$, 4 and 8 Hz, respectively. The unforced layer is noted to have linear growth rate. From this Figure, it may also be seen that the width of the forced layer is greater than the unforced layer and increases with downstream

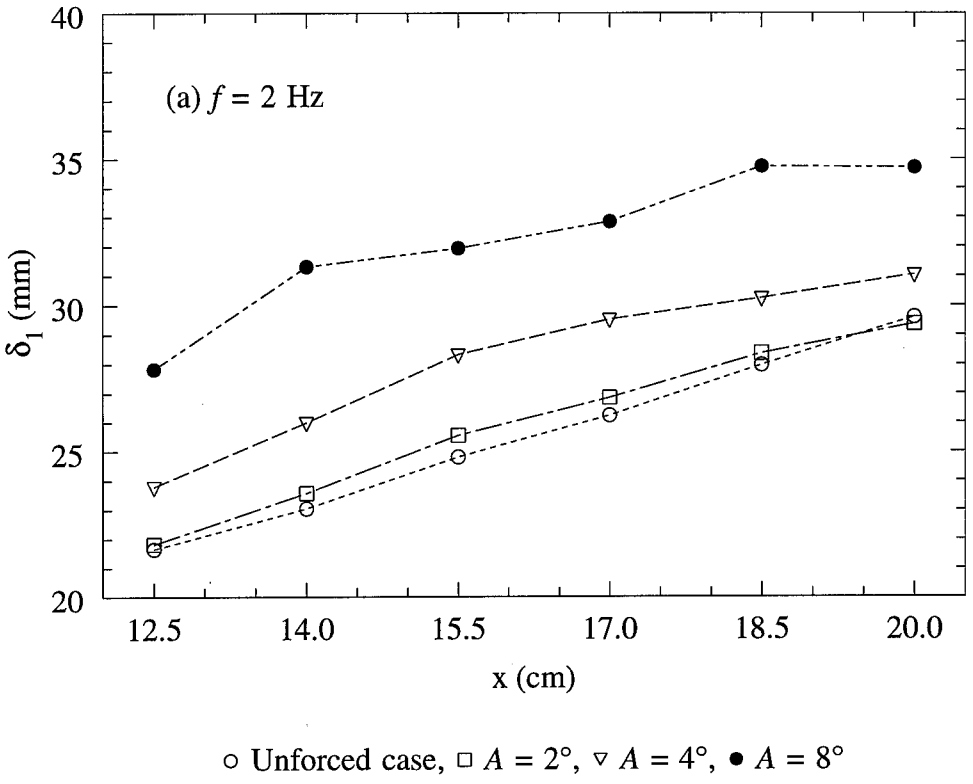

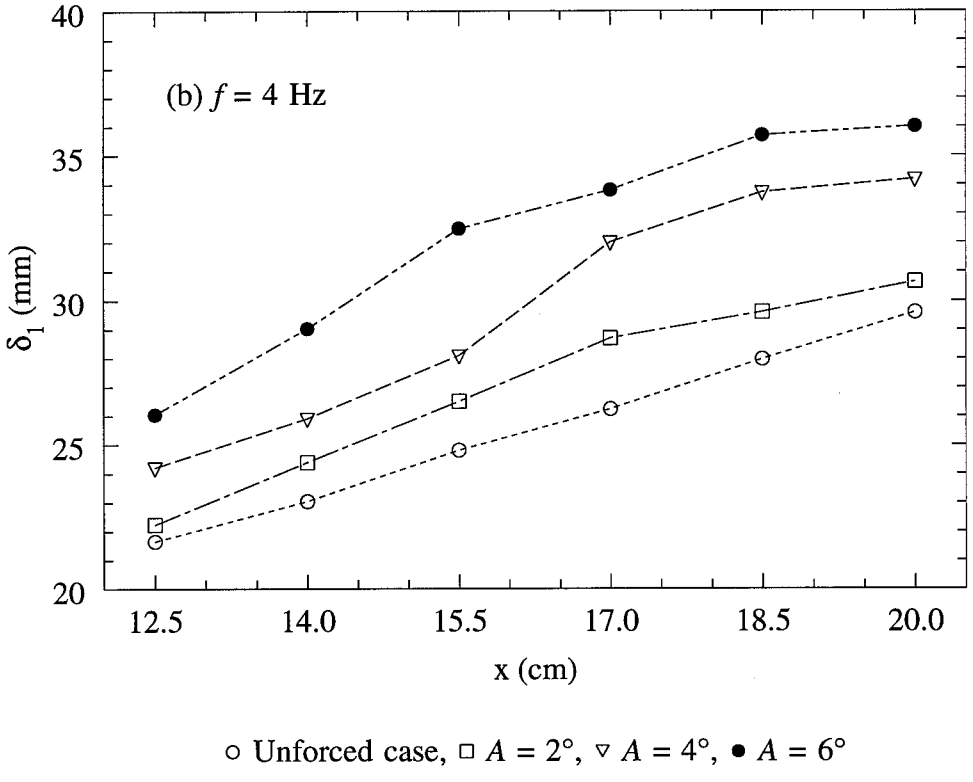

Figure 26. Streamwise evolution of the shear layer width δ_1 as a function of the forcing amplitude A compared to the unforced case.

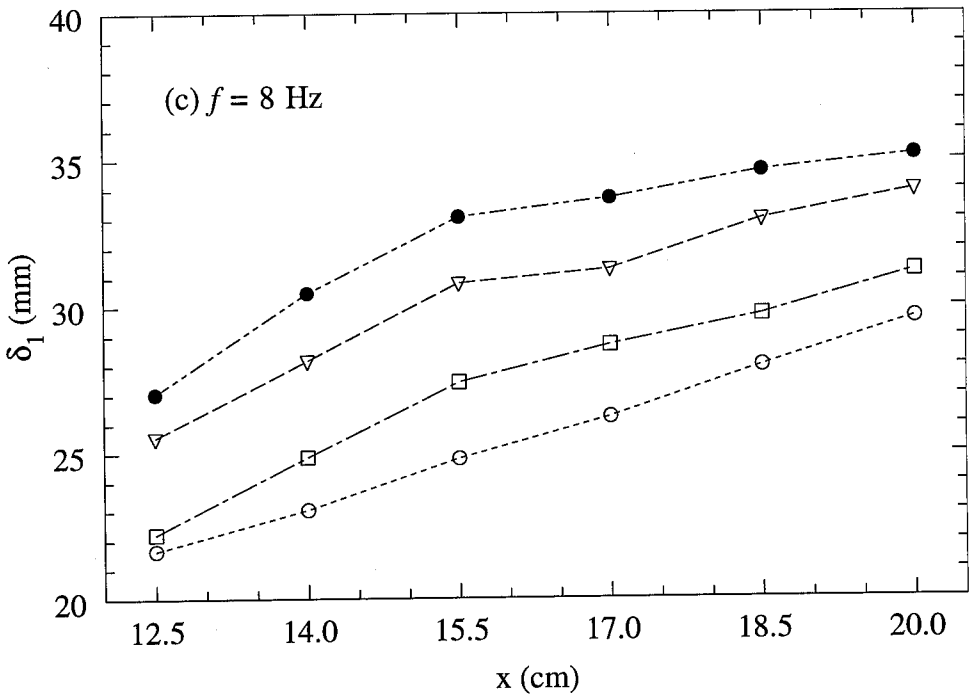

○ Unforced case, □ A = 2°, ▽ A = 4°, • A = 6°

Figure 26. Streamwise evolution of the shear layer width δ_1 as a function of the forcing amplitude A compared to the unforced case.

distance. The highest amplitude cases all seem to saturate at approximately 35 mm in width. The forced layer is expected to initially have enhanced growth rate, then taper off (saturate) and finally resume the natural growth rate, see section 1.2. The growth of the forced layers may be hindered by the finite size (height) of the test section, $2h$ = 40 mm; or may be reaching the saturation point at $x^* = 1$.

The total amount of mixed fluid in terms of the mixed fluid thickness δ_m is plotted in Figure 27. The amplitude dependence for the f = 2 Hz cases are shown in Figure 27 (a). Only at the largest amplitude A = 8° was there a significant increase, approximately 11%, in the mixed fluid thickness. There was less than a 2% change in

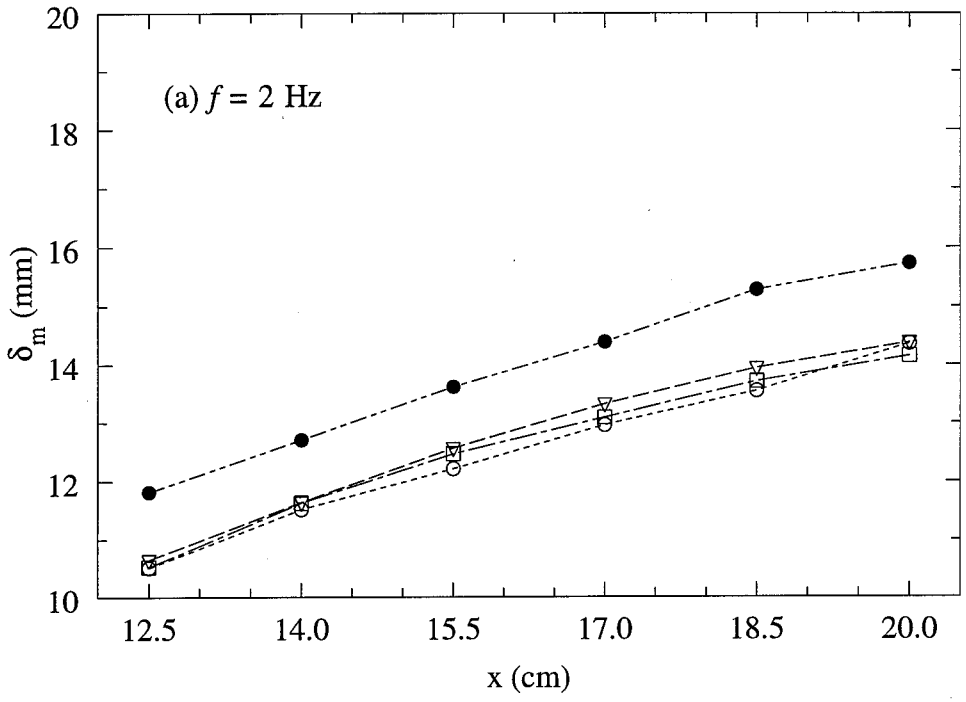

○ Unforced case, □ A = 2°, ▽ A = 4°, ● A = 8°

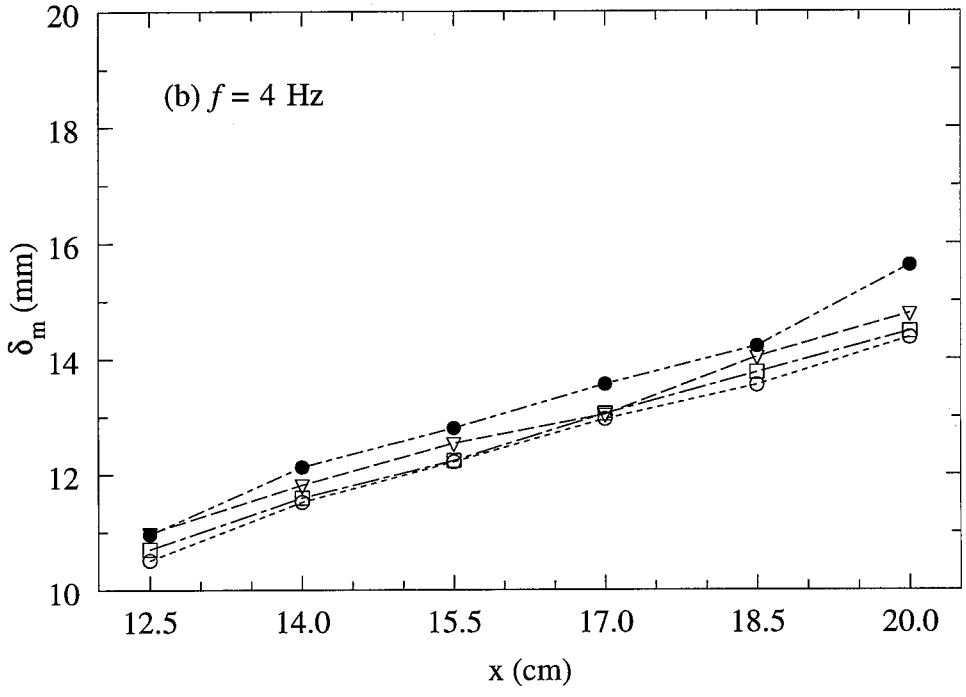

○ Unforced case, □ A = 2°, ▽ A = 4°, ● A = 6°

Figure 27. Streamwise evolution of the mixed fluid thickness δ_m as a function of the forcing amplitude A compared to the unforced case.

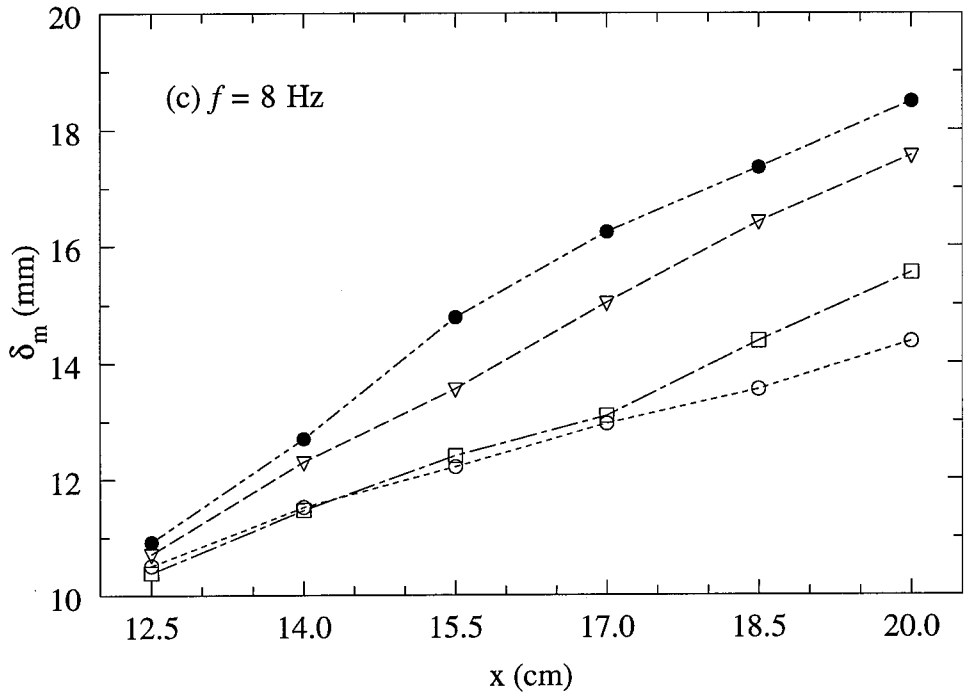

Figure 27. Streamwise evolution of the mixed fluid thickness δ_m as a function of the forcing amplitude A compared to the unforced case.

the mixed fluid thickness when compared to the unforced shear layer at the two smaller amplitudes. Small increases, 5% at most, were similarly noted for the cases forced at f = 4 Hz, see Figure 27 (b). There was, however, a marked increase in the amount of mixed fluid at all amplitudes when the layer was forced at 8 Hz, Figure 27 (c). The largest change observed in this study was 29%, when the layer was forced at f = 8 Hz, A = 6°.

It was noted above that the largest increase in the mixed fluid thickness compared to the unforced layer was 29%, for the case forced at f = 8 Hz, A = 6°. The shear layer width in this case was δ_1 = 35.2 mm, an increase of 19% over the unforced layer (δ_1 =

29.6 mm), see Figure 26 (c). One way to quantify the amount of mixing, while taking into account the increasing width of the layer is to use the mixed fluid fraction δ_m/δ_1, the fraction of the layer width occupied by mixed fluid. δ_m/δ_1. In Figure 28, the mixed fluid fraction is shown as a function of amplitude. In most cases the forced layer has less mixed fluid per unit width than the unforced layer, and in that sense, is a less efficient mixer. The exceptions are the cases forced at f = 8 Hz, A = 4° and 6° at the farthest downstream locations x = 18.5 and all amplitudes at x = 20.0 cm. The reduction in the mixed fluid fraction as a result of forcing was similarly reported by Koochesfahani and M^{ac}Kinnon (1991). It is interesting to note that the mixed fluid fraction for the cases presented here are at best no greater than 0.52; only slightly more than half of the fluid

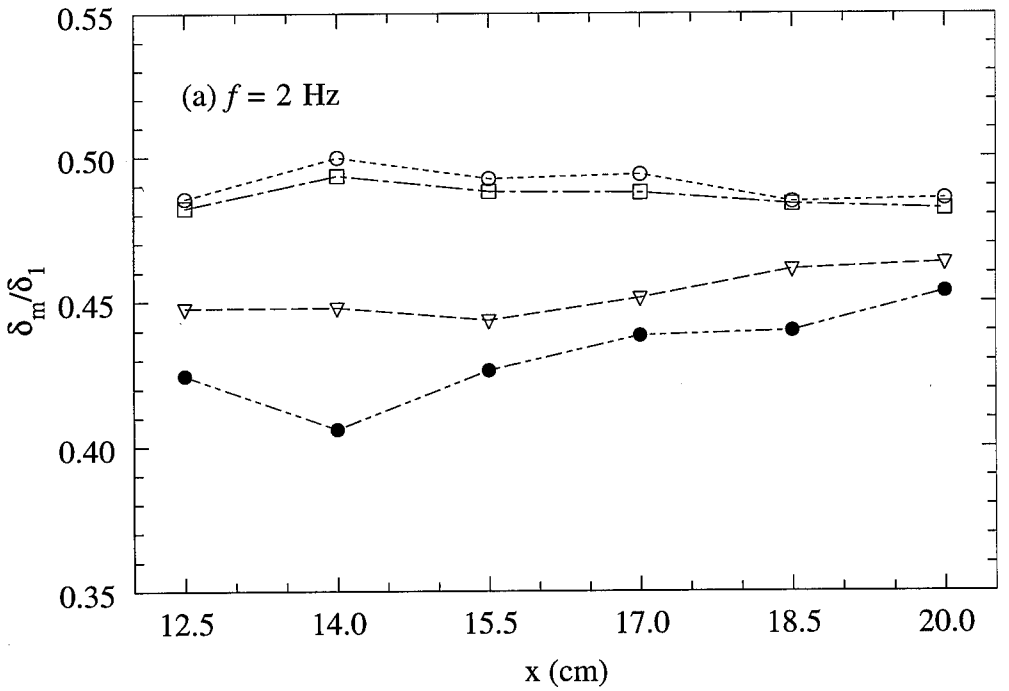

Figure 28. Streamwise evolution of the mixed fluid fraction δ_m/δ_1 as a function of the forcing amplitude A compared to the unforced case.

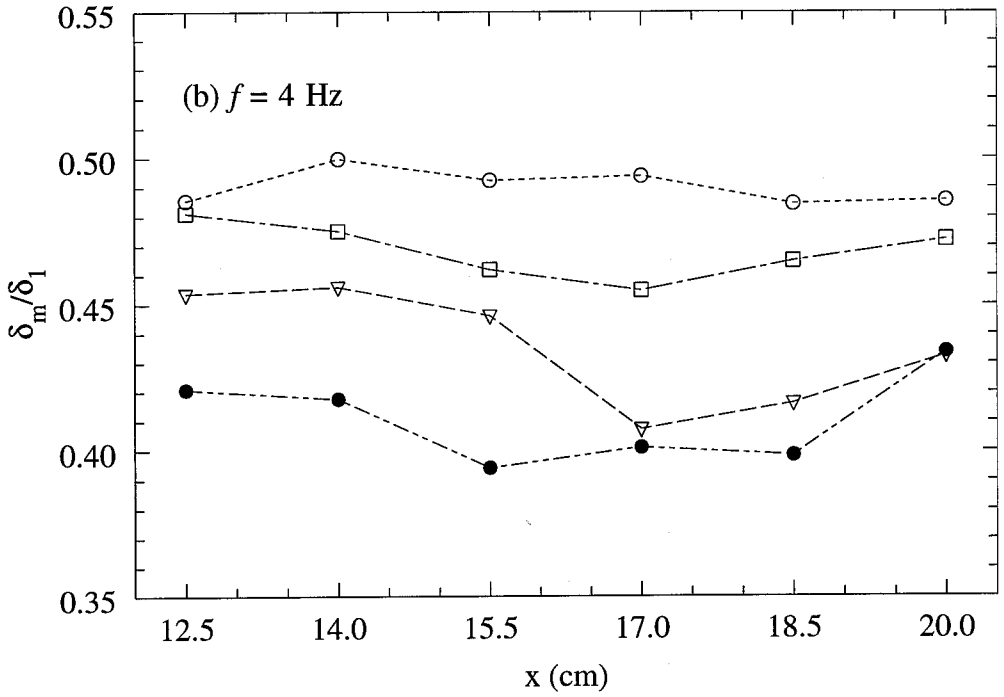

○ Unforced case, □ A = 2°, ▽ A = 4°, ● A = 6°

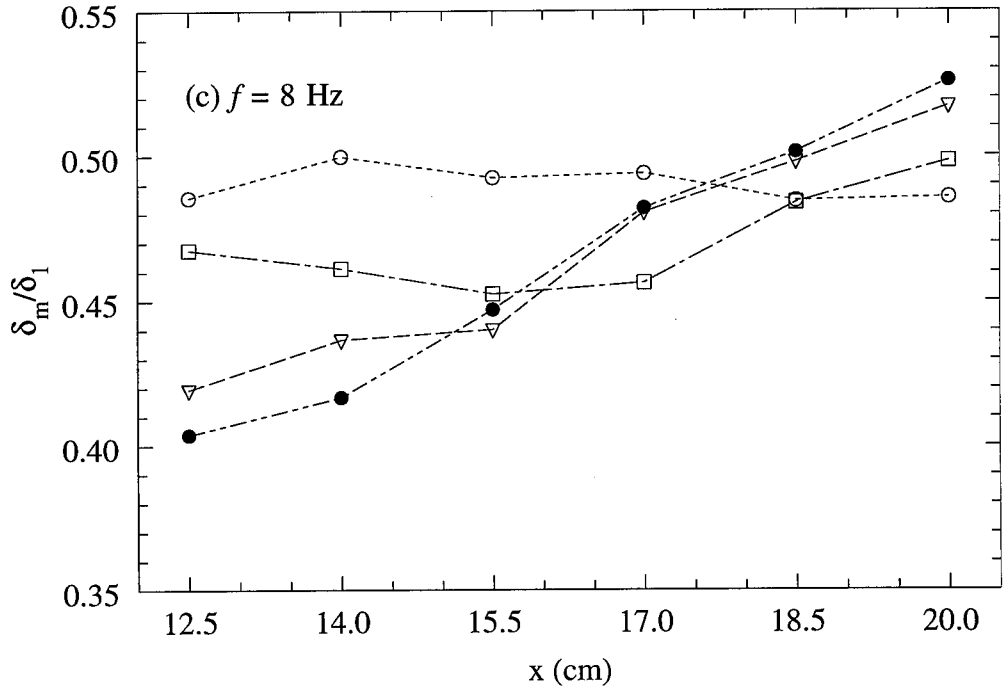

○ Unforced case, □ A = 2°, ▽ A = 4°, ● A = 6°

Figure 28. Streamwise evolution of the mixed fluid fraction δ_m/δ_1 as a function of the forcing amplitude A compared to the unforced case.

within the shear layer is mixed (to within the measurement resolution 200 μm).

The amount of mixed fluid in the center of the layer is characterized by the peak of the mixed fluid probability curve $(p_m)_{max}$. The amplitude dependence of $(p_m)_{max}$ is shown as a function of x in Figure 29. It is observed that there is more mixed fluid in the center of the unforced shear layer compared to *all* of the forced cases. For the cases forced at f = 2 Hz, $(p_m)_{max}$ is in general decreasing with amplitude and downstream distance. The 4 Hz cases exhibit a similar behavior with the exception of a slight increase at x = 20.0 cm for the two larger amplitudes. When forced at f = 8 Hz, A = 2° $(p_m)_{max}$ initially decreases then continually increases; while at higher amplitudes the amount of mixed fluid in the center of the layer is observed to continually increase. It

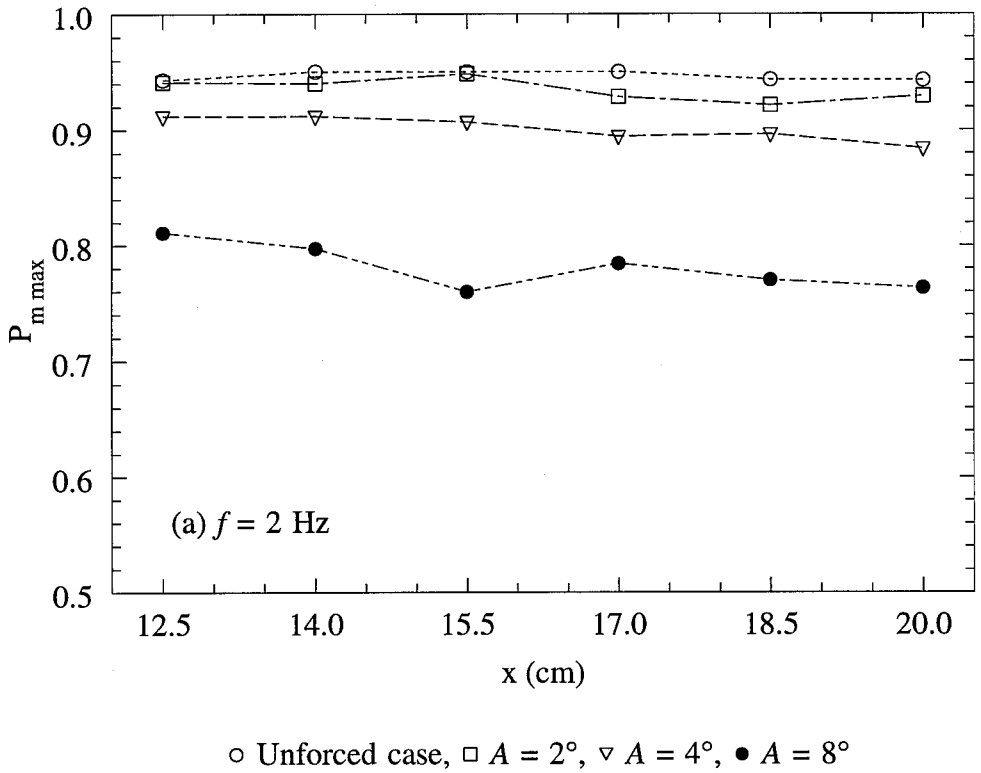

Figure 29. Streamwise evolution of the amount of mixed fluid in the center of the layer as a function of the forcing amplitude A compared to the unforced case.

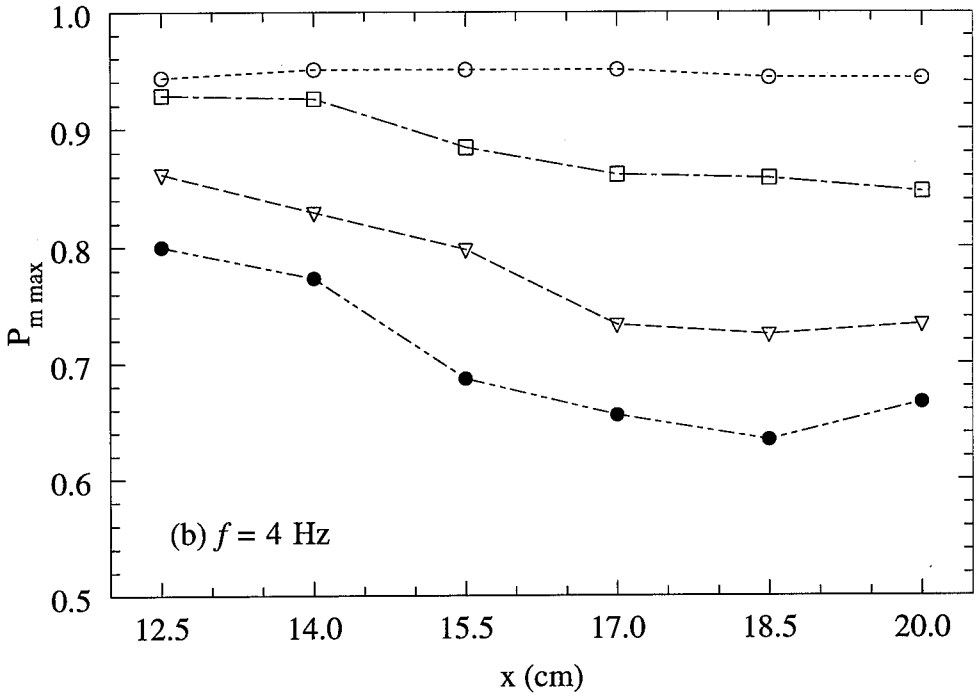

○ Unforced case, □ A = 2°, ▽ A = 4°, ● A = 6°

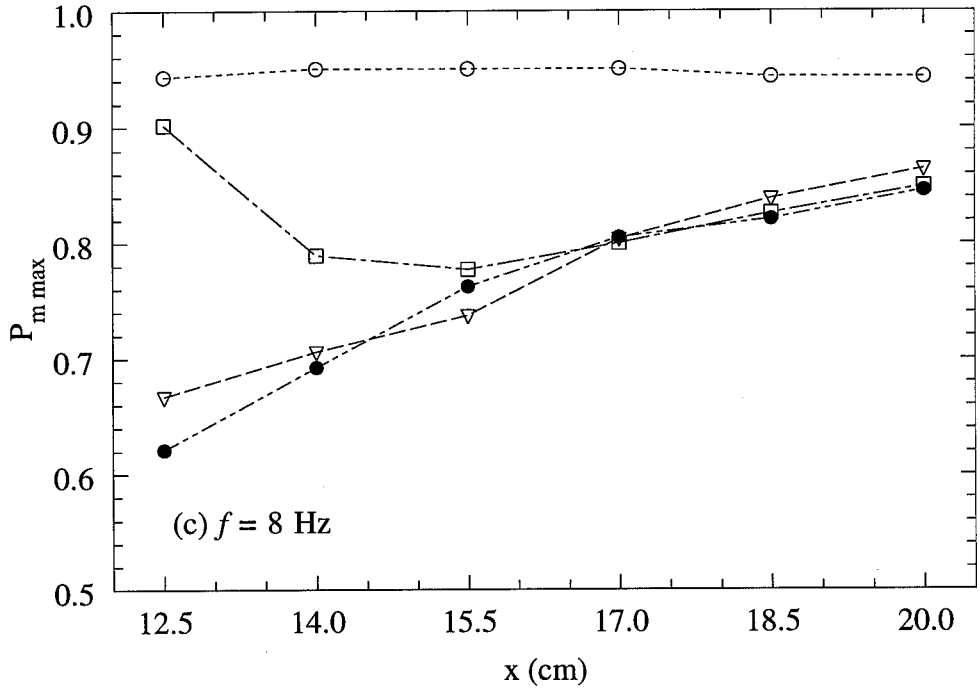

○ Unforced case, □ A = 2°, ▽ A = 4°, ● A = 6°

Figure 29. Streamwise evolution of the amount of mixed fluid in the center of the layer as a function of the forcing amplitude A compared to the unforced case.

is interesting to note that $(p_m)_{max}$ reaches a minimum (in the 4 Hz cases) at $x^* \approx 1$, when the structures saturate; this will be further discussed in section 3.4.

3.4 Nondimensional streamwise variation of δ_1, δ_m, δ_m/δ_1 and $(p_m)_{max}$

The previous sections discussed the evolution of the shear layer in terms of the downstream coordinate x; now flow evolution will be discussed in terms of the nondimensional streamwise coordinate $x^* = \lambda x f / U_c$. The shear layer width δ_1 and mixed fluid thickness δ_m normalized by the forcing wavelength U_c/f are shown in Figure 30 and 31 versus x^*. These Figures display all of the forced cases from Figures

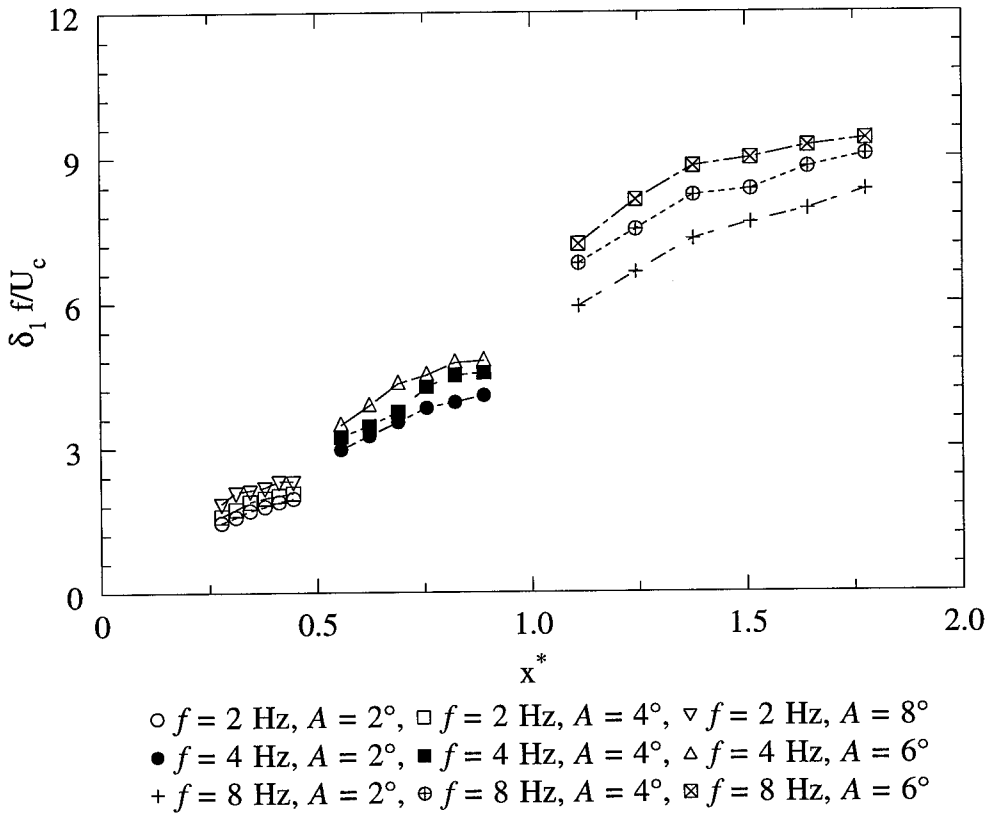

Figure 30. Nondimensional streamwise evolution of the shear layer width normalized by the forcing wavelength for the various forcing conditions.

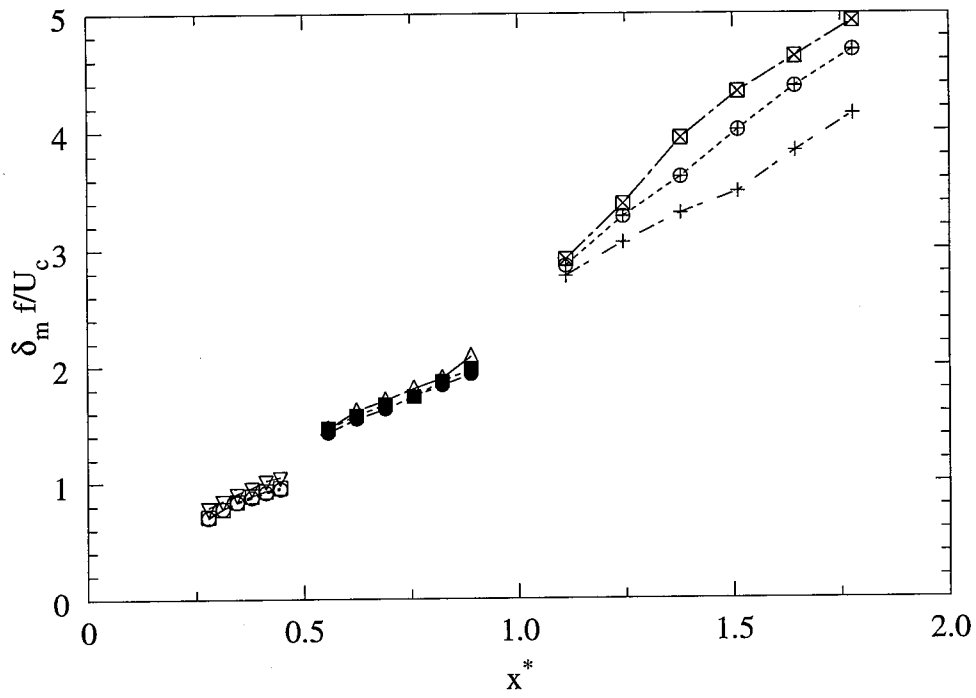

○ f = 2 Hz, A = 2°, □ f = 2 Hz, A = 4°, ▽ f = 2 Hz, A = 8°
● f = 4 Hz, A = 2°, ■ f = 4 Hz, A = 4°, △ f = 4 Hz, A = 6°
+ f = 8 Hz, A = 2°, ⊕ f = 8 Hz, A = 4°, ⊠ f = 8 Hz, A = 6°

Figure 31. Nondimensional streamwise evolution of the mixed fluid thickness normalized by the forcing wavelength for the various forcing conditions.

26 and 27 in nondimensional form. As expected, with increasing x^* the shear layer width continually increases. The saturation of the structures may also be seen in the frequency locked region, near $x^* = 1.5$. The amplitude effects are also observed to increase the shear layer width. Similarly, the amount of mixed fluid increases with increasing x^*. There is, however, no saturation effect in the frequency locked region.

The mixed fluid fraction δ_m / δ_1 is displayed in Figure 32 as a function of x^*. Noteworthy features of this Figure are a local minimum occurring near $x^* = 0.8$; and a

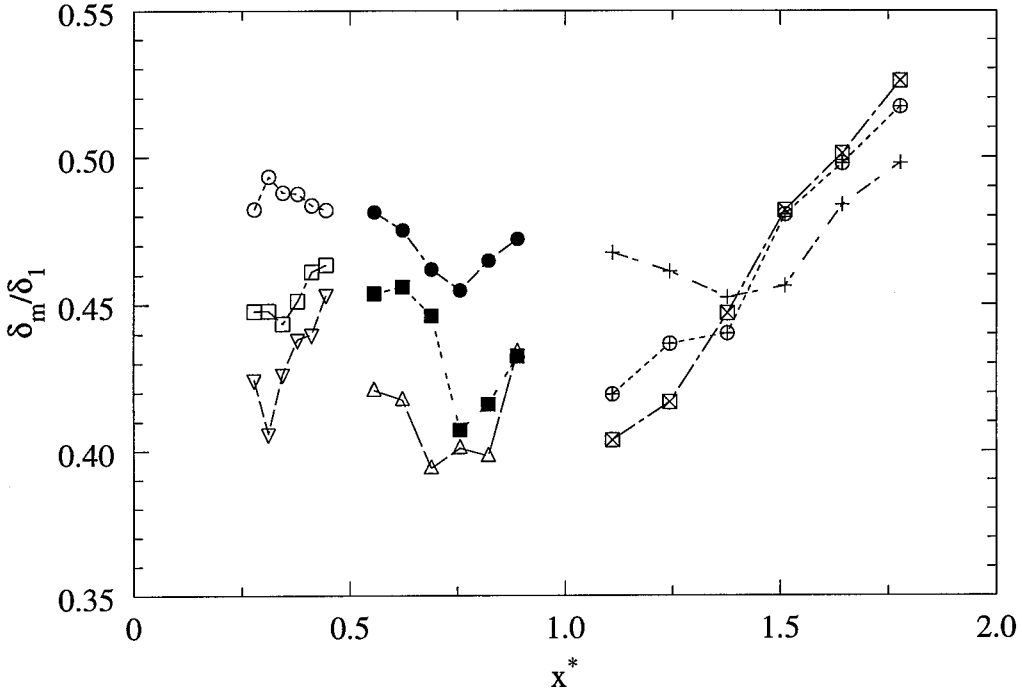

○ f = 2 Hz, A = 2°, □ f = 2 Hz, A = 4°, ▽ f = 2 Hz, A = 8°
● f = 4 Hz, A = 2°, ■ f = 4 Hz, A = 4°, △ f = 4 Hz, A = 6°
+ f = 8 Hz, A = 2°, ⊕ f = 8 Hz, A = 4°, ⊠ f = 8 Hz, A = 6°

Figure 32. Nondimensional streamwise evolution of the mixed fluid fraction for the various forcing conditions.

general increase in the mixed fluid fraction for $x^* > 1.0$. Figure 33 shows the probability of mixed fluid in the center of the layer $(p_m)_{max}$, which is proportional to the amount of mixed fluid in the central of the layer. It is seen that $(p_m)_{max}$, in general, decrease while $x^* < 1.0$ and increase for $x^* > 1.0$. These observations are connected to the growth rate, size and spacing of the structures. The local minimum appears to be connected to the enhanced growth rate of the layer; in this region the layer width is increasing faster than the amount of mixed fluid in the layer. In the frequency locked region the opposite is true, layer growth rate is not increasing as fast as the amount of

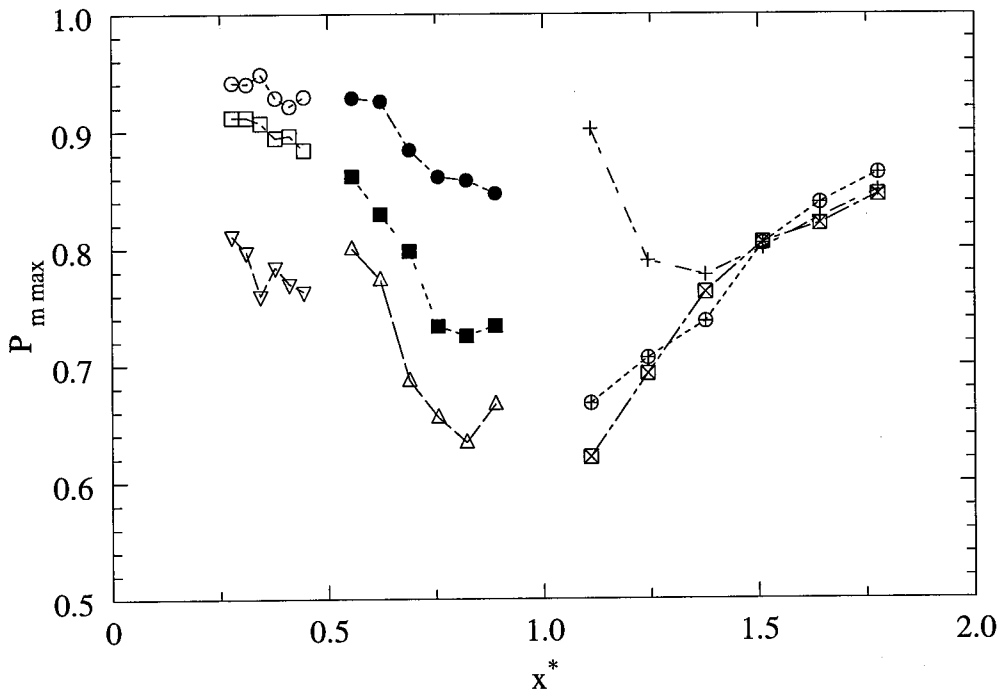

○ f = 2 Hz, A = 2°, □ f = 2 Hz, A = 4°, ▽ f = 2 Hz, A = 8°
● f = 4 Hz, A = 2°, ■ f = 4 Hz, A = 4°, △ f = 4 Hz, A = 6°
+ f = 8 Hz, A = 2°, ⊕ f = 8 Hz, A = 4°, ⊠ f = 8 Hz, A = 6°

Figure 33. Nondimensional streamwise evolution of the amount of mixed fluid in the center of the layer for the various forcing conditions.

mixed fluid in the layer, see Figures 26 and 27. Physically, the reason that the frequency locked region, ie. 8 Hz cases, has more mixed fluid is that the structures, although roughly the same size as the 4 Hz cases, are twice as many in number.

The above nondimensional analysis used the shear layer width δ_1 and the forcing wavelength U_c/f as length scales. The shear layer width, recall is computed similar to boundary layer thickness, in that the edge of the layer is defined by the points where the total mixed fluid probability curve reaches 1% of its maximum value. It suffers from resolution problems, due the non-reacting experiments used in this work over-estimating

the amount of mixed fluid. In some cases the $p_m(y)$ curves asymptotically approach zero, artificially increasing the shear layer width. Perhaps a more robust length scale would be the concentration thickness θ_ξ, an integral quantity analogous to momentum thickness (introduced in section 2.4) based on average concentration measurements. The relationship between the concentration thickness and momentum thickness is displayed in Figure 34. For the unforced layer the relationship is nearly linear, as the frequency and amplitude increase there is an apparent scatter in the plot at large δ_1. This scatter may be the result of deficiencies on the part of both δ_1 and θ_ξ. The concentration thickness may suffer when there is a well developed flat region on the average concentration profile.

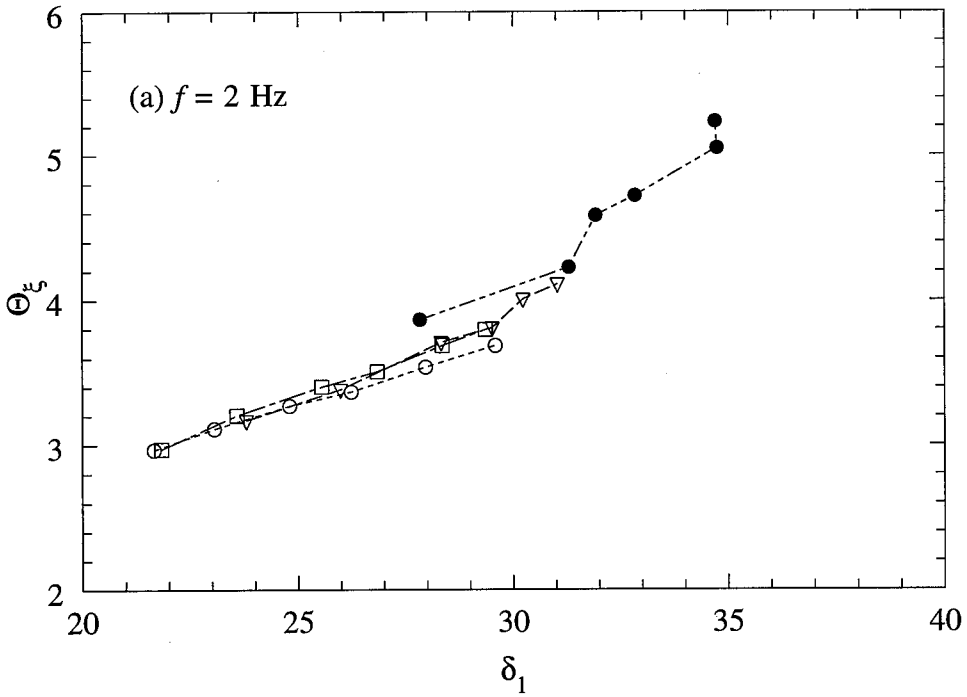

Figure 34. Streamwise evolution of the concentration thickness as a function of the forcing amplitude A compared to the unforced case.

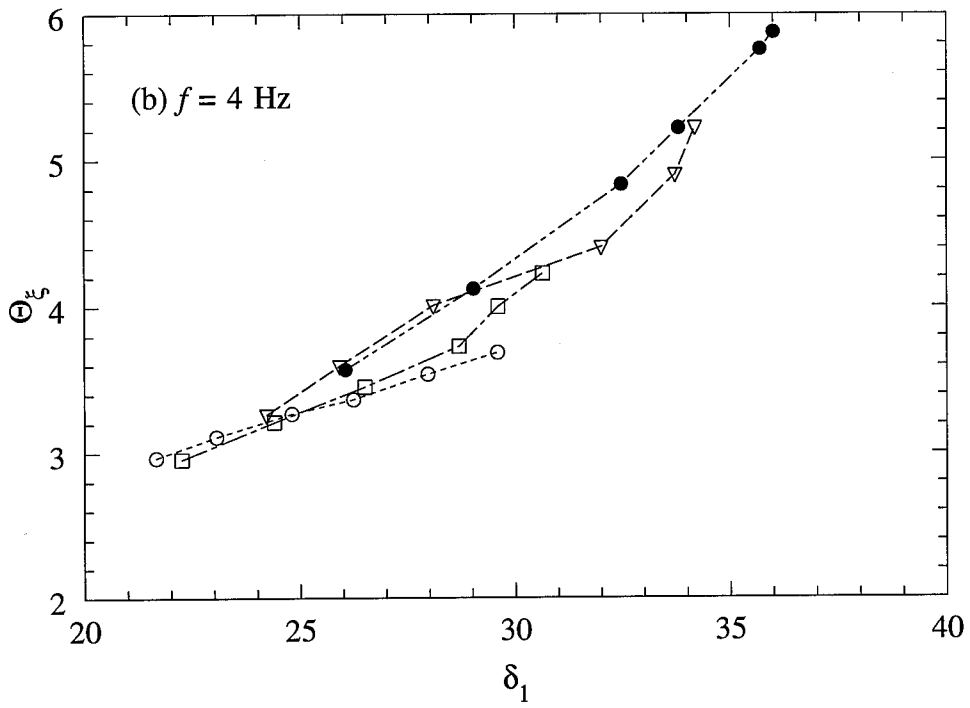

○ Unforced case, □ A = 2°, ▽ A = 4°, ● A = 6°

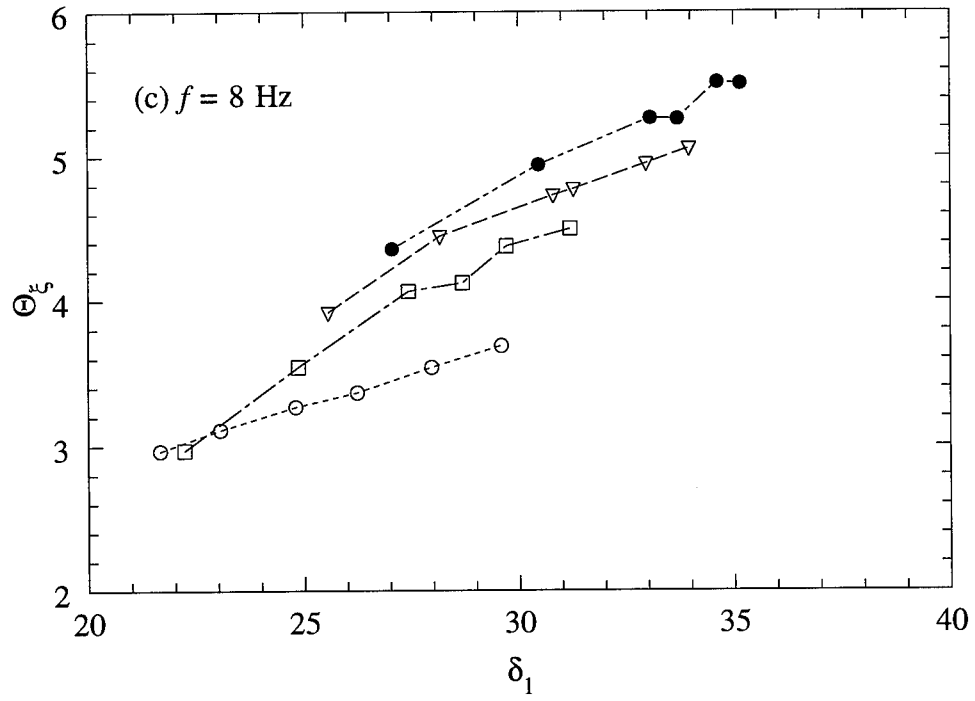

○ Unforced case, □ A = 2°, ▽ A = 4°, ● A = 6°

Figure 34. Streamwise evolution of the concentration thickness as a function of the forcing amplitude A compared to the unforced case.

The concentration thickness normalized by the forcing wavelength $\theta_\xi f/U_c$ is shown versus x^* in Figure 35; note the similarity to Figure 30.

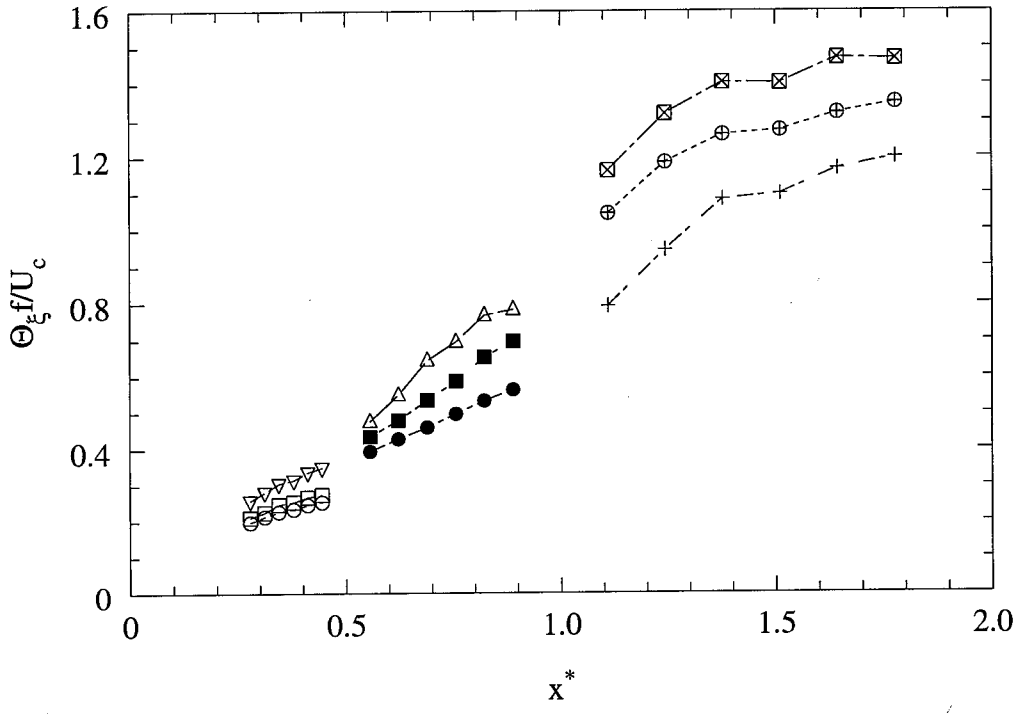

○ f = 2 Hz, A = 2°, □ f = 2 Hz, A = 4°, ▽ f = 2 Hz, A = 8°
● f = 4 Hz, A = 2°, ■ f = 4 Hz, A = 4°, △ f = 4 Hz, A = 6°
+ f = 8 Hz, A = 2°, ⊕ f = 8 Hz, A = 4°, ⊠ f = 8 Hz, A = 6°

Figure 35. Nondimensional streamwise evolution of the concentration thickness normalized by the forcing wavelength for the various forcing conditions.

The mixed fluid thickness normalized by the concentration thickness δ_m/θ_ξ, Figure 36, shows a trend very similar to the mixed fluid fraction versus x^*, see Figure 32. The most notable feature, again, is the local minimum occurring in the vicinity of x^* = 1.0, the end of the enhanced growth rate region. As x^* increases past 1.0, a steady increase

in δ_m/θ_ξ is observed. Trends in Figure 36 are the same as those shown in Figure 32, the only difference being the lack of the scatter in Figure 32.

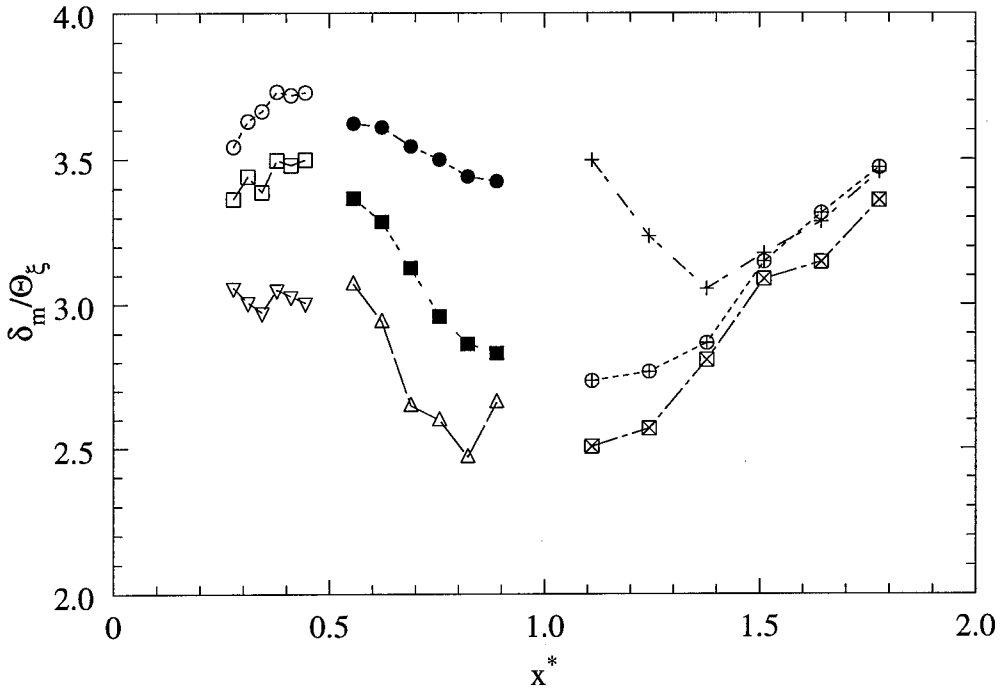

○ f = 2 Hz, A = 2°, □ f = 2 Hz, A = 4°, ▽ f = 2 Hz, A = 8°
● f = 4 Hz, A = 2°, ■ f = 4 Hz, A = 4°, △ f = 4 Hz, A = 6°
+ f = 8 Hz, A = 2°, ⊕ f = 8 Hz, A = 4°, ⊠ f = 8 Hz, A = 6°

Figure 36. Nondimensional streamwise evolution of the mixed fluid thickness normalized by the concentration thickness for the various forcing conditions.

The plots in this section were normalized with respect to the forcing frequency only; effects of the forcing amplitude are *not* effected by this normalization. It is not clear at this time if the amplitude effect can be properly normalized.

3.5 Probability density function of ξ

Results thus far have addressed mixing in terms of mixed fluid at *all* concentrations. The influence of forcing on the actual distribution of the mixed fluid composition will now be discussed in terms of the average probability density function $P(\xi, y)$. According to Koochesfahani and MacKinnon (1991), the use of a single pdf to characterize the composition field of both the unforced and the forced layers is warranted here, since the shape of the pdf was observed to be nearly invariant across the layer width. The composition distribution for the unforced and forced shear layers are presented in Appendix B.

3.5.1 Streamwise variation of the total pdf

Figures 37 displays the streamwise evolution of the total pdf of ξ for the unforced shear layer. The general shape of the pdf is preserved as downstream distance increases. An increase in mixed fluid with increasing downstream distance is seen by the increased height of the peak of the pdf located near $\xi \approx 0.75$. This peak in the pdf will be referred to as the most probable concentration. It is interesting to note how the pdf fills in around the most probable concentration, but not at very low concentrations. It is also observed that the peak tends to shift slightly toward lower values as x increases. Initially the layer has an excess of high-speed fluid ($\xi = 1$) resulting in a most probable concentration at very high values of ξ. As the mixing process continues the most probable concentration shifts toward the low-speed side ($\xi = 0$). This result was first reported by Koochesfahani and Dimotakis (1986).

The streamwise dependence of the pdf for the shear layer forced at $f = 2$, 4 and 8 Hz, $A = 4°$ are displayed in Figures 38 - 40, respectively. The remaining forced cases

are presented in Appendix C. In all cases mixing is enhanced mostly at high values of concentration with increasing downstream distance. Unlike the unforced layer which shows a slight shift in the most probable concentration to lower values, some of the more highly forced cases exhibit a slight shift toward higher values, see Figures 39 and 40.

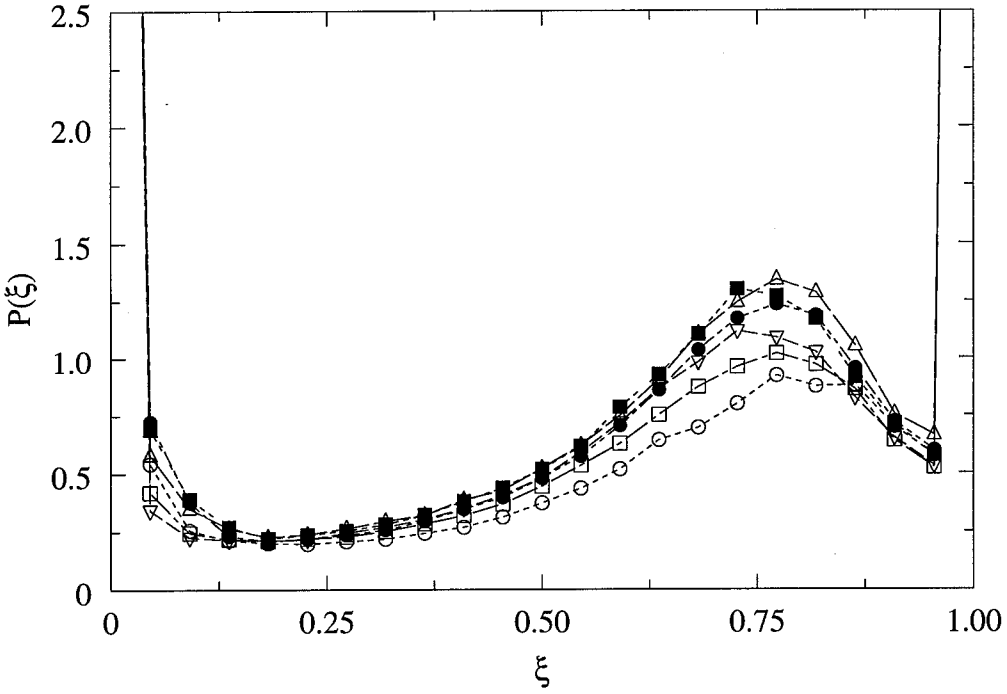

○ x = 12.5, □ x = 14.0, ▽ x = 15.5, ● x = 17.0, ■ x = 18.5, △ x = 20.0 cm

Figure 37. Streamwise evolution of the total pdf of the unforced shear layer.

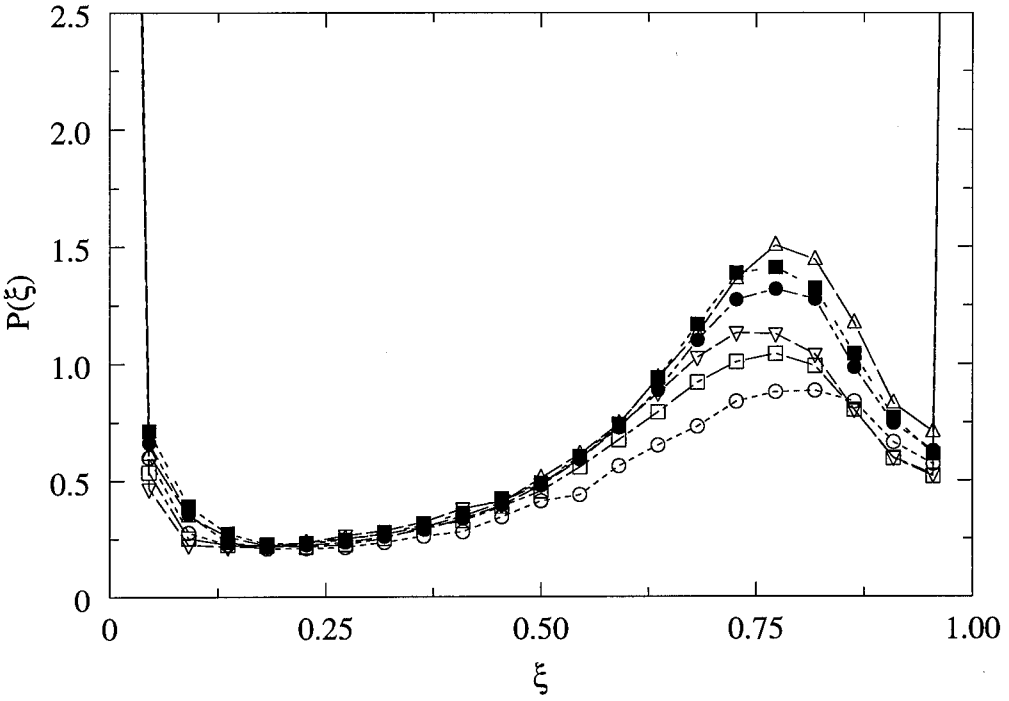

○ $x^* = 0.28$, □ $x^* = 0.31$, ▽ $x^* = 0.34$, ● $x^* = 0.37$, ■ $x^* = 0.41$, △ $x^* = 0.44$

Figure 38. Nondimensional streamwise evolution of the total pdf for the shear layer forced at $f = 2$ Hz, $A = 4°$.

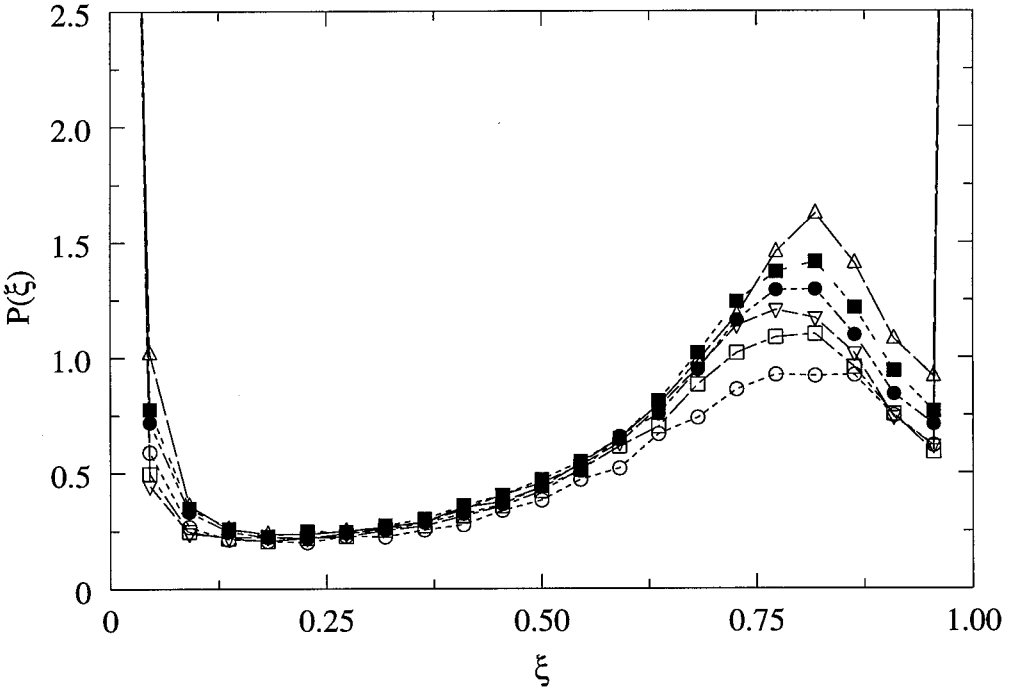

○ $x^* = 0.56$, □ $x^* = 0.62$, ▽ $x^* = 0.68$, ● $x^* = 0.75$, ■ $x^* = 0.82$, △ $x^* = 0.88$

Figure 39. Nondimensional streamwise evolution of the total pdf for the shear layer forced at $f = 4$ Hz, $A = 4°$.

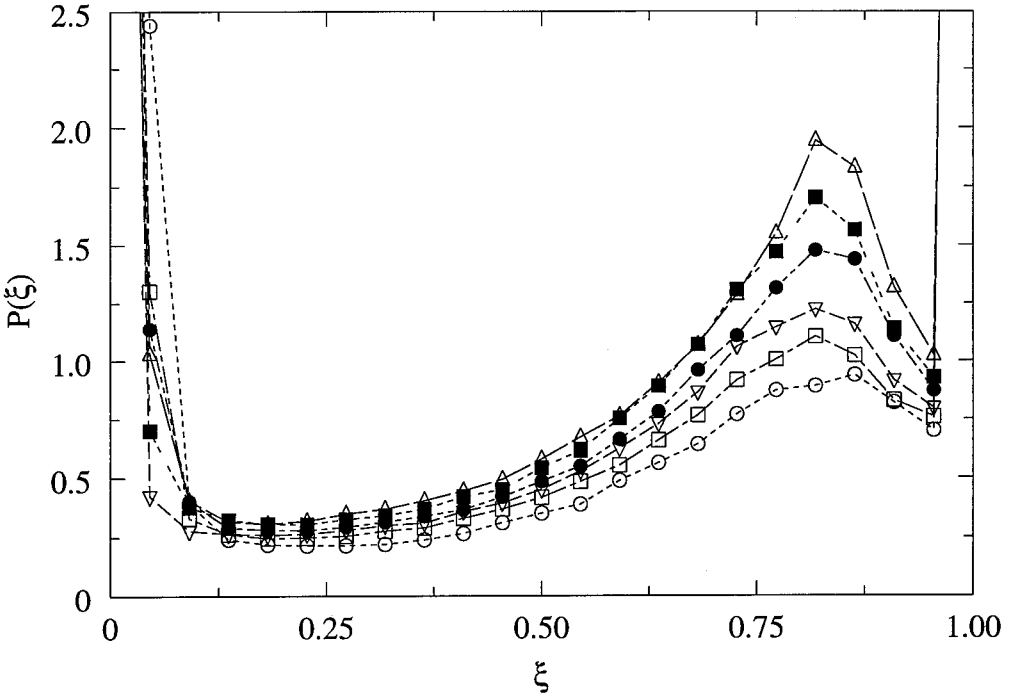

○ $x^* = 1.11$, □ $x^* = 1.24$, ▽ $x^* = 1.38$, ● $x^* = 1.51$, ■ $x^* = 1.64$, △ $x^* = 1.78$

Figure 40. Nondimensional streamwise evolution of the total pdf for the shear layer forced at $f = 8$ Hz, $A = 4°$.

3.5.2 Amplitude dependence of the total pdf

The forcing amplitude dependence is shown in Figures 41 - 43 for the cases forced at $f = 2$, 4 and 8 Hz at the farthest downstream location $x = 20.0$ cm, corresponding to $x^* = 0.44$, 0.88, 1.78, respectively. The remaining cases are presented in Appendix D. The main result is that in all cases mixing is enhanced mostly at high values of concentration. The effect of the forcing amplitude is simply to increase the proportion of fluid mixed at higher values of concentration. In addition to enhanced mixing, there is a change in the composition field. In all cases the most probable concentration is shifted slightly toward higher values of ξ. A shift in the predominate mixed-fluid concentration was also noted by Koochesfahani and M^{ac}Kinnon (1991).

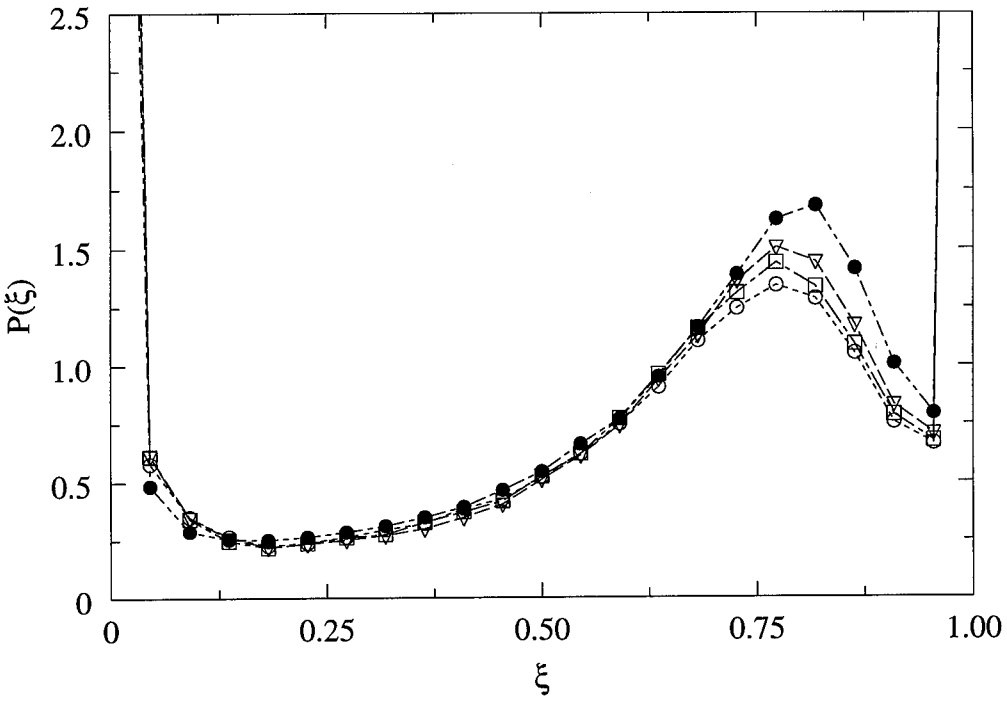

○ Unforced case, □ $A = 2°$, ▽ $A = 4°$, ● $A = 8°$

Figure 41. Amplitude dependence of the total pdf for the shear layer forced at $f = 2$ Hz, at $x = 20.0$ cm ($x^* = 0.44$), compared to the unforced case.

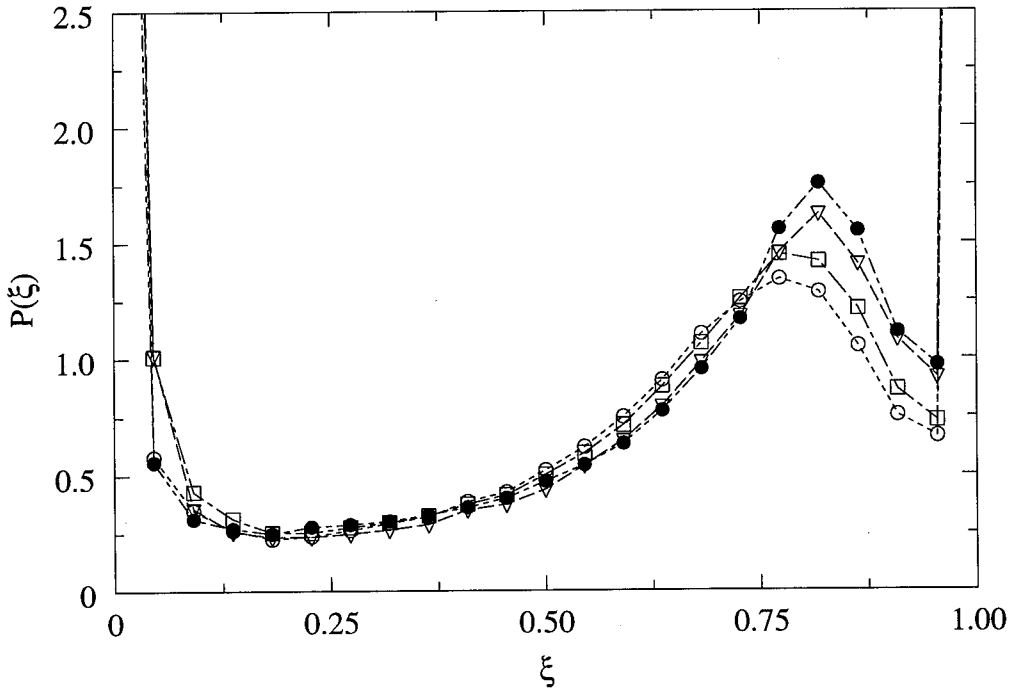

○ Unforced case, □ $A = 2°$, ▽ $A = 4°$, ● $A = 6°$

Figure 42. Amplitude dependence of the total pdf for the shear layer forced at $f = 4$ Hz, at $x = 20.0$ cm ($x^* = 0.88$), compared to the unforced case.

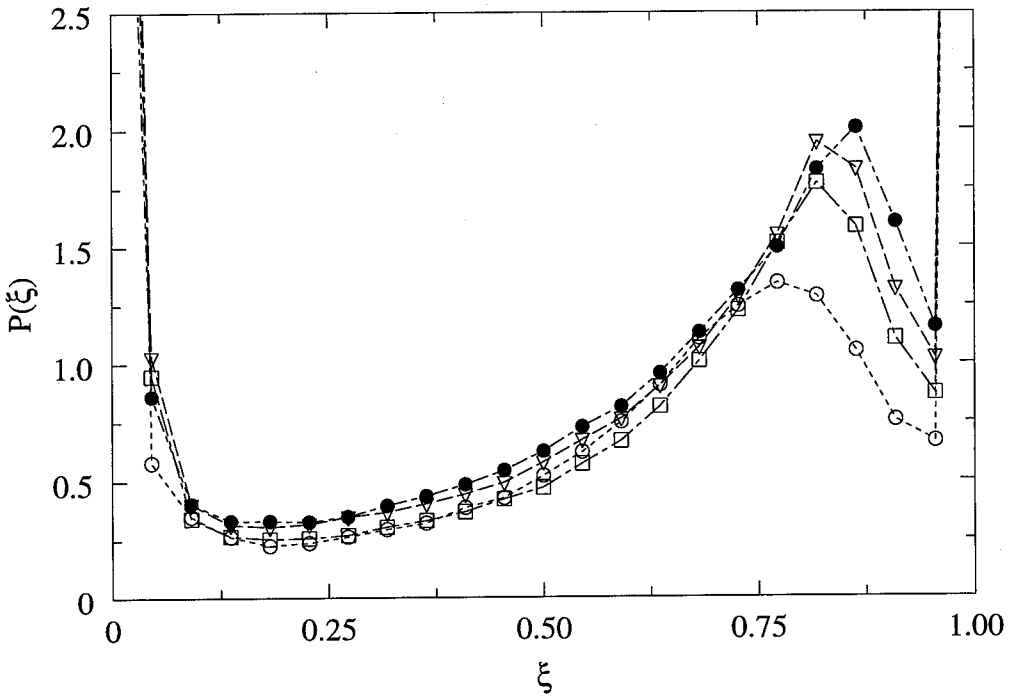

○ Unforced case, □ A = 2°, ▽ A = 4°, ● A = 6°

Figure 43. Amplitude dependence of the total pdf for the shear layer forced at f = 8 Hz, at x = 20.0 cm (x^* = 1.78), compared to the unforced case.

3.6 Comparison with Koochesfahani and M^{ac}Kinnon (1991)

The current flow conditions, U_1 = 40 cm/sec and U_2 = 20 cm/sec, were chosen to be the same as those in Koochesfahani and M^{ac}Kinnon (1991), to allow comparison of the forcing mechanism on the development of the forced shear layer. The facility used in the current experiment was the same facility used by Koochesfahani and M^{ac}Kinnon (1991). In the previous work, data were presented at a single downstream position, x = 20 cm, where the local Reynolds number $Re_{\delta_1} = \Delta U\, \delta_1/\nu$, was approximately 6,600. In the current work $Re_{\delta_1} \approx$ 6,000 at x = 20.0 cm. Due to the finite size (height and length) of the test section it was not possible to match the Reynolds numbers of the two

experiments.

As stated earlier, the unforced layer in the current study is *not* the same as the natural layer, due to the presence of the airfoil; the main difference being a reduction in the width of the unforced layer. A summary of shear layer width δ_1, mixed fluid thickness δ_m and the mixed fluid fraction δ_m/δ_1, for the natural and unforced layers are given in Table 2.

Table 2. Summary of shear layer width, mixed fluid thicknesses and mixed fluid fraction for the natural and unforced layers.

	δ_m (mm)	δ_1 (mm)	δ_m/δ_1
Natural	16.1	33.3	0.483
Unforced	14.4	29.6	0.486

The natural layer of Koochesfahani and M^{ac}Kinnon has width $\delta_{1_{nat}}$ = 33.3 mm and the unforced layer in the current investigation was δ_1 = 29.6 cm. This is approximately an 11% reduction. The reduction in the width of the layer due to the presence of an airfoil is consistent with the results reported by Koochesfahani and Dimotakis (1989). The peak of the mixed fluid probability curve, $(p_m)_{max}$, in the central region of the shear layer is nearly the same, implying that the amount of mixed fluid at x = 20.0 cm is not changed due to the presence of the airfoil. Therefore, the changes in δ_m between the unforced and natural layers are due purely to the reduced width of the shear layer.

In the forced layers of Koochesfahani and M^{ac}Kinnon (1991), perturbations were induced by sinusoidally oscillating the high-speed freestream at frequencies of 4 and 8

Hz, with rms amplitude of about 1.0% of the freestream speed. There is some ambiguity in the comparing these cases to the present work since the perturbation methods are different and the amplitudes are characterized differently. It is not clear if the methods by which each of these forcing techniques are quantified are related to each other. The effect of the different forcing mechanisms on the scalar mixing field does, however, show the same trend. In Figure 44, the forcing frequency and amplitude dependence of the

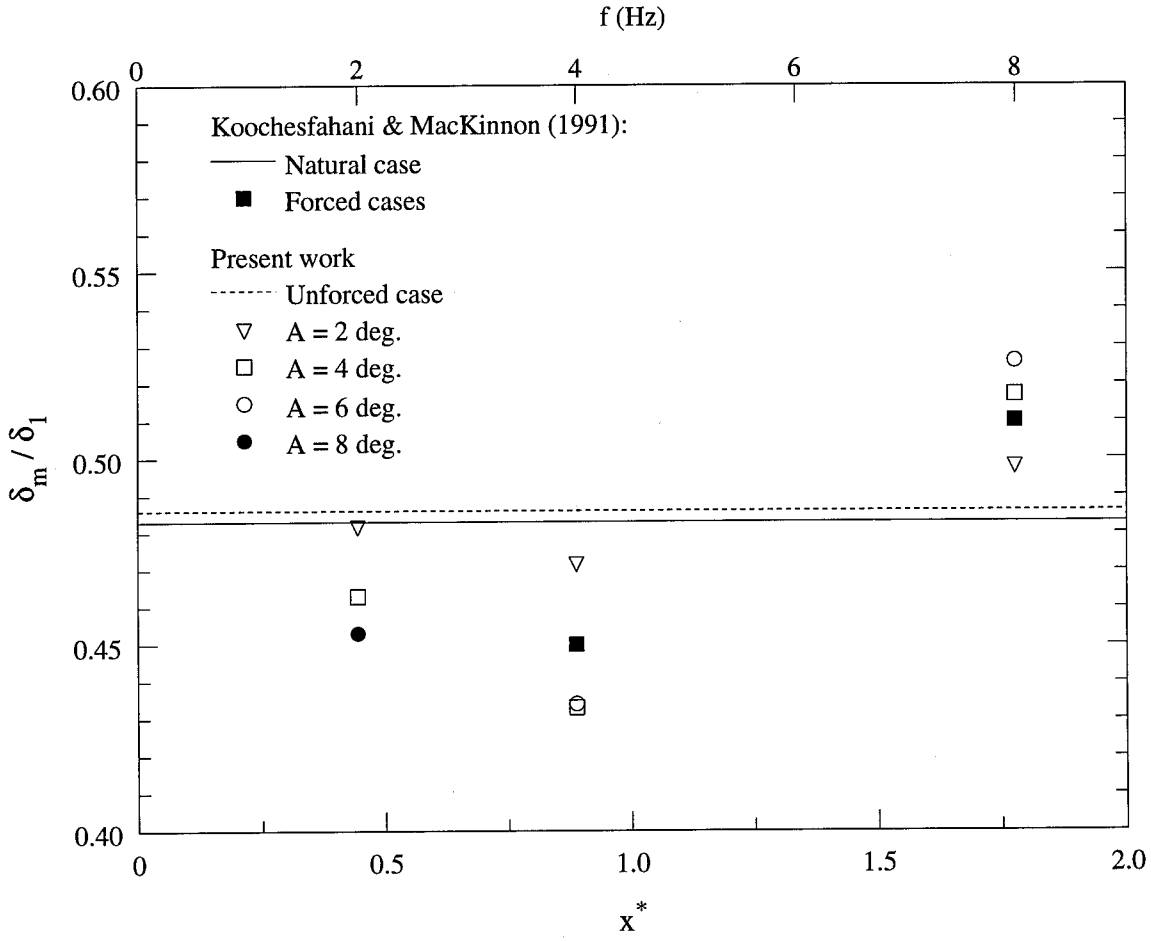

Figure 44. Nondimensional streamwise (frequency) dependence of the mixed fluid fraction for various forced cases compared with Koochesfahani and M[ac]Kinnon (1991).

mixed-fluid fraction for the two forcing mechanisms are displayed. At a fixed downstream location the nondimensional streamwise coordinate $x^* = \lambda x f / U_c$ is directly proportional to the forcing frequency f. Therefore the frequency scale of Figure 44 may also be viewed as an evolutionary scale. Only for the cases forced at f = 8 Hz is there more mixed-fluid per unit width of the layer than in the unforced case at this downstream location; if the flow is examined farther downstream, further increases in the mixing would be expected. Table 3 summarizes the shear layer width δ_1, mixed fluid thickness δ_m and the mixed fluid fraction δ_m/δ_1 for the forced cases in both of these studies.

Table 3. Summary of shear layer width, mixed fluid thickness and mixed fluid fraction for the different forcing conditions.

	δ_m (mm)	δ_1 (mm)	δ_m/δ_1
Koochesfahani and M^{ac}Kinnon			
f = 4 Hz	18.3	40.5	0.452
f = 8 Hz	19.3	37.5	0.515
Present work			
f = 2 Hz, A = 2°	14.2	29.4	0.482
f = 2 Hz, A = 4°	14.4	31.0	0.463
f = 2 Hz, A = 8°	15.7	34.7	0.453
f = 4 Hz, A = 2°	14.5	30.6	0.472
f = 4 Hz, A = 4°	14.8	34.2	0.433
f = 4 Hz, A = 6°	15.6	36.0	0.434
f = 8 Hz, A = 2°	15.5	31.2	0.498
f = 8 Hz, A = 4°	17.6	34.0	0.517
f = 8 Hz, A = 6°	18.5	35.2	0.526

The total pdf for the oscillating freestream experiments showed trends similar to the present work. In both cases the effect of forcing was to increase mixing at mainly higher values of concentration. It is noted, however, that the predominant concentration of mixed fluid shows only slight variations relative to the unforced case, in contrast to the oscillating freestream experiment which showed a larger shift to higher concentrations. It is not clear at this time why the current forcing method results in smaller shifts of the predominant mixed fluid concentration. It is possible that the wake of the airfoil may be a contributing factor.

3.7 Comparison with Roberts and Roshko (1985)

In the work of Roberts and Roshko (1985) the effect of a periodic disturbance on the amount of chemical product in a forced shear layer was examined at pre-transitional and post-transitional Reynolds numbers. Forcing was achieved by sinusoidally oscillating the high-speed freestream, at 2% (rms) of the freestream speed. The chemical product was measured using a laser absorption technique. In this work the amount of mixing was quantified by the product thickness, defined by

$$\delta_{p_2} = \frac{1}{C_{2_0}} \int_{-h}^{+h} \overline{c_p}(y)\, dy,$$

where C_{2_0} is the low-speed feestream reactant concentration and $\overline{c_p}(y)$ is the average product concentration defined as

$$\overline{c_p}(y) = C_{2_0} \int_{\varepsilon}^{1-\varepsilon} (1-\xi)\, p(\xi, y)\, d\xi.$$

The product thickness for the various forcing conditions was noted relative to the product thickness of the unforced layer, denoted by the ratio $(\delta_{p_2})_F/(\delta_{p_2})_N$, where δ_{p_2} is the product thickness and the subscripts F and N refer to the forced and natural layers, respectively.

In these experiments the unit Reynolds number $Re' = \Delta U/\nu$ of the pre-transitional (low Reynolds number) case was 905 cm^{-1}/sec, and for the post-transitional (high Reynolds number) case 4340 cm^{-1}/sec. The natural frequency for the low Reynolds number case was f_0 = 8.3 Hz and for the high Reynolds number case f_0 = 62.7 Hz. In the current work the unit Reynolds number is 2000 cm^{-1}/sec, corresponding to the later stages of the mixing transition. The natural frequency for the unforced case is $f_0 \approx 27$ Hz.

It was found, in the work of Roberts and Roshko, for the low Reynolds number case that forcing had steadily increased the ratio of the product thicknesses $(\delta_{p_2})_F/(\delta_{p_2})_N$ through the enhanced growth region, reaching a local maximum near $x^* = 2$. Once past the frequency locked region the product thicknesses steadily decreased. The ratio of forced product thickness to the natural product thickness $(\delta_{p_2})_F/(\delta_{p_2})_N$ is shown in Figure 45 as a function of x^* for the low Reynolds number case. In the high Reynolds number case, the forced product thickness is initially as much as 4 times larger than the unforced product thickness; their ratio $(\delta_{p_2})_F/(\delta_{p_2})_N$ steadily decreases through the enhanced growth region. In the frequency locked region and beyond, $x^* > 1$, the ratio of the forced to the natural product thickness remains slightly less than the one, see Figure 46. This indicates that there is actually slightly less chemical product, on average, in the forced layer than in the unforced layer.

In the present work, the ratio of the forced mixed fluid thickness to the unforced

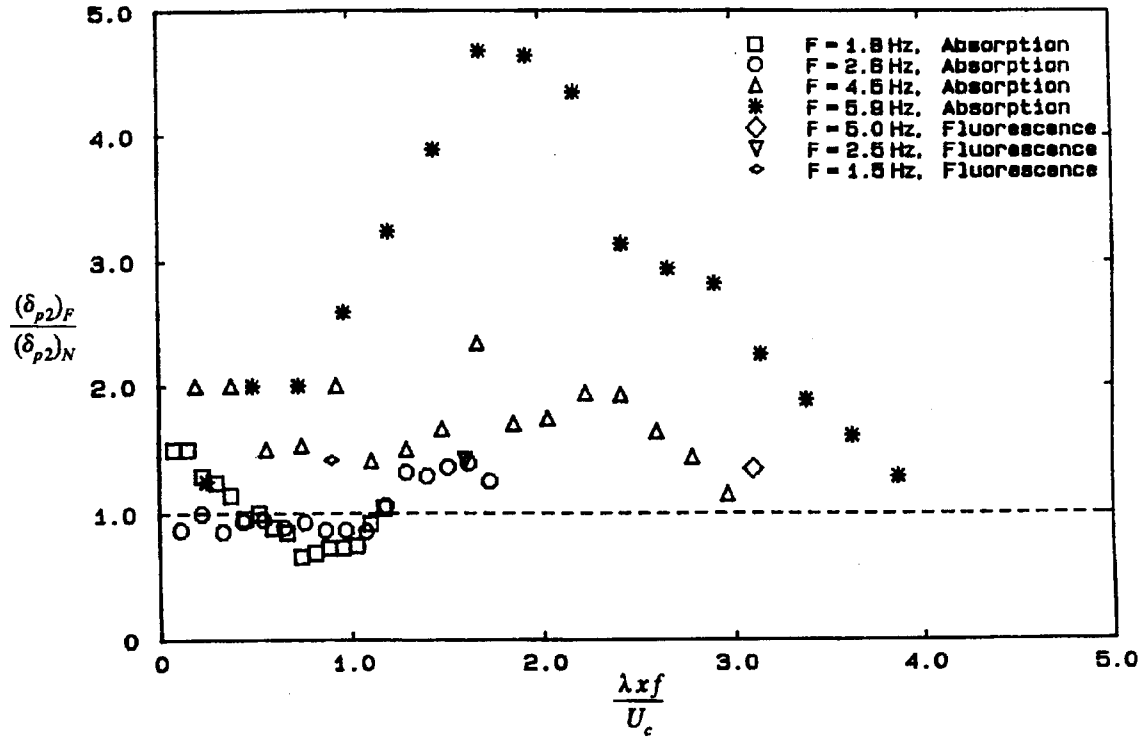

Figure 45. Ratio of forced product thickness to natural product thickness as a function of x^* : low Reynolds number case, reprinted from Roberts (1985).

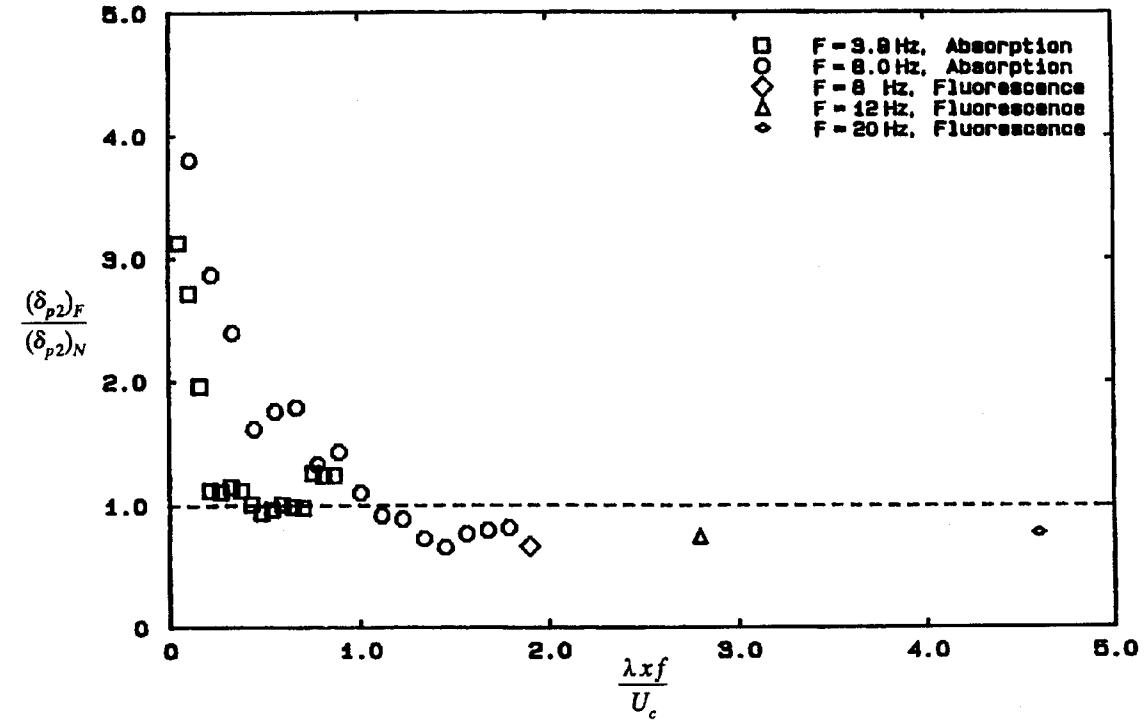

Figure 46. Ratio of forced product thickness to natural product thickness as a function of x^* : high Reynolds number case, reprinted from Roberts (1985).

mixed fluid thickness $(\delta_m)_F/(\delta_m)_U$ is analogous to the ratio of the forced to natural product thickness, see Figure 47. It should be noted that the current experiments were done using a non-reacting technique which over-estimates the amount of mixed fluid. Therefore, the trends shown in the data are of interest not the actual values of the quantities. The trends observed in the present data are most similar to the trends shown in the low Reynolds number case, Figure 45. In the enhanced growth region there is a slight increase in mixed fluid thickness over the unforced case; and in the frequency locked region there is a large increase in δ_m that seems to peak near $x^* = 2$. Note the expanded scale of Figure 47.

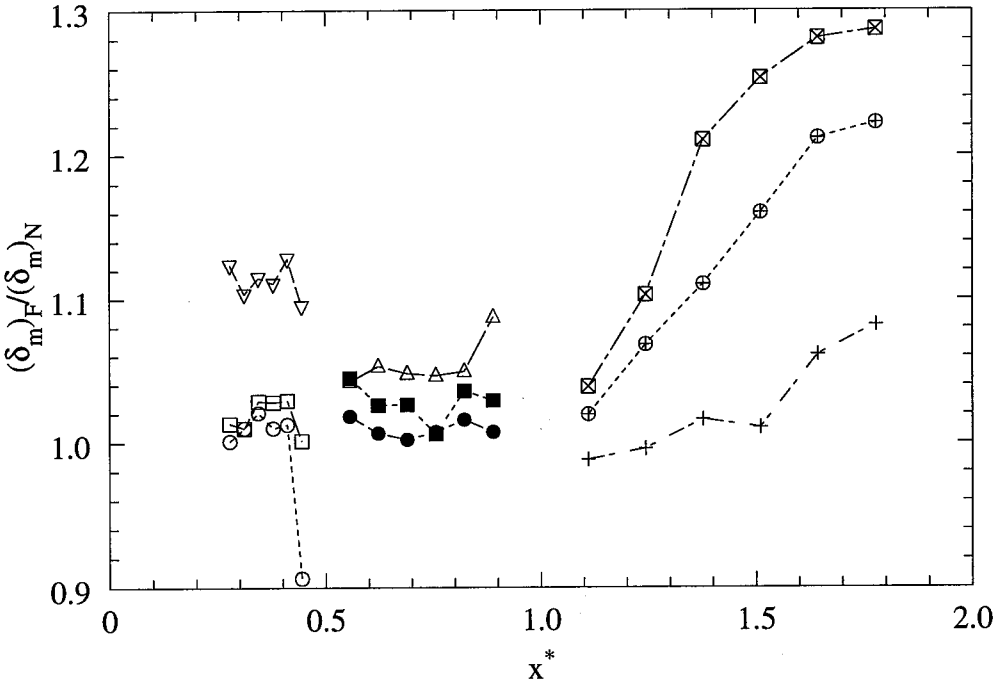

○ f = 2 Hz, A = 2°, □ f = 2 Hz, A = 4°, ▽ f = 2 Hz, A = 8°
● f = 4 Hz, A = 2°, ■ f = 4 Hz, A = 4°, △ f = 4 Hz, A = 6°
+ f = 8 Hz, A = 2°, ⊕ f = 8 Hz, A = 4°, ⊠ f = 8 Hz, A = 6°

Figure 47. Ratio of forced product thickness to unforced product thickness as a function of x^*.

Chapter 4

CONCLUSIONS

The structure and the scalar mixing field in a shear layer forced by an oscillating airfoil were investigated over a range of amplitudes, frequencies and streamwise locations using laser induced fluorescence in the passive scalar mode. One purpose of this study was to compare the mixing characteristics of a shear layer which is forced by two different methods. Comparisons were made with previous results from a shear layer perturbed by the oscillation of one freestream.

It was observed that the general structure and the growth characteristics of the forced shear layer here were similar to previous results. As either the forcing frequency or amplitude was increased, there was, in most cases, a significant increase in the shear layer width. Results show a reduction of the amount of mixed fluid in the central portion of the forced layer, an increase in the width of the region where mixed fluid is found, and an increase in the total amount of mixed fluid in the layer. The fraction of the layer width occupied by mixed fluid was found to vary slightly, however, when compared to the unforced case. These results are consistent with those from a shear layer forced by the oscillating freestream method. The predominant mixed fluid concentration showed similar variation as a result of forcing, when compared to previous results from oscillating freestream forcing studies. The composition distribution for the unforced and the forced

shear layers was reported to be essentially uniform across the width of the layer again. This result is consistent with the oscillating freestream experiment.

The effect of downstream evolution was found to increase shear layer width and increase the total amount of mixed fluid in the layer. The amount of mixed fluid in the center of the layer and the mixed fluid thickness were found to vary depending the stage of the evolution as defined by the nondimensional streamwise parameter $x^* = \lambda x f / U_c$. A local minimum was reported near the end of the enhanced growth region for both the mixed fluid fraction and the amount of mixed fluid in the center of the layer. The choice of length scale when computing the mixed fluid thickness as noted to have a slight effect on the reported efficiency of the mixing layer. In most cases the unforced layer was observed to be more efficient, in terms of the amount of mixed fluid per unit width of the layer, than the forced layer.

APPENDICES

APPENDIX A

Amplitude dependence of the transverse profiles

Amplitude dependence of the transverse profiles of average concentration $\overline{\xi}$, total mixed fluid probability p_m, pure low-speed fluid probability p_0 and pure high-speed fluid probability p_1 at the downstream locations not presented in Section 3.2.2 are shown in Figures A.1 - A.15.

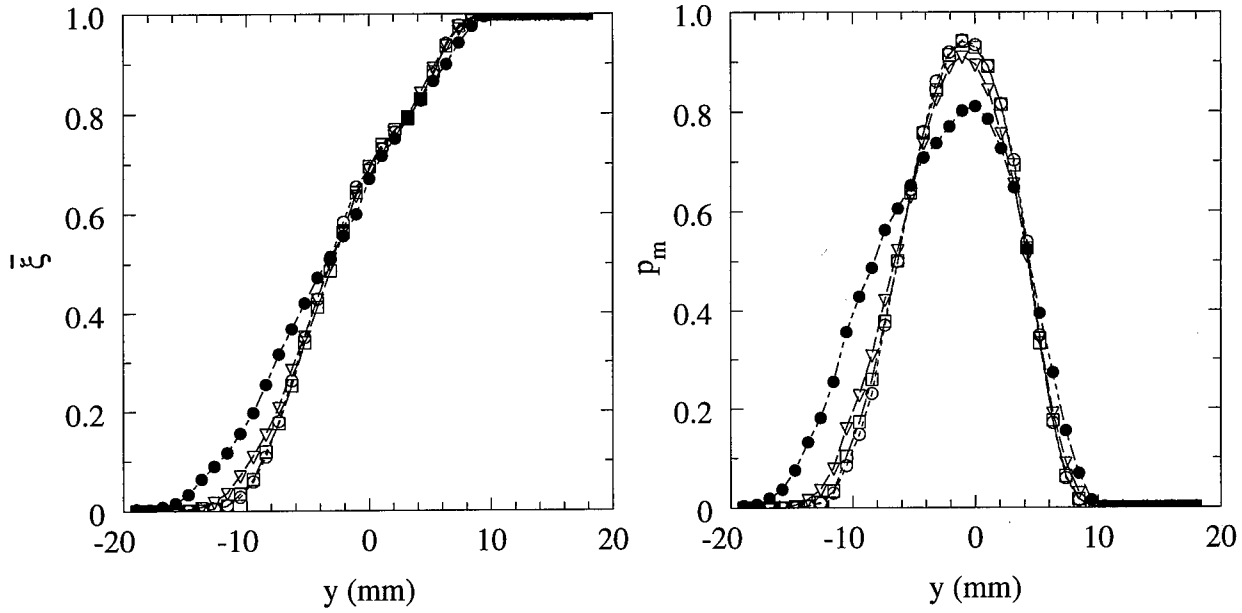

(a) Average concentration

(b) Total mixed fluid probability

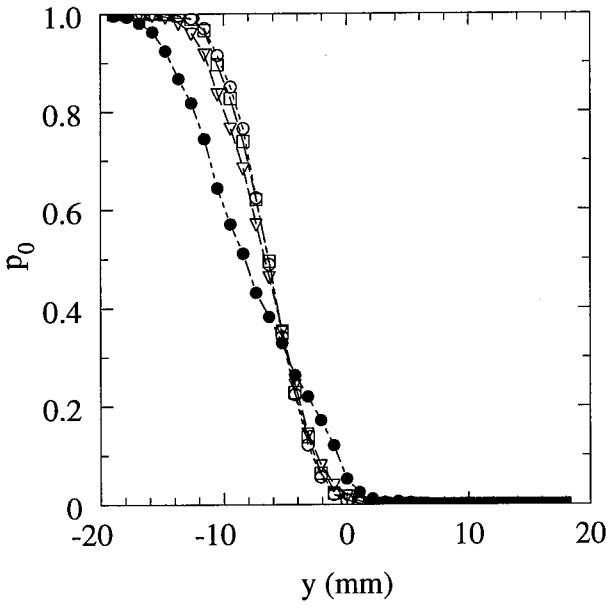

(c) Pure low-speed fluid probability

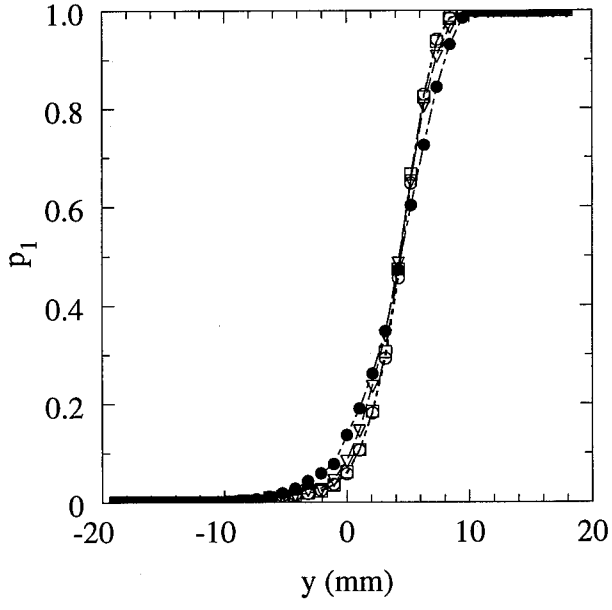

(d) Pure high-speed fluid probability

○ Unforced case, □ A = 2°, ▽ A = 4°, ● A = 8°

Figure A.1. Transverse profiles for the shear layer forced at f = 2 Hz as a function of the forcing amplitude A, at x^* = 0.28, compared to the unforced case.

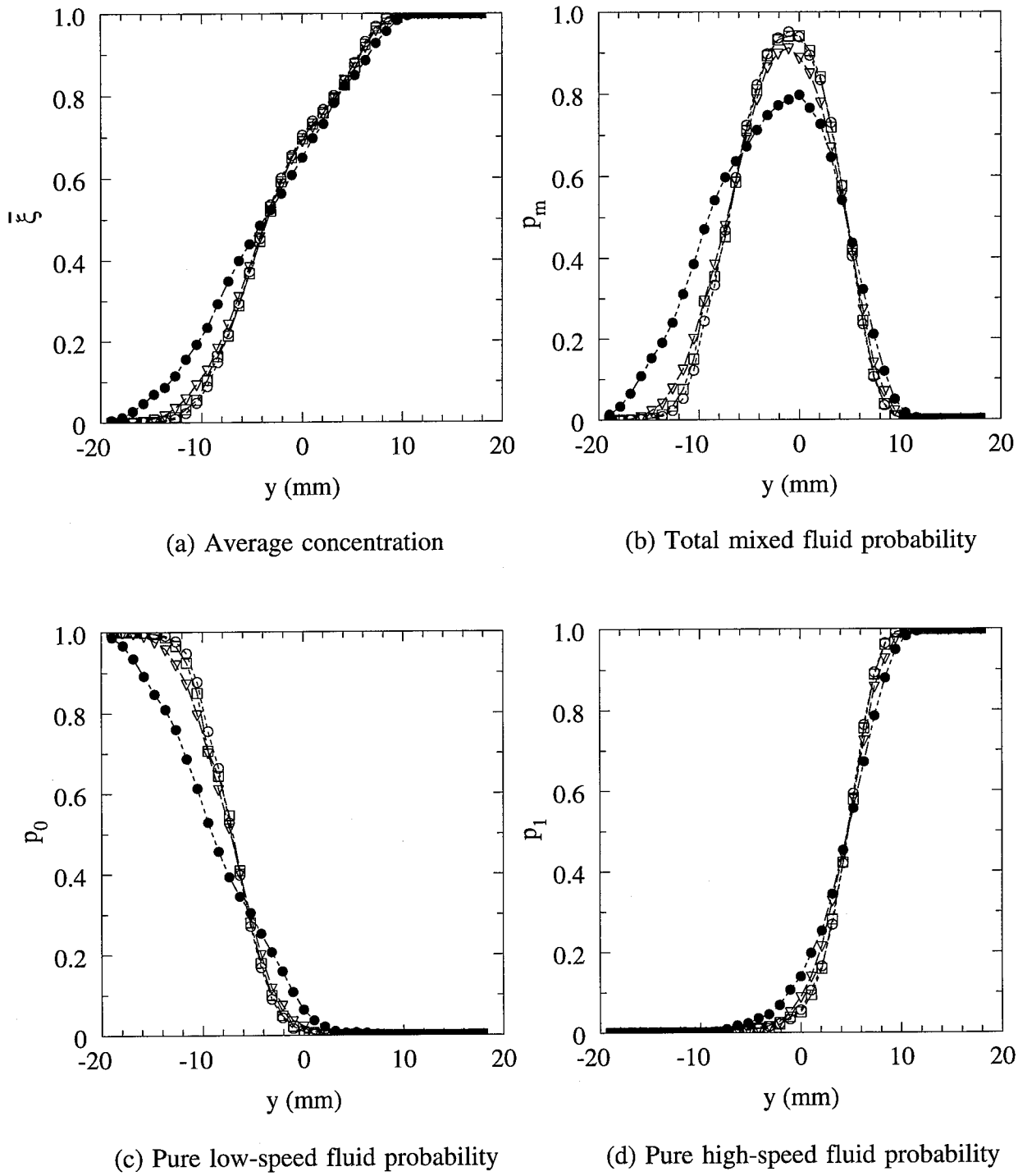

(a) Average concentration

(b) Total mixed fluid probability

(c) Pure low-speed fluid probability

(d) Pure high-speed fluid probability

○ Unforced case, □ $A = 2°$, ▽ $A = 4°$, ● $A = 8°$

Figure A.2. Transverse profiles for the shear layer forced at $f = 2$ Hz as a function of the forcing amplitude A, at $x^* = 0.31$, compared to the unforced case.

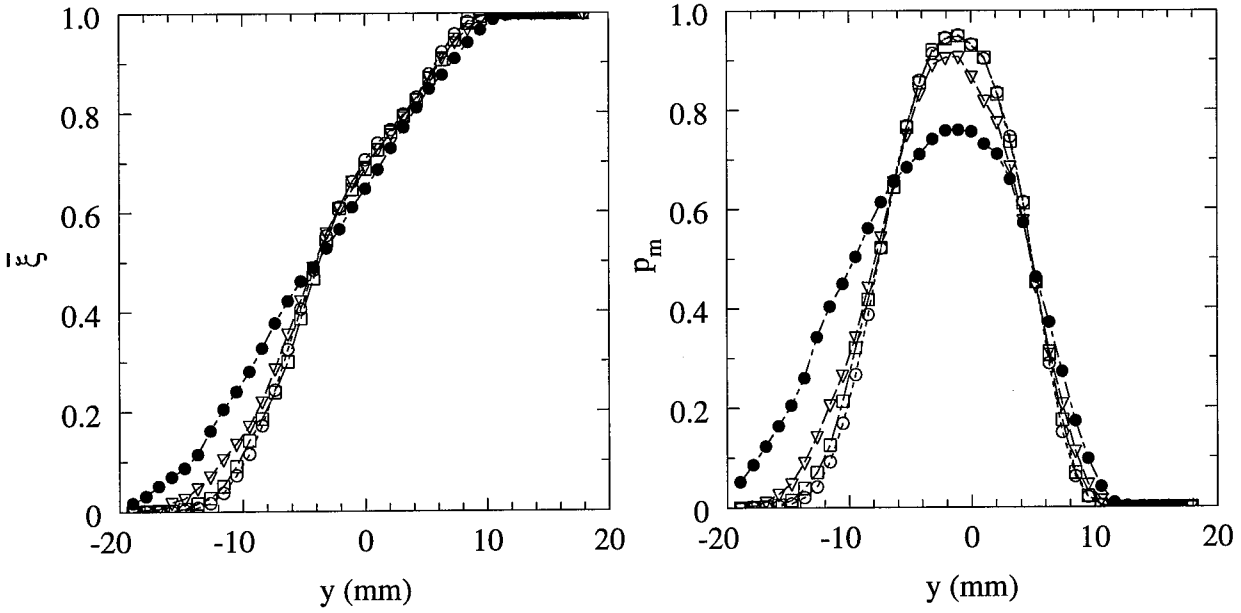

(a) Average concentration

(b) Total mixed fluid probability

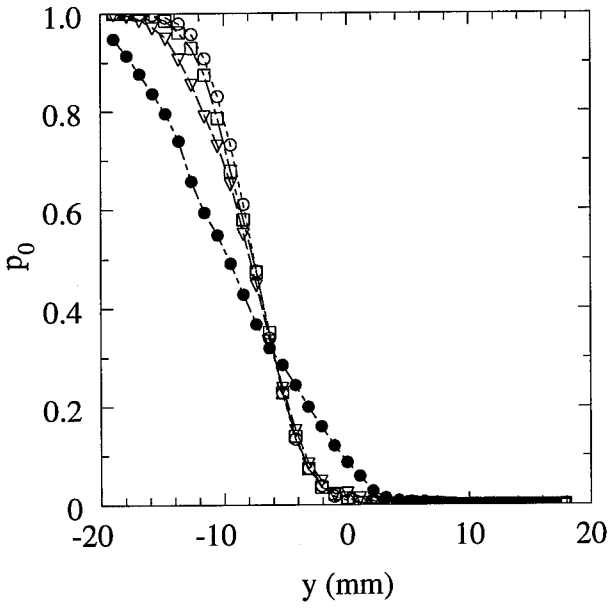

(c) Pure low-speed fluid probability

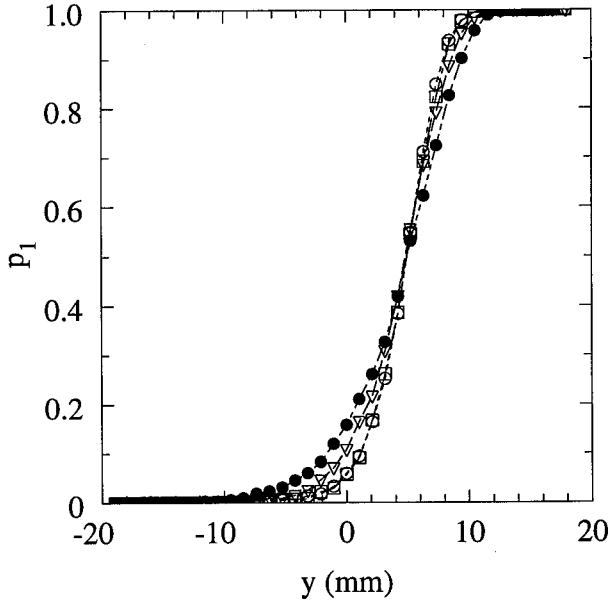

(d) Pure high-speed fluid probability

○ Unforced case, □ $A = 2°$, ▽ $A = 4°$, ● $A = 8°$

Figure A.3. Transverse profiles for the shear layer forced at $f = 2$ Hz as a function of the forcing amplitude A, at $x^* = 0.34$, compared to the unforced case.

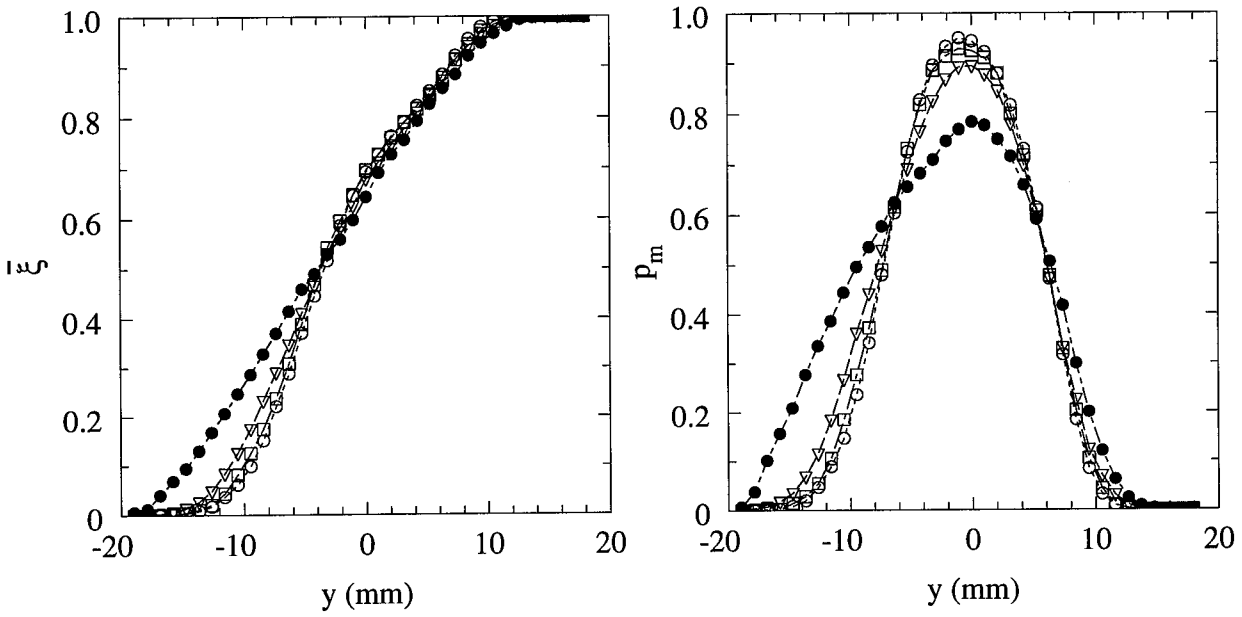

(a) Average concentration

(b) Total mixed fluid probability

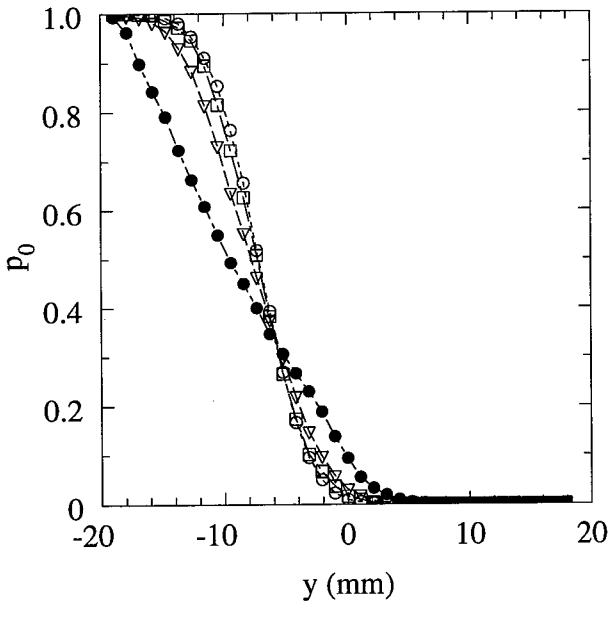

(c) Pure low-speed fluid probability

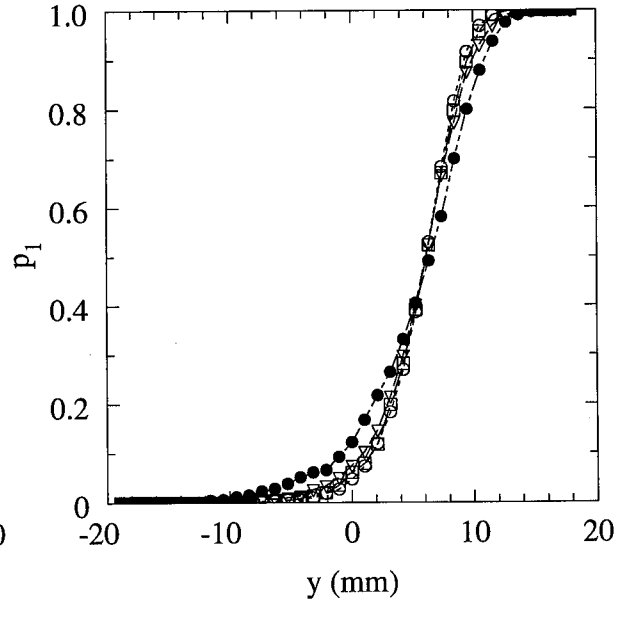

(d) Pure high-speed fluid probability

○ Unforced case, □ $A = 2°$, ▽ $A = 4°$, ● $A = 8°$

Figure A.4. Transverse profiles for the shear layer forced at $f = 2$ Hz as a function of the forcing amplitude A, at $x^* = 0.37$, compared to the unforced case.

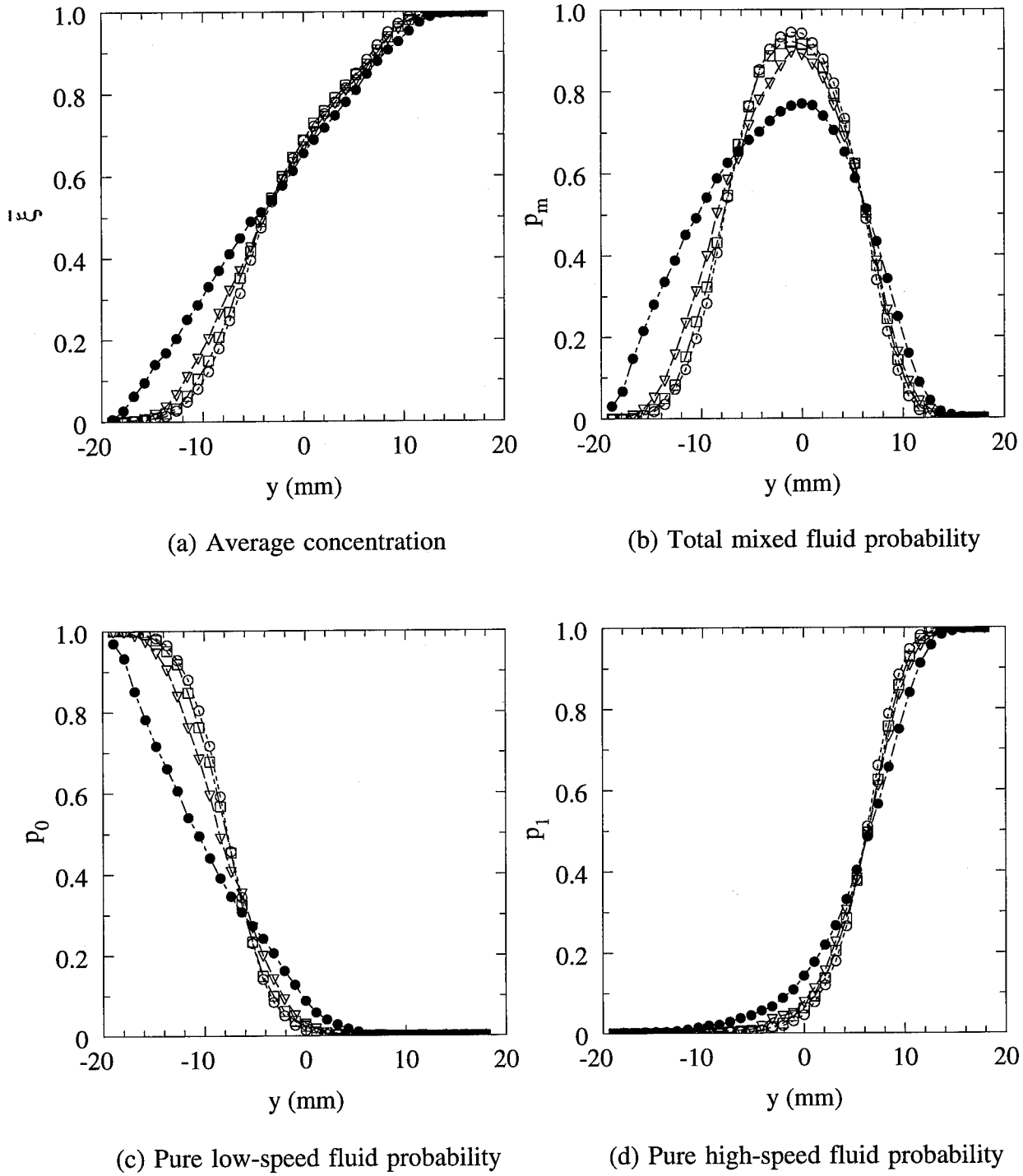

(a) Average concentration

(b) Total mixed fluid probability

(c) Pure low-speed fluid probability

(d) Pure high-speed fluid probability

○ Unforced case, □ $A = 2°$, ▽ $A = 4°$, ● $A = 8°$

Figure A.5. Transverse profiles for the shear layer forced at $f = 2$ Hz as a function of the forcing amplitude A, at $x^* = 0.41$, compared to the unforced case.

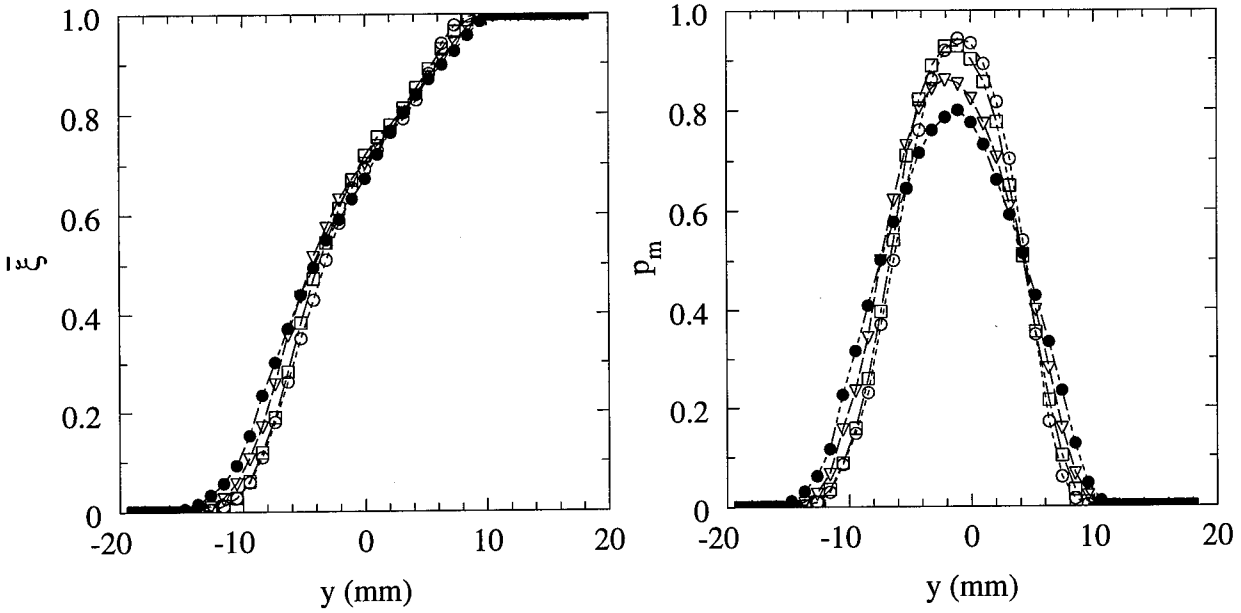

(a) Average concentration

(b) Total mixed fluid probability

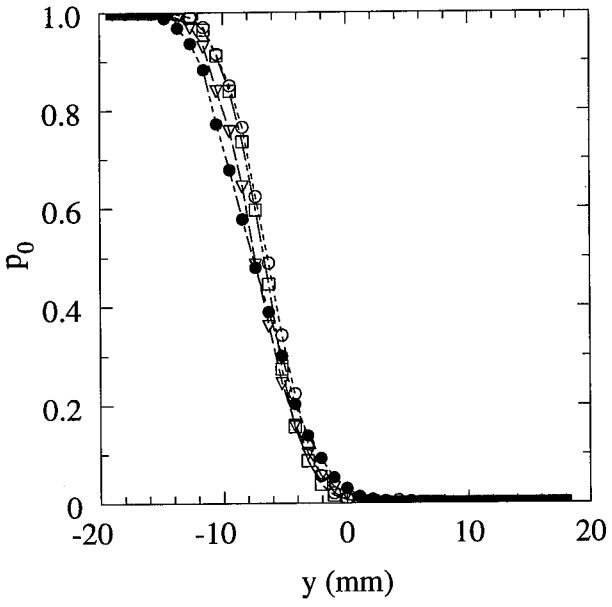

(c) Pure low-speed fluid probability

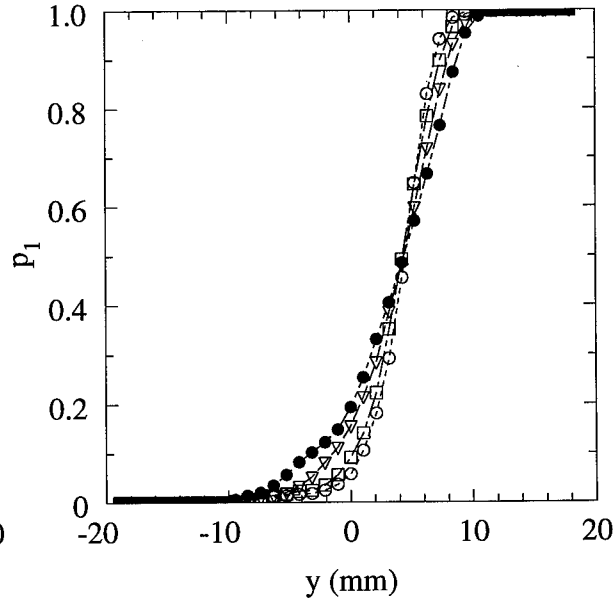

(d) Pure high-speed fluid probability

○ Unforced case, □ $A = 2°$, ▽ $A = 4°$, ● $A = 6°$

Figure A.6. Transverse profiles for the shear layer forced at $f = 4$ Hz as a function of the forcing amplitude A, at $x^* = 0.56$, compared to the unforced case.

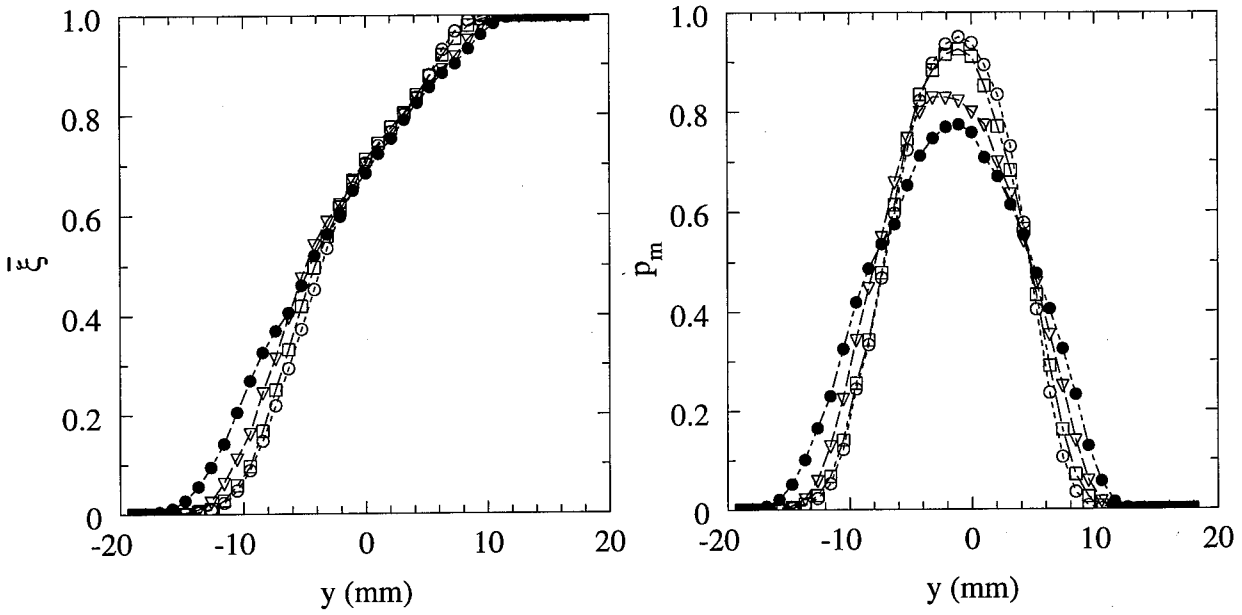

(a) Average concentration

(b) Total mixed fluid probability

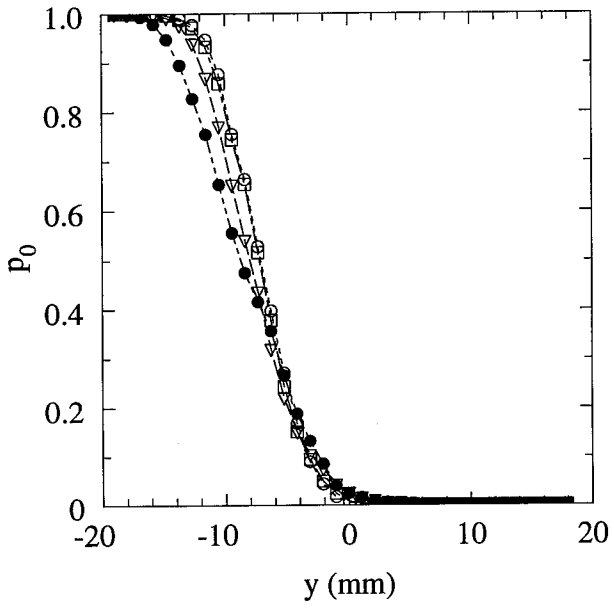

(c) Pure low-speed fluid probability

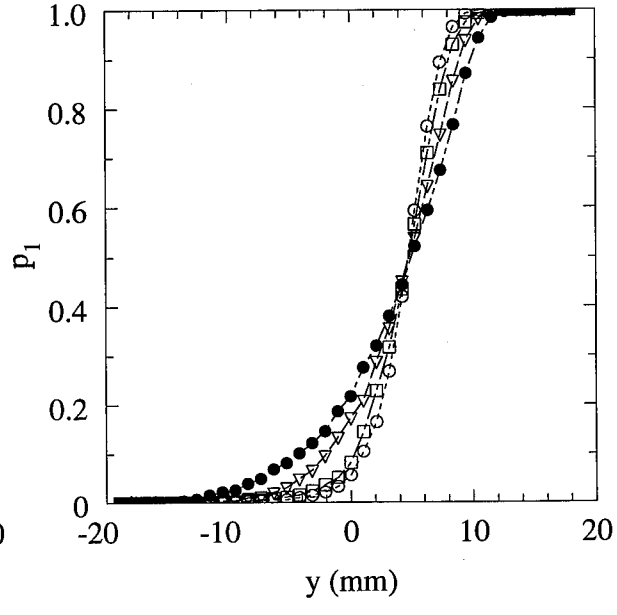

(d) Pure high-speed fluid probability

○ Unforced case, □ $A = 2°$, ▽ $A = 4°$, ● $A = 6°$

Figure A.7. Transverse profiles for the shear layer forced at $f = 4$ Hz as a function of the forcing amplitude A, at $x^* = 0.62$, compared to the unforced case.

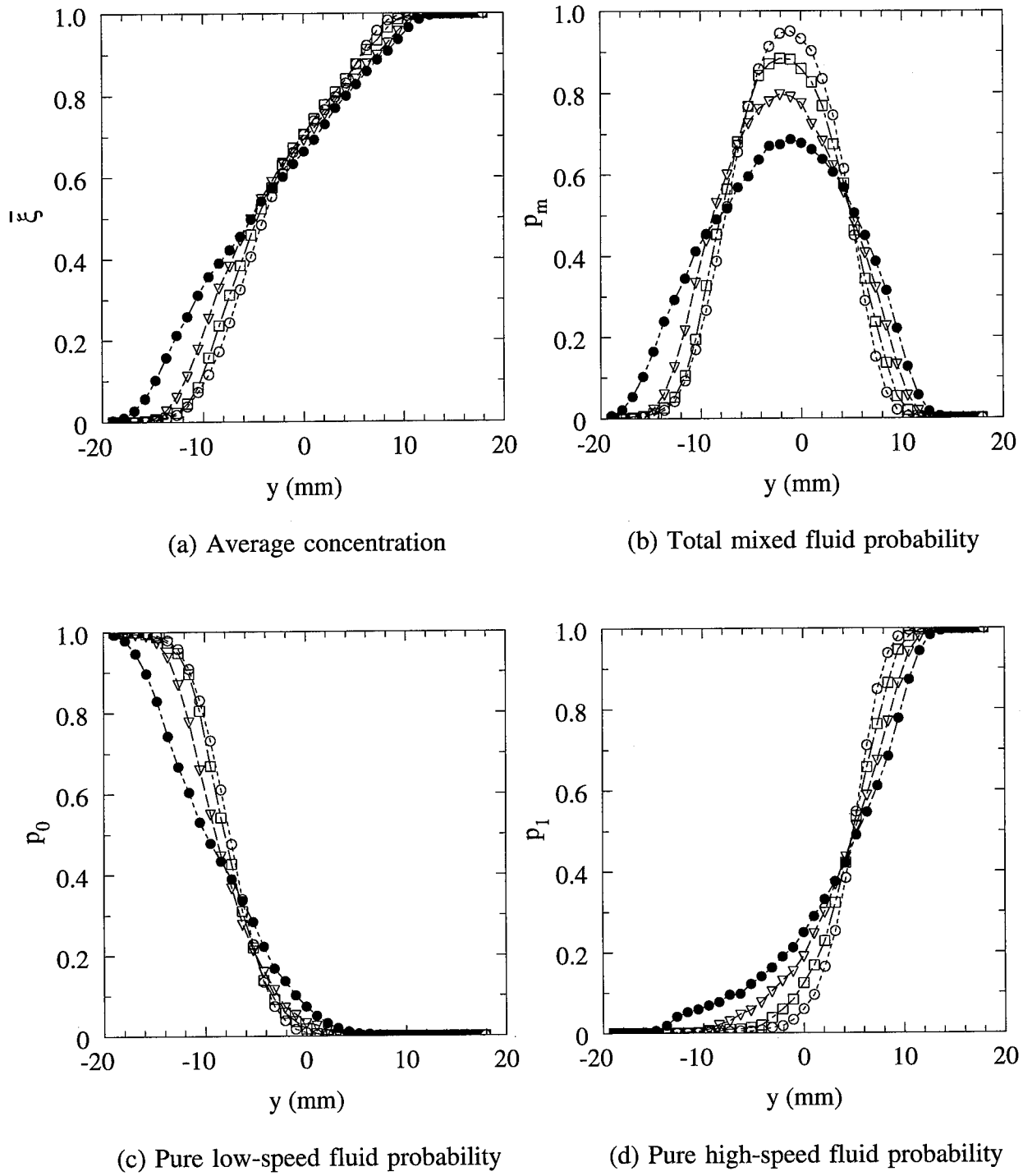

(a) Average concentration

(b) Total mixed fluid probability

(c) Pure low-speed fluid probability

(d) Pure high-speed fluid probability

○ Unforced case, □ $A = 2°$, ▽ $A = 4°$, ● $A = 6°$

Figure A.8. Transverse profiles for the shear layer forced at $f = 4$ Hz as a function of the forcing amplitude A, at $x^* = 0.68$, compared to the unforced case.

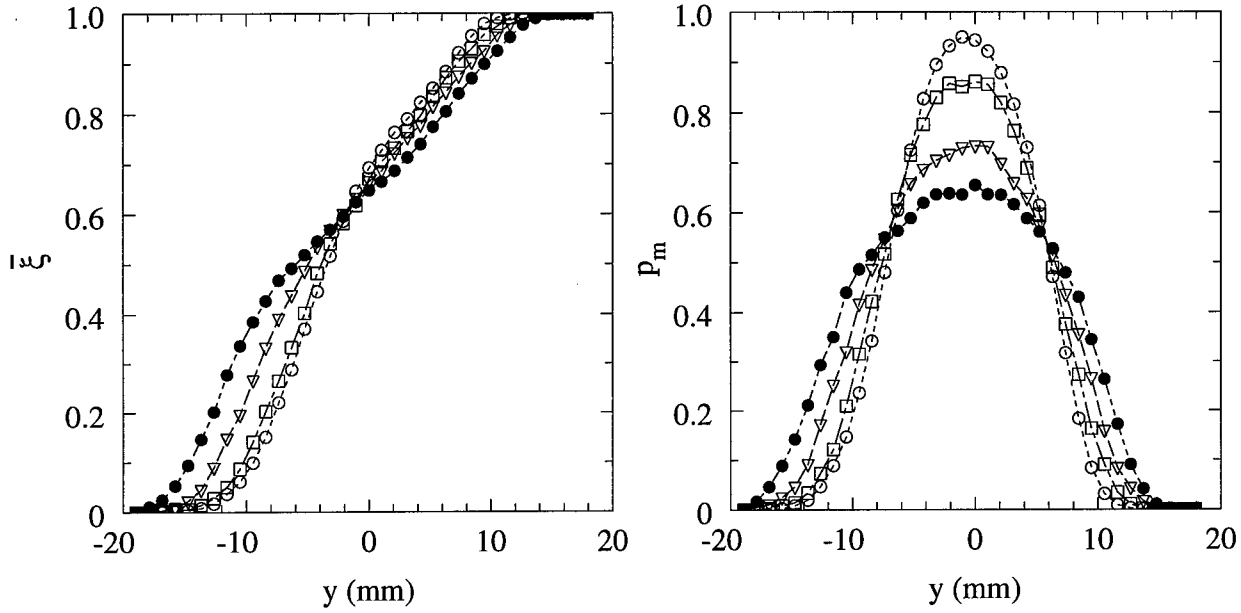

(a) Average concentration

(b) Total mixed fluid probability

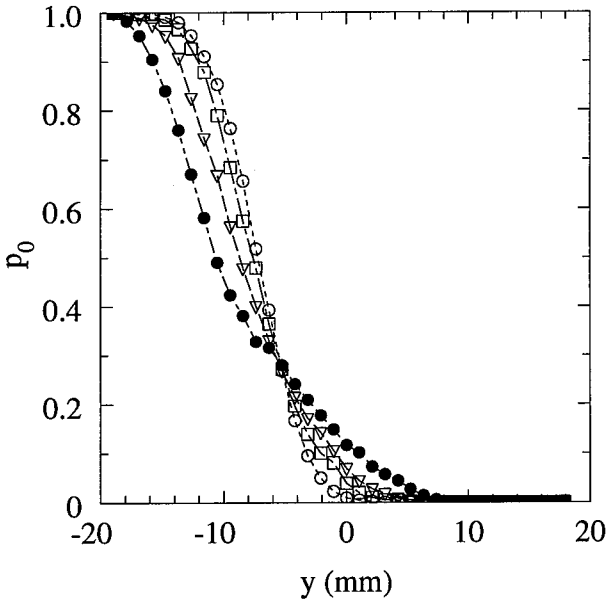

(c) Pure low-speed fluid probability

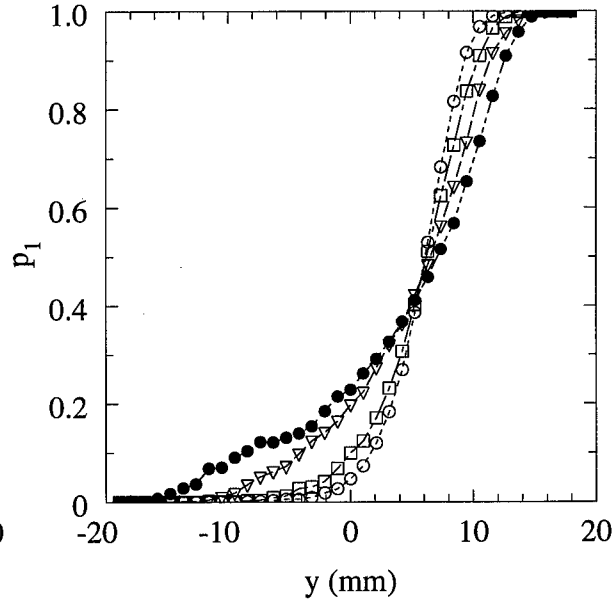

(d) Pure high-speed fluid probability

○ Unforced case, □ $A = 2°$, ▽ $A = 4°$, ● $A = 6°$

Figure A.9. Transverse profiles for the shear layer forced at $f = 4$ Hz as a function of the forcing amplitude A, at $x^* = 0.75$, compared to the unforced case.

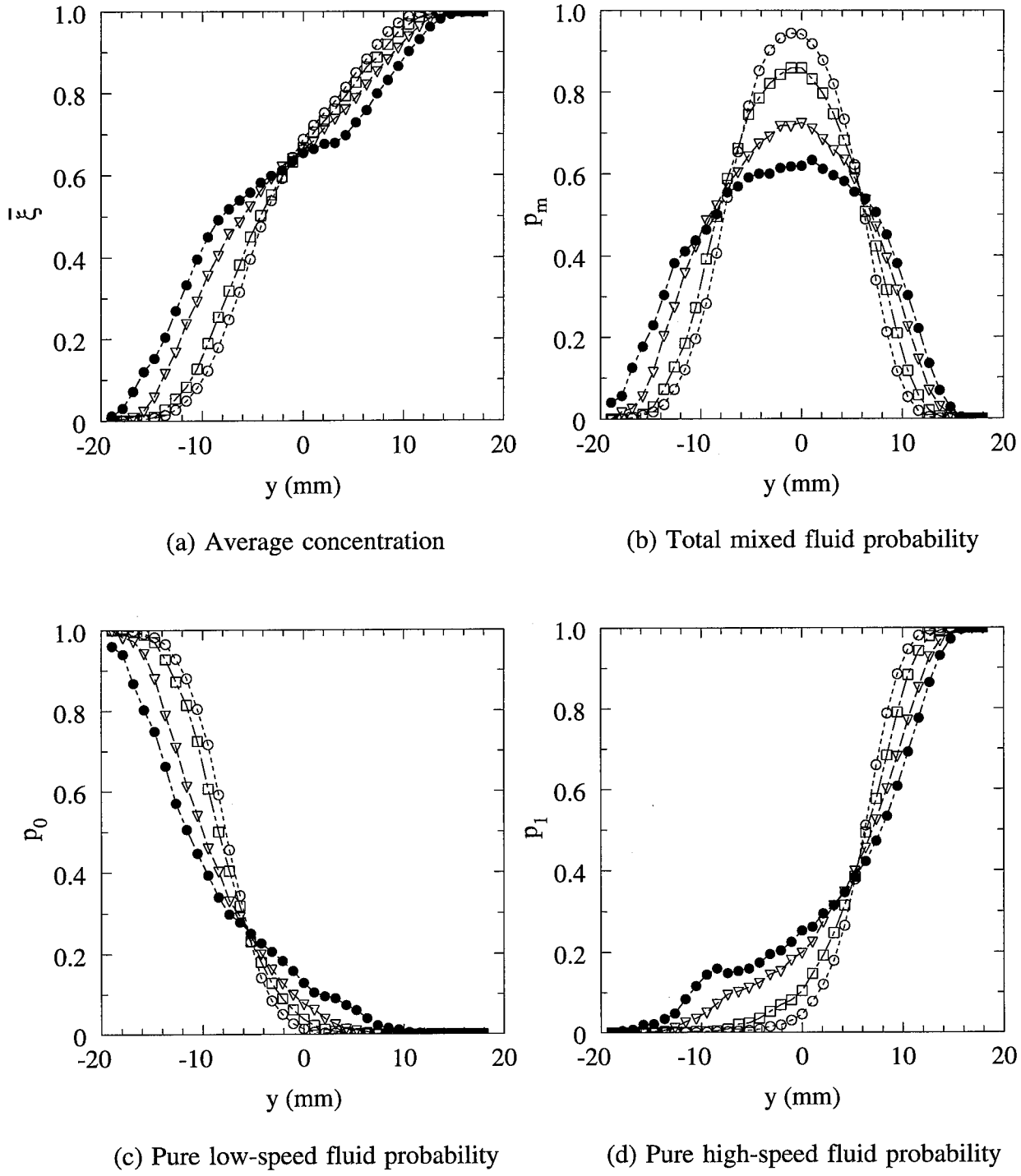

(a) Average concentration

(b) Total mixed fluid probability

(c) Pure low-speed fluid probability

(d) Pure high-speed fluid probability

○ Unforced case, □ A = 2°, ▽ A = 4°, ● A = 6°

Figure A.10. Transverse profiles for the shear layer forced at f = 4 Hz as a function of the forcing amplitude A, at x^* = 0.82, compared to the unforced case.

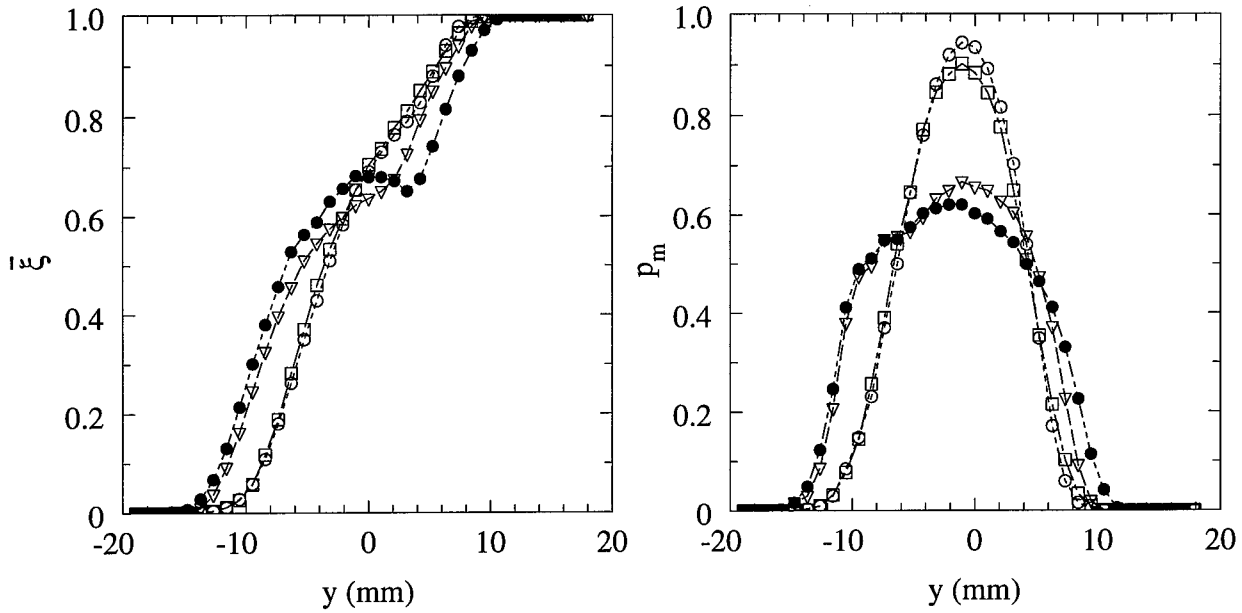

(a) Average concentration

(b) Total mixed fluid probability

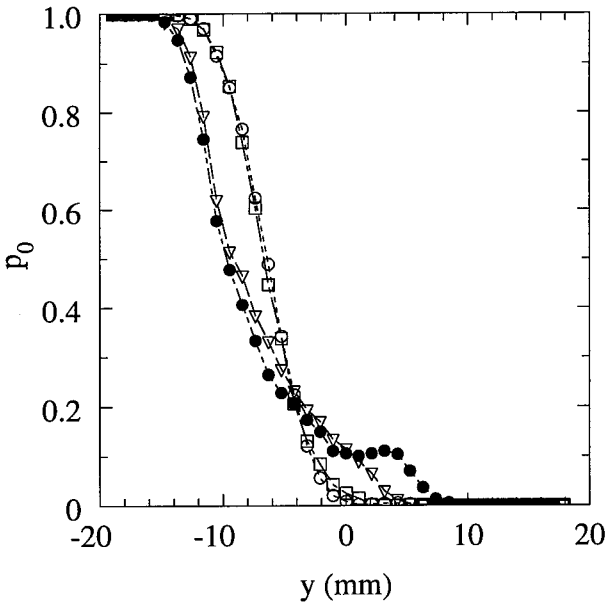

(c) Pure low-speed fluid probability

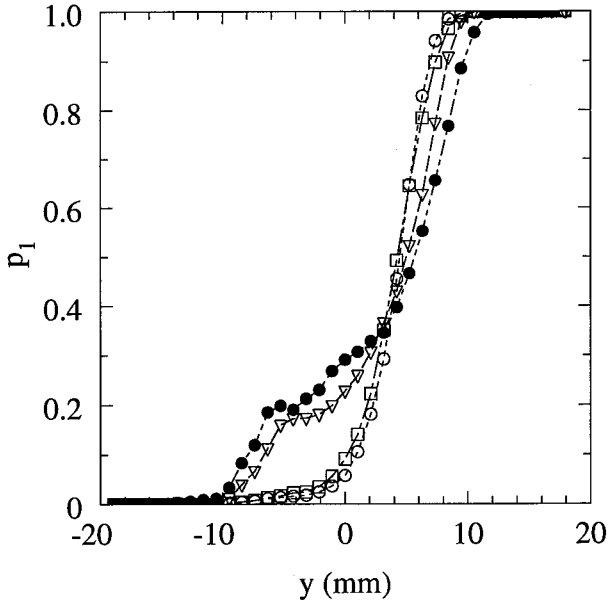

(d) Pure high-speed fluid probability

○ Unforced case, □ $A = 2°$, ▽ $A = 4°$, ● $A = 6°$

Figure A.11. Transverse profiles for the shear layer forced at $f = 8$ Hz as a function of the forcing amplitude A, at $x^* = 1.11$, compared to the unforced case.

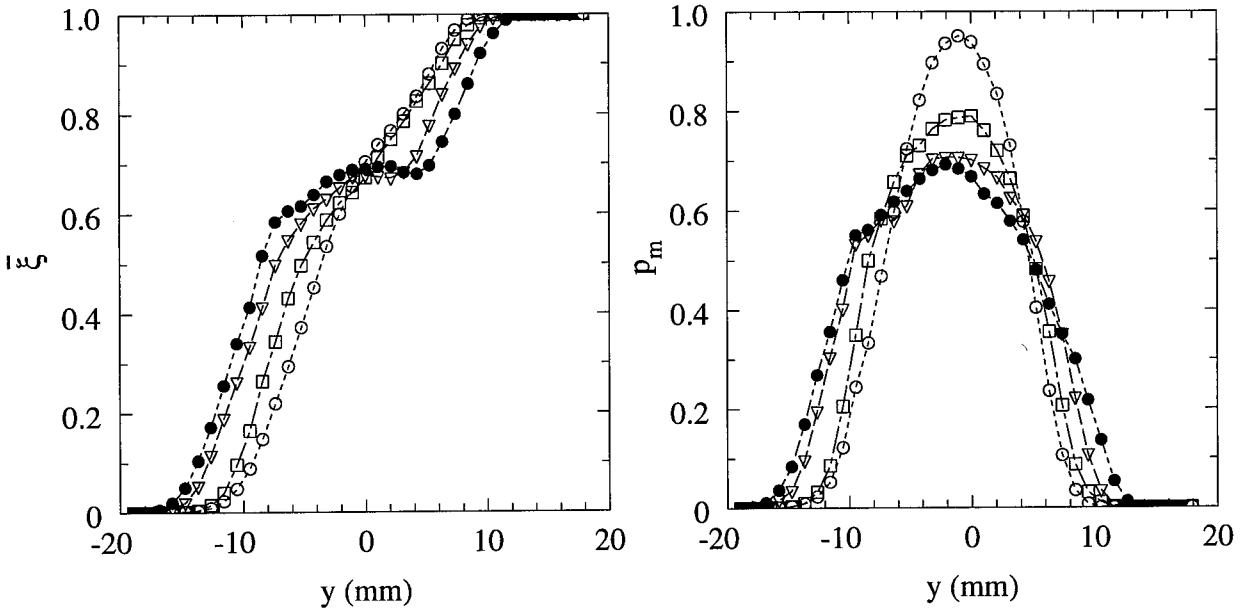

(a) Average concentration

(b) Total mixed fluid probability

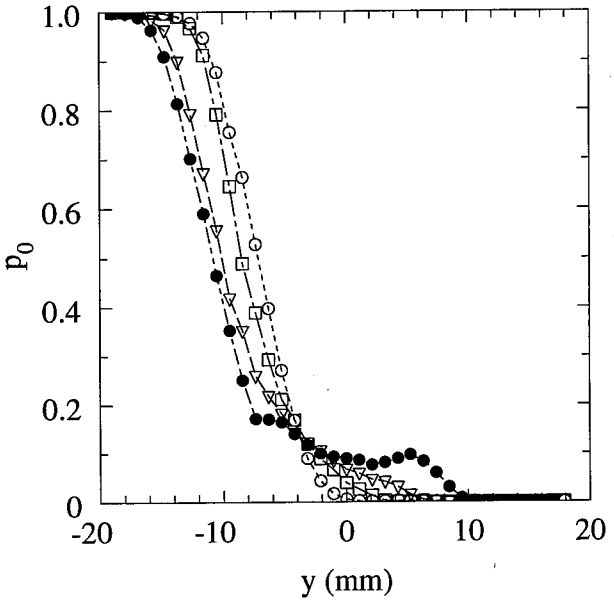

(c) Pure low-speed fluid probability

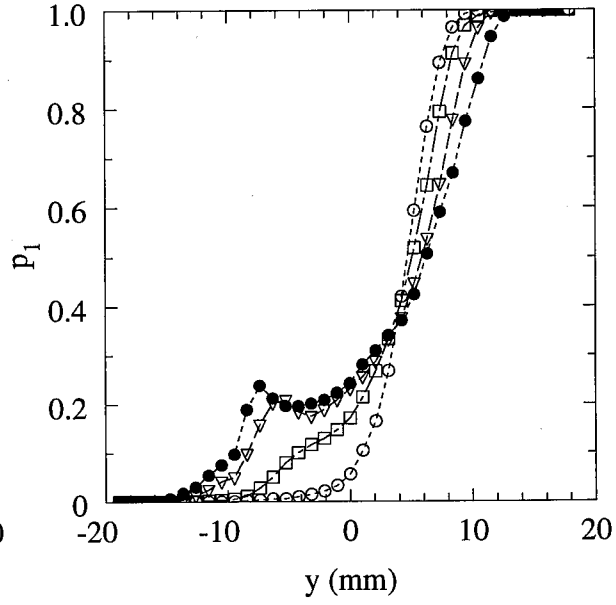

(d) Pure high-speed fluid probability

○ Unforced case, □ A = 2°, ▽ A = 4°, ● A = 6°

Figure A.12. Transverse profiles for the shear layer forced at f = 8 Hz as a function of the forcing amplitude A, at x^* = 1.24, compared to the unforced case.

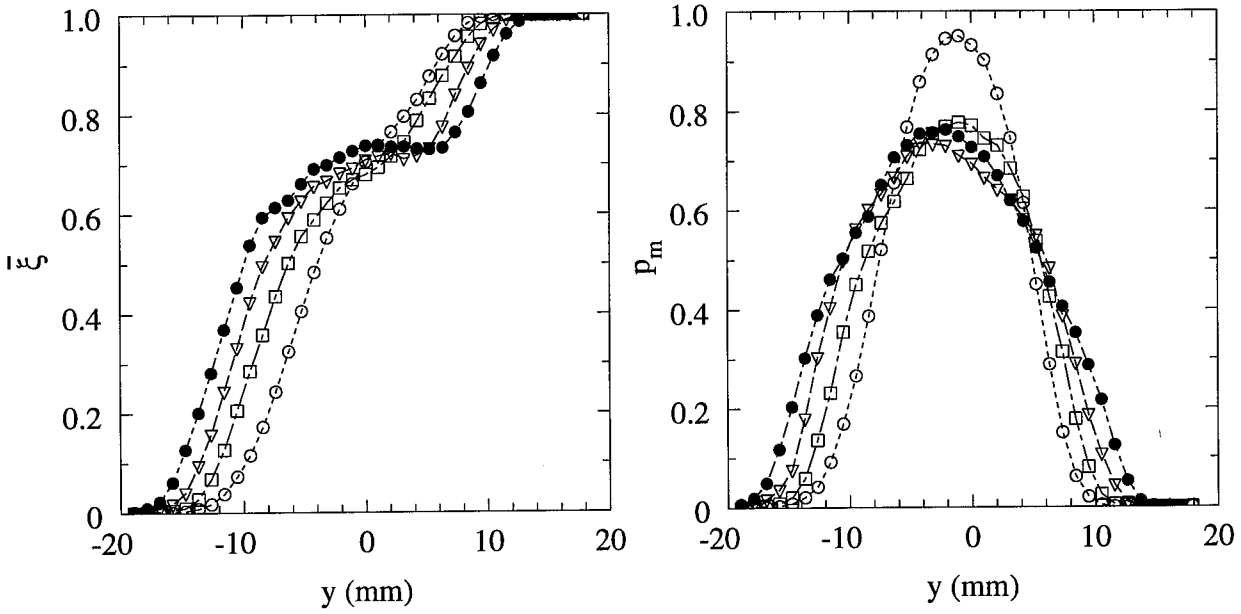

(a) Average concentration

(b) Total mixed fluid probability

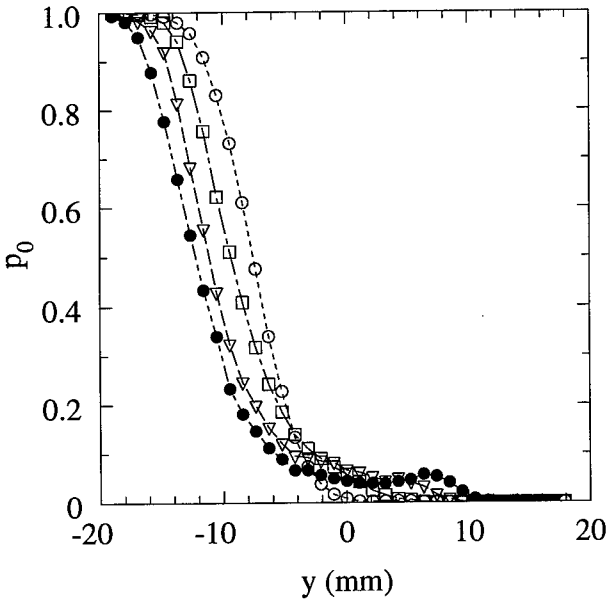

(c) Pure low-speed fluid probability

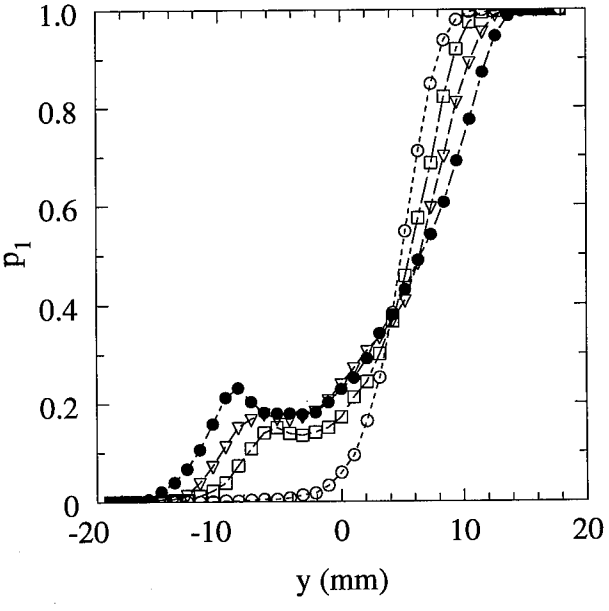

(d) Pure high-speed fluid probability

○ Unforced case, □ $A = 2°$, ▽ $A = 4°$, ● $A = 6°$

Figure A.13. Transverse profiles for the shear layer forced at $f = 8$ Hz as a function of the forcing amplitude A, at $x^* = 1.38$, compared to the unforced case.

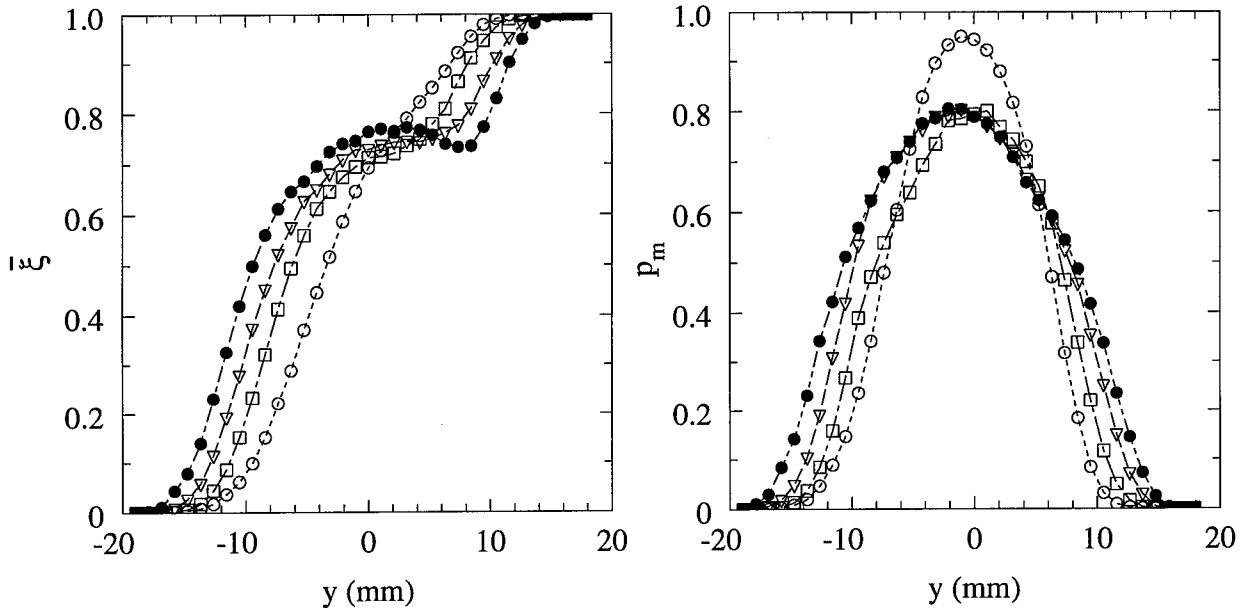

(a) Average concentration

(b) Total mixed fluid probability

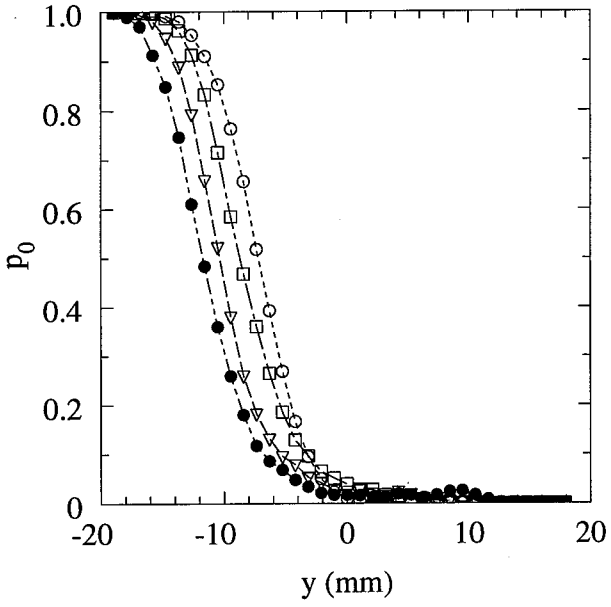

(c) Pure low-speed fluid probability

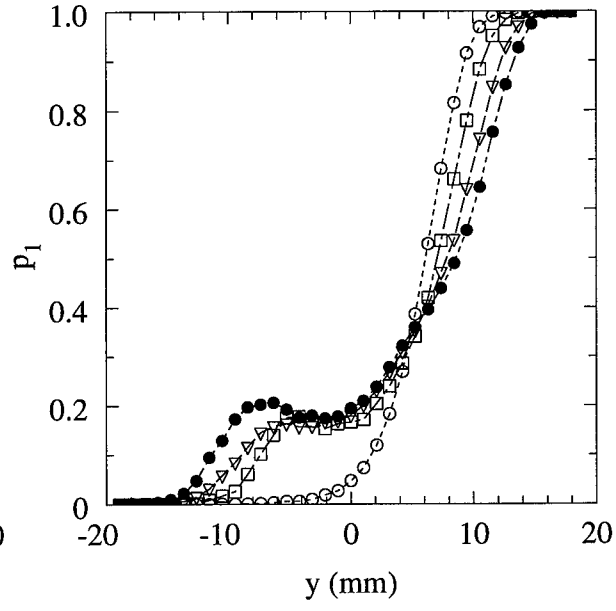

(d) Pure high-speed fluid probability

○ Unforced case, □ $A = 2°$, ▽ $A = 4°$, ● $A = 6°$

Figure A.14. Transverse profiles for the shear layer forced at $f = 8$ Hz as a function of the forcing amplitude A, at $x^* = 1.51$, compared to the unforced case.

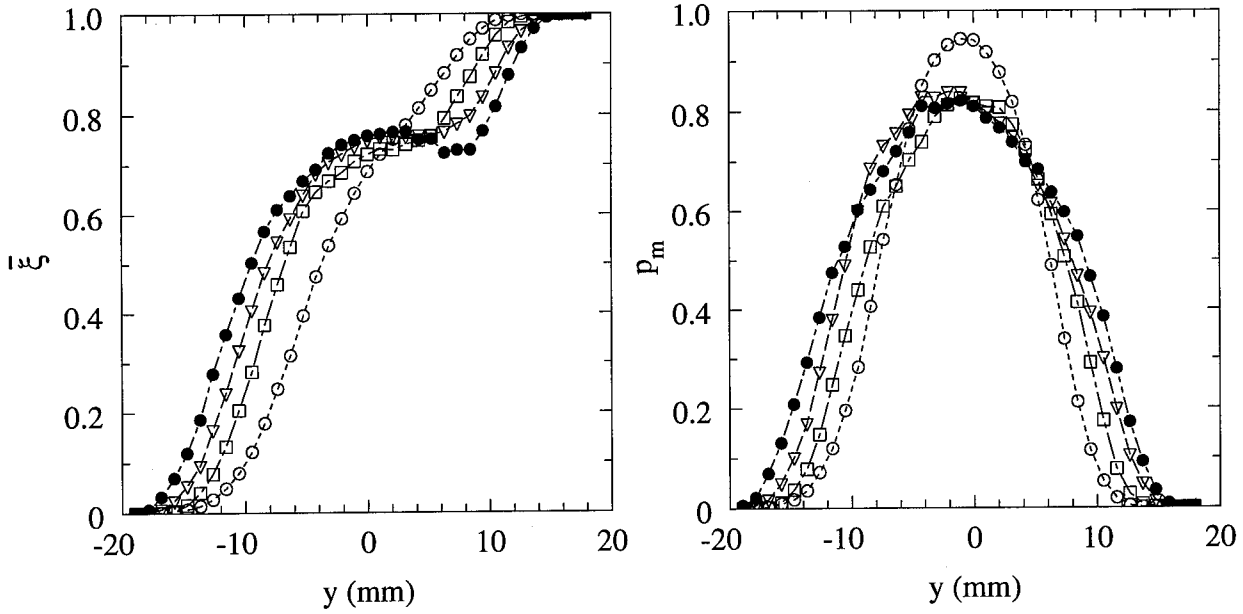

(a) Average concentration

(b) Total mixed fluid probability

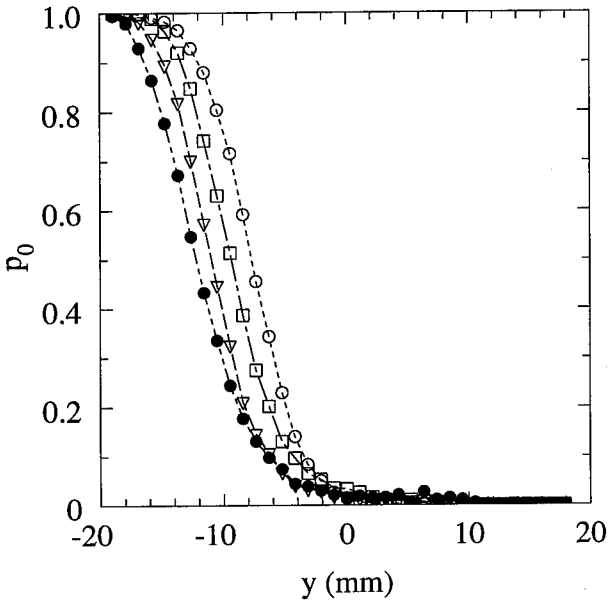

(c) Pure low-speed fluid probability

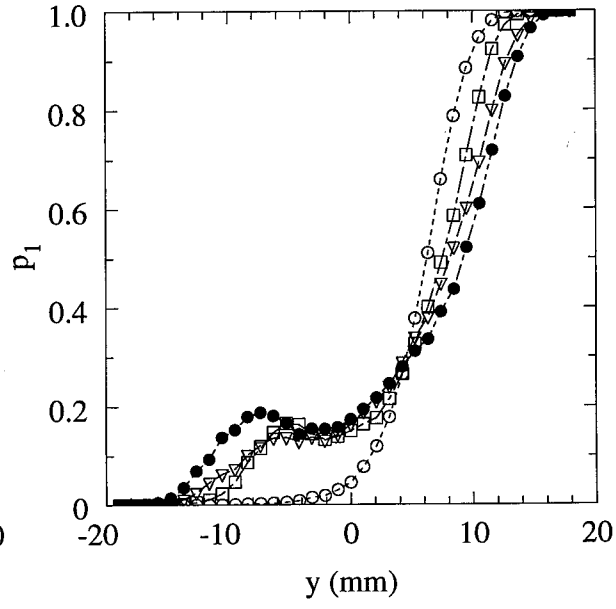

(d) Pure high-speed fluid probability

○ Unforced case, □ $A = 2°$, ▽ $A = 4°$, ● $A = 6°$

Figure A.15. Transverse profiles for the shear layer forced at $f = 8$ Hz as a function of the forcing amplitude A, at $x^* = 1.64$, compared to the unforced case.

APPENDIX B

Distribution of mixed fluid composition

The distribution of mixed fluid composition across the height of the test section for the unforced and forced shear layers are shown in Figures B.1 - B.10 as a function of the streamwise coordinate. From these Figures it is noted that the pdf is essentially uniform across the height of the test section, similar to the results of Koochesfahani (1984) and Koochesfahani and M^{ac}Kinnon (1991).

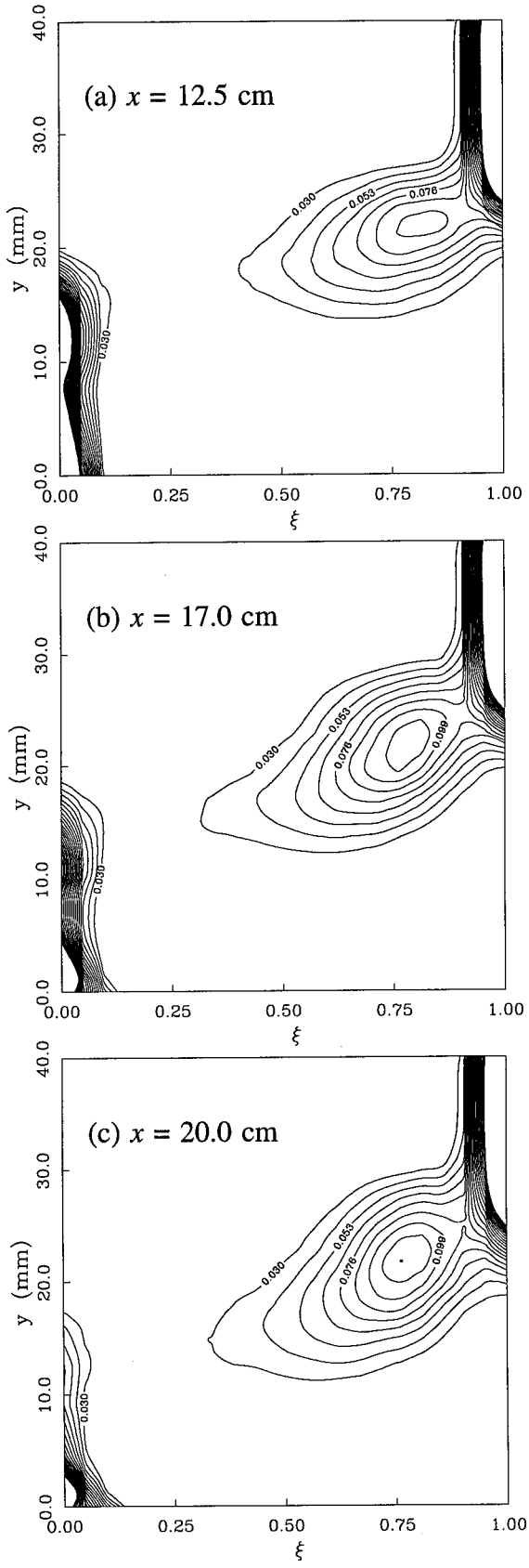

Figure B.1. Composition distribution for the unforced shear layer.

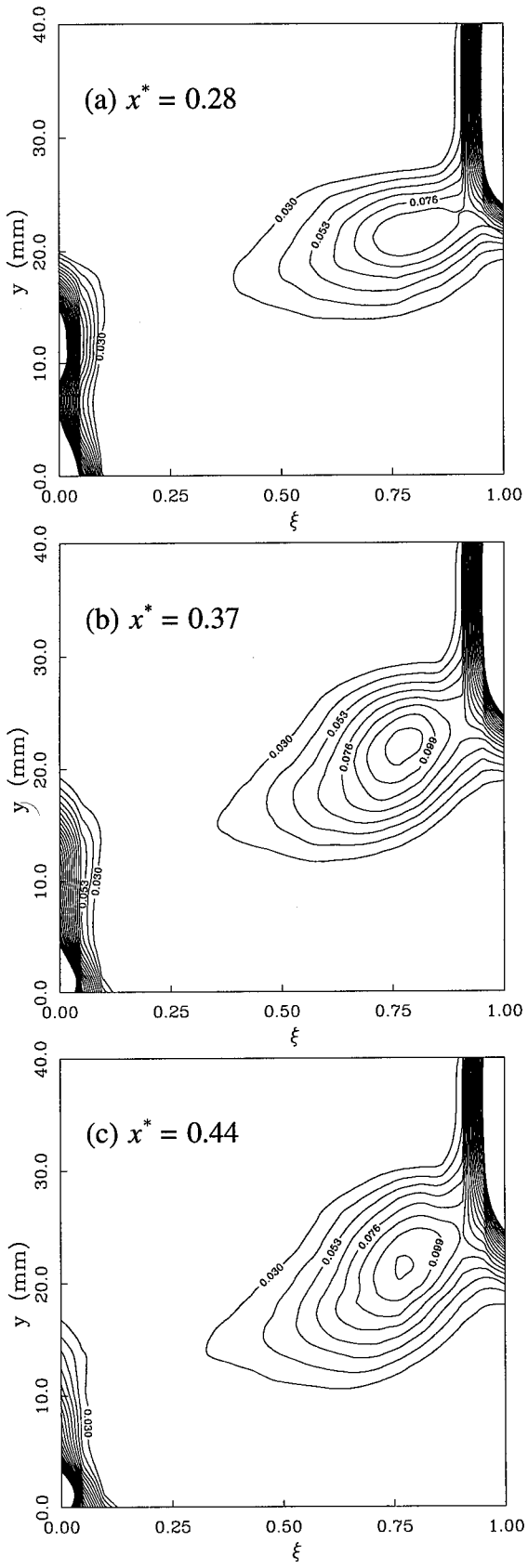

Figure B.2. Composition distribution for the shear layer forced at $f = 2$ Hz, $A = 2°$.

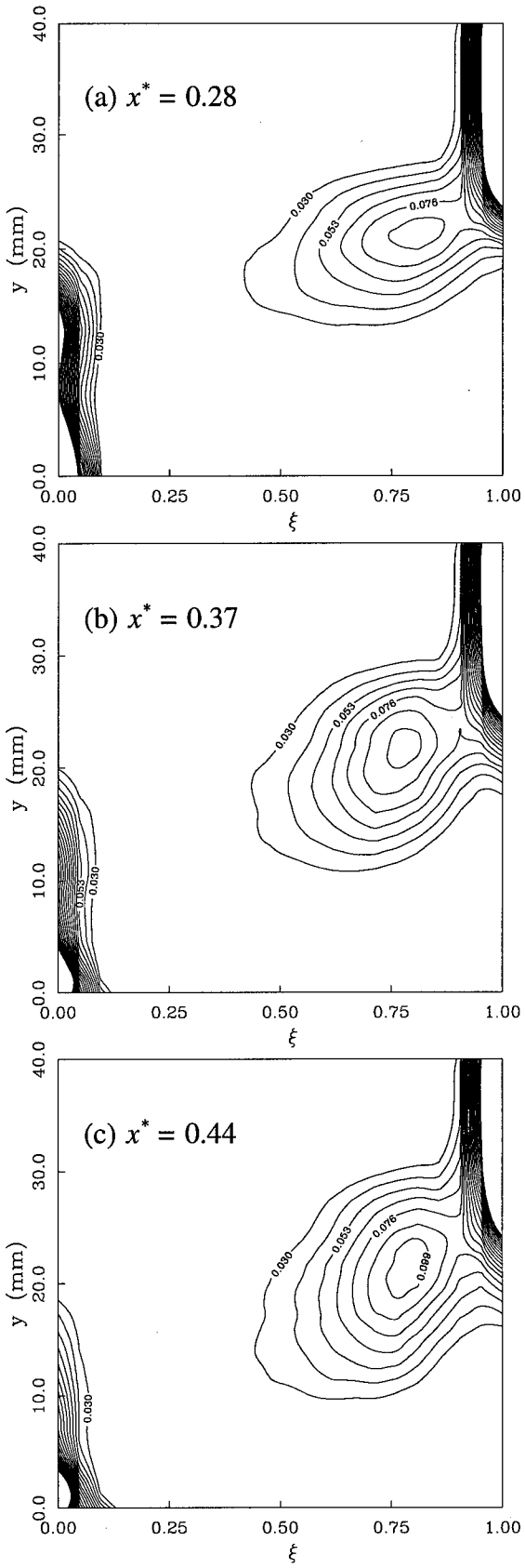

Figure B.3. Composition distribution for the shear layer forced at $f = 2$ Hz, $A = 4°$.

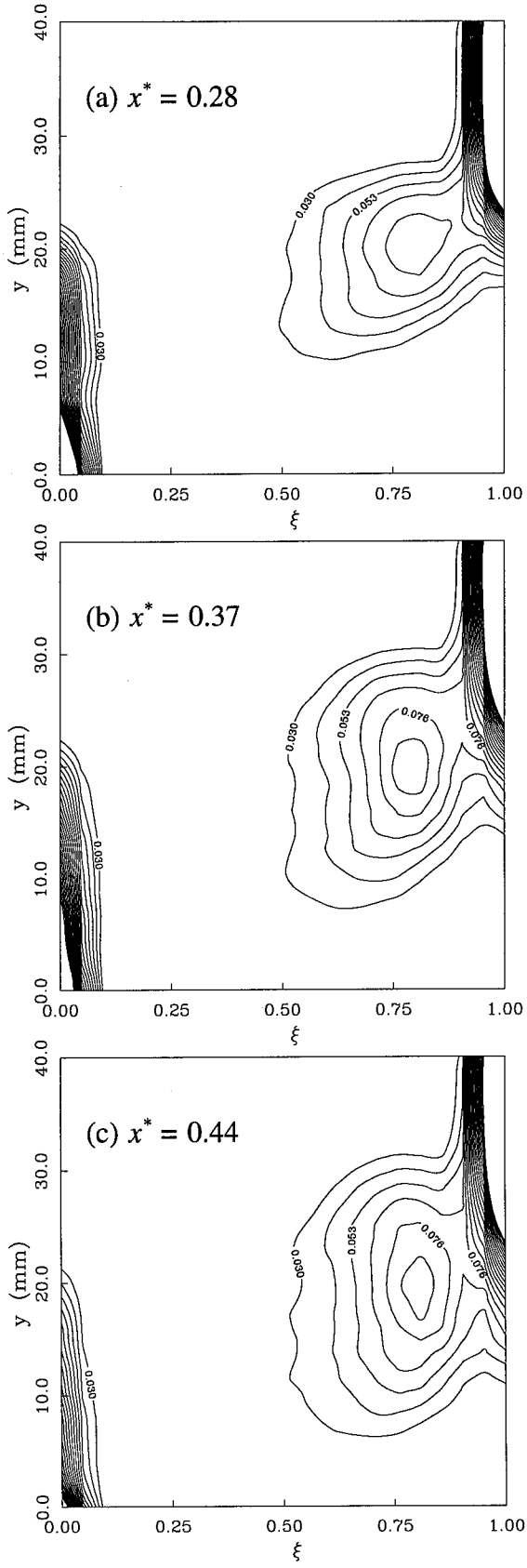

Figure B.4. Composition distribution for the shear layer forced at $f = 2$ Hz, $A = 8°$.

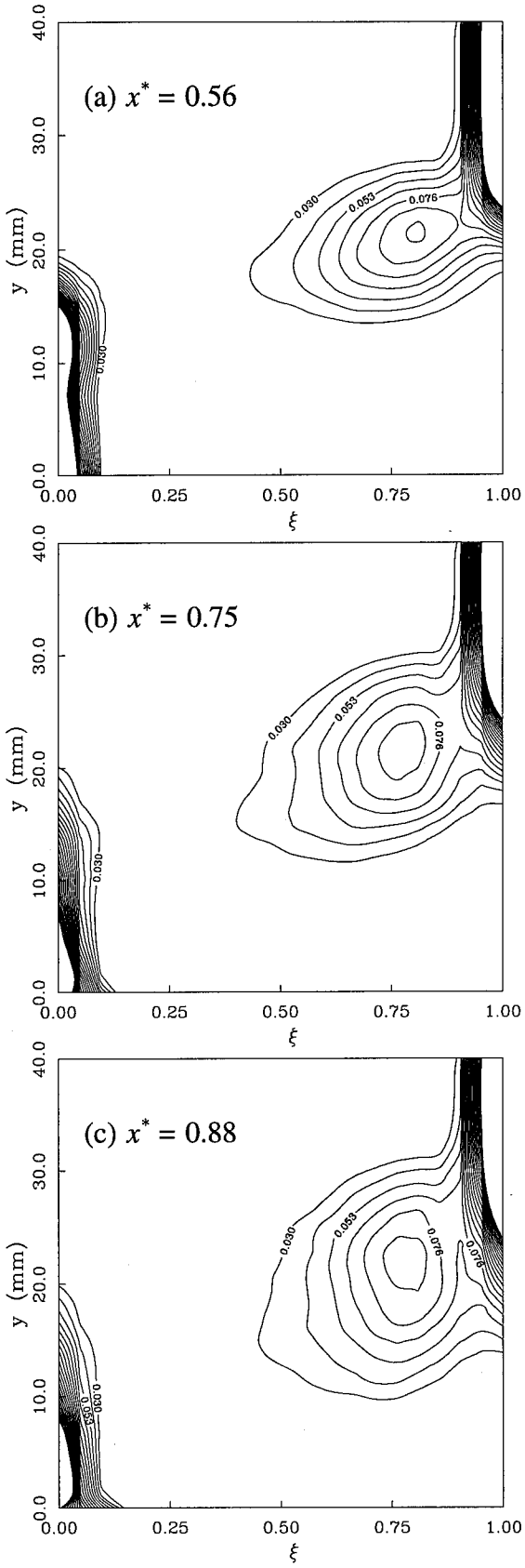

Figure B.5. Composition distribution for the shear layer forced at f = 4 Hz, A = 2°.

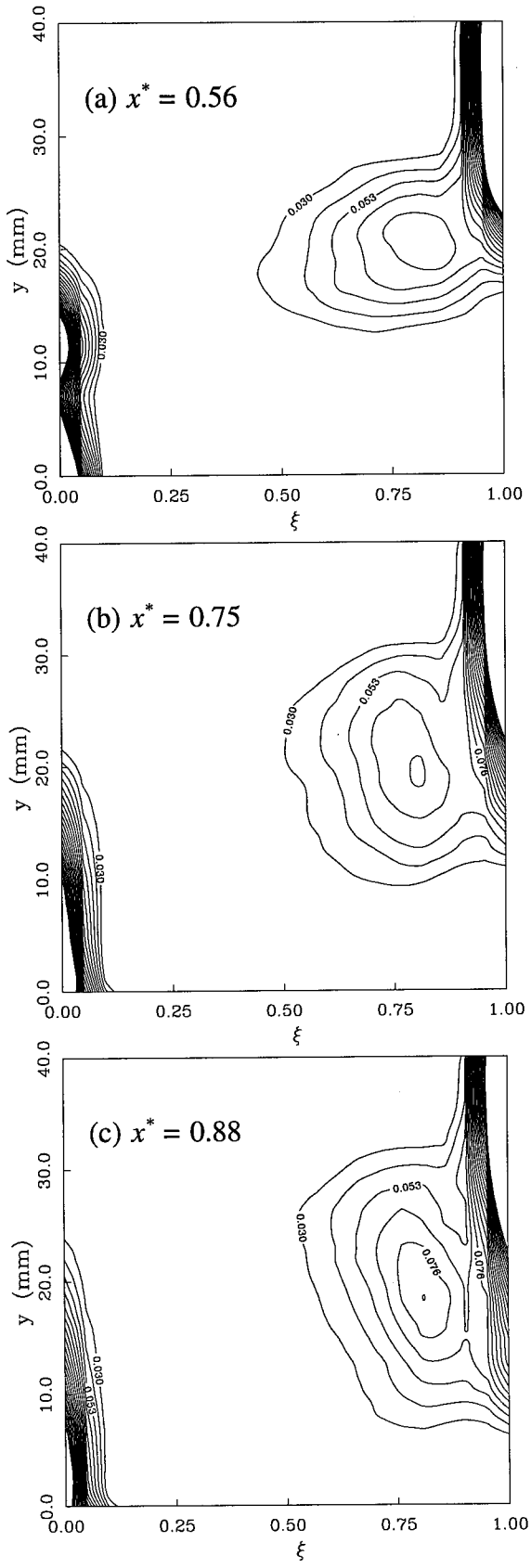

Figure B.6. Composition distribution for the shear layer forced at $f = 4$ Hz, $A = 4°$.

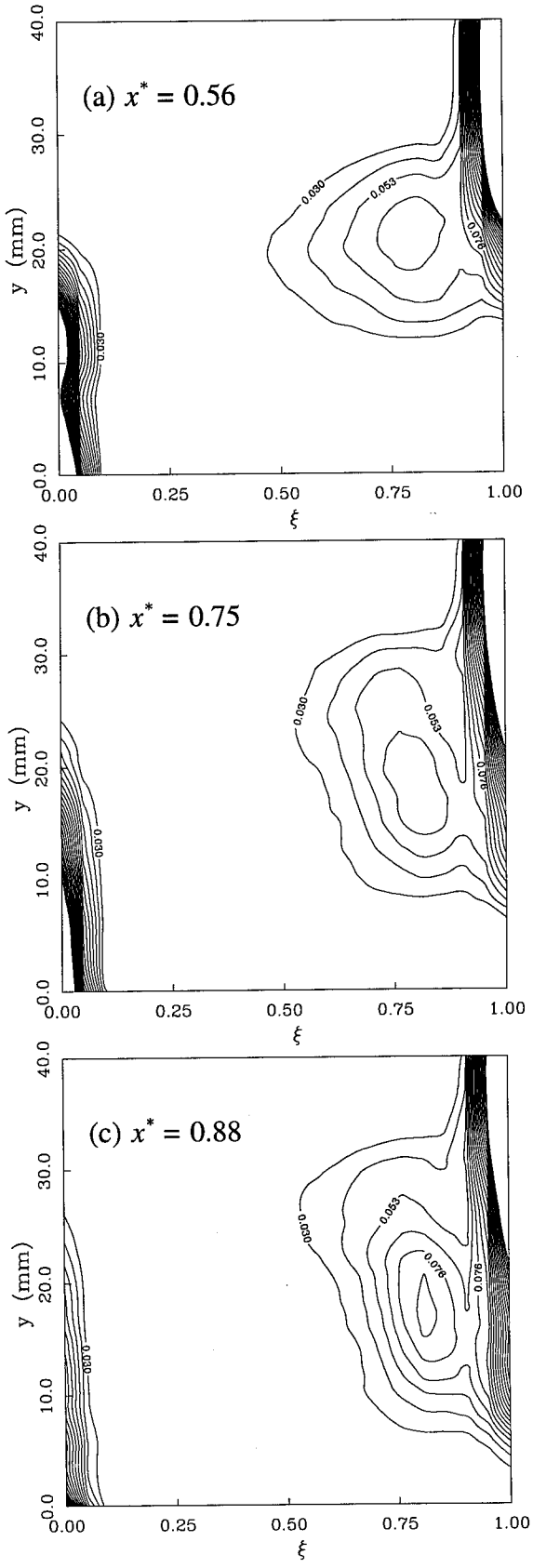

Figure B.7. Composition distribution for the shear layer forced at $f = 4$ Hz, $A = 6°$.

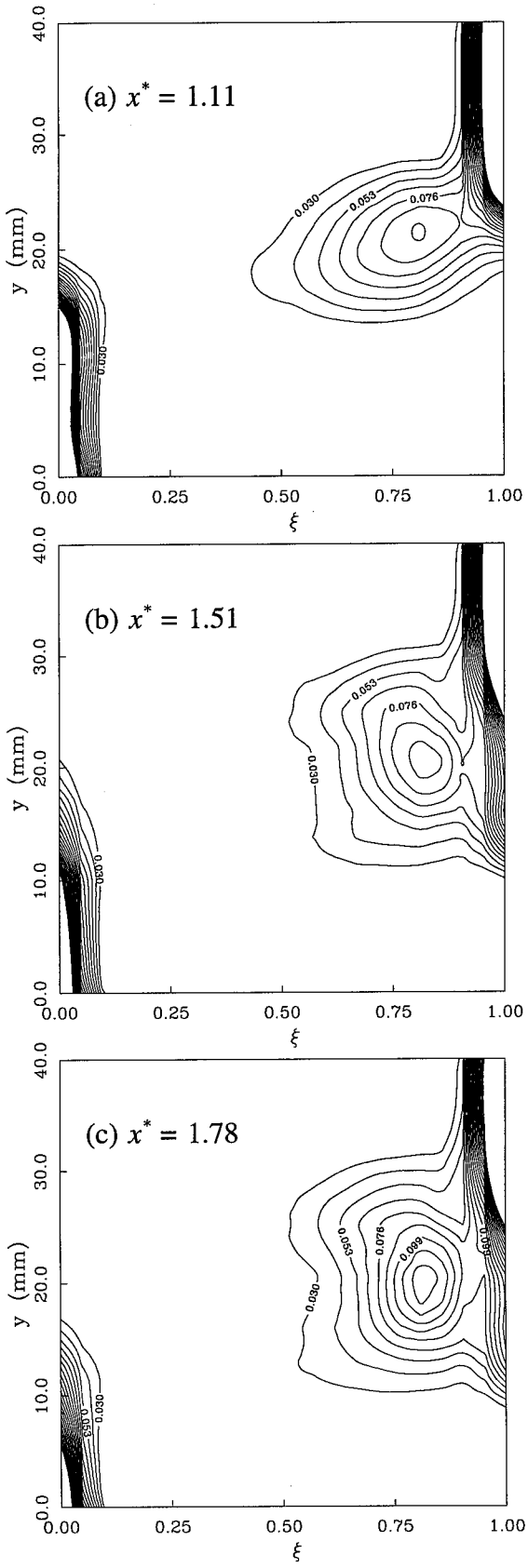

Figure B.8. Composition distribution for the shear layer forced at $f = 8$ Hz, $A = 2°$.

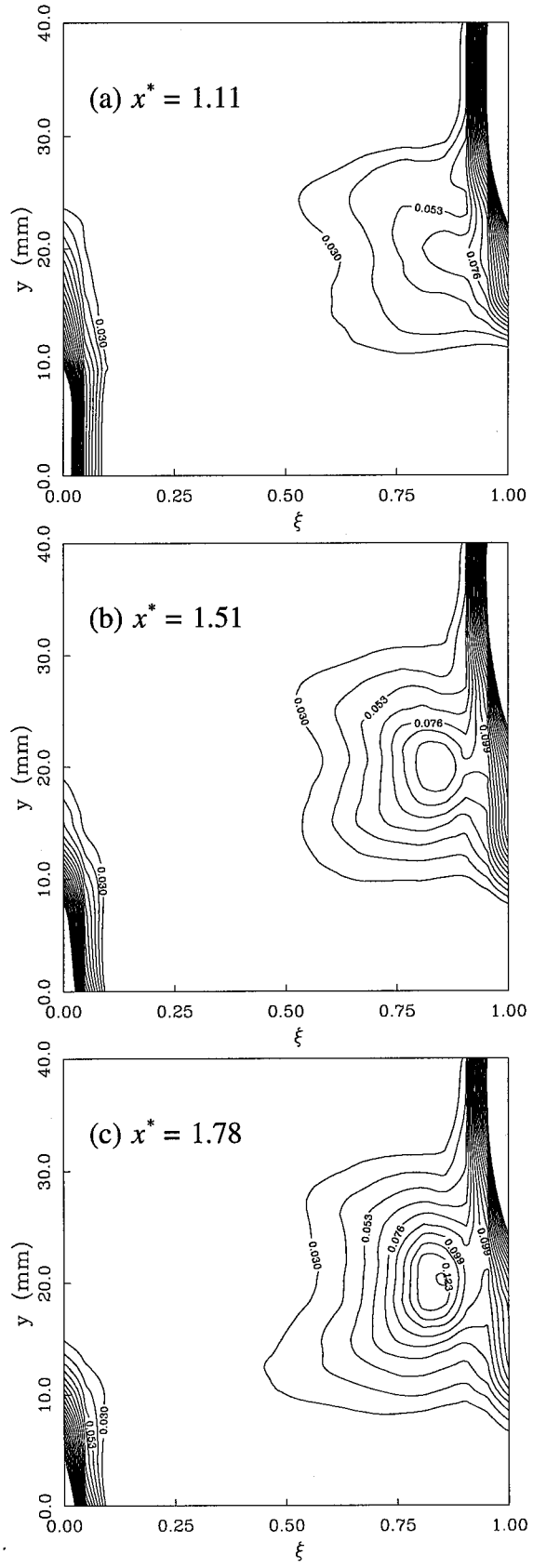

Figure B.9. Composition distribution for the shear layer forced at f = 8 Hz, A = 4°.

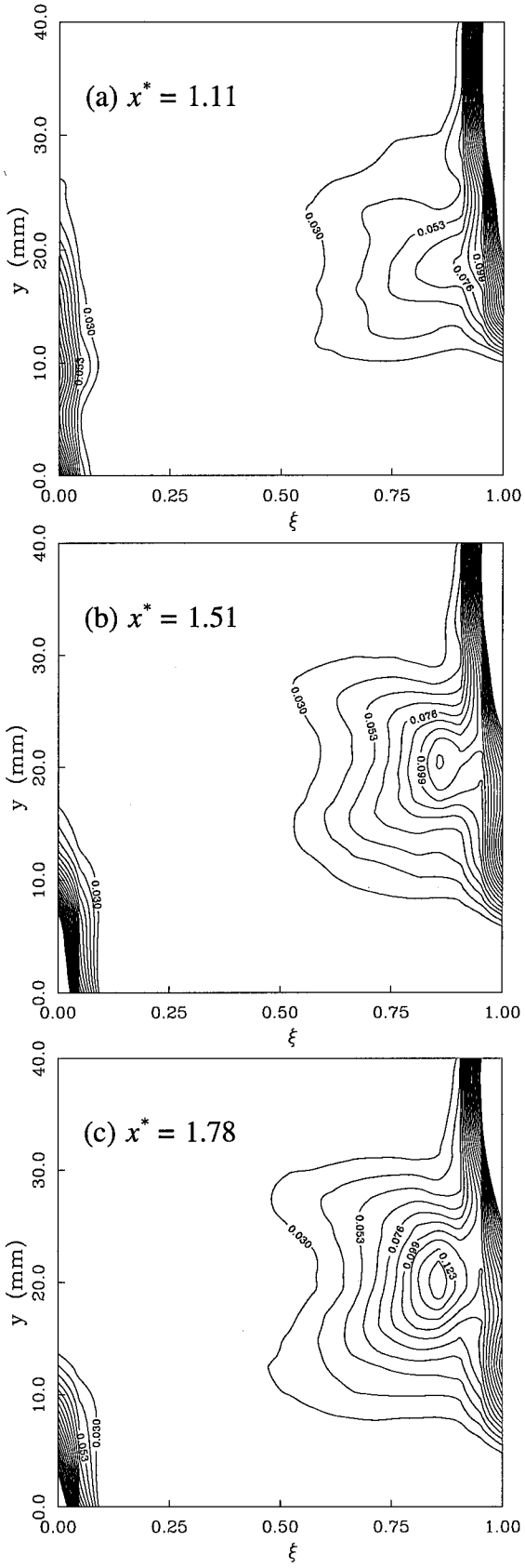

Figure B.10. Composition distribution for the shear layer forced at f = 8 Hz, A = 6°.

APPENDIX C

Streamwise evolution of the total pdf

Streamwise evolution of the total pdf for the forced shear layers not presented in Section 3.5.1 are shown in Figures C.1 - C.6.

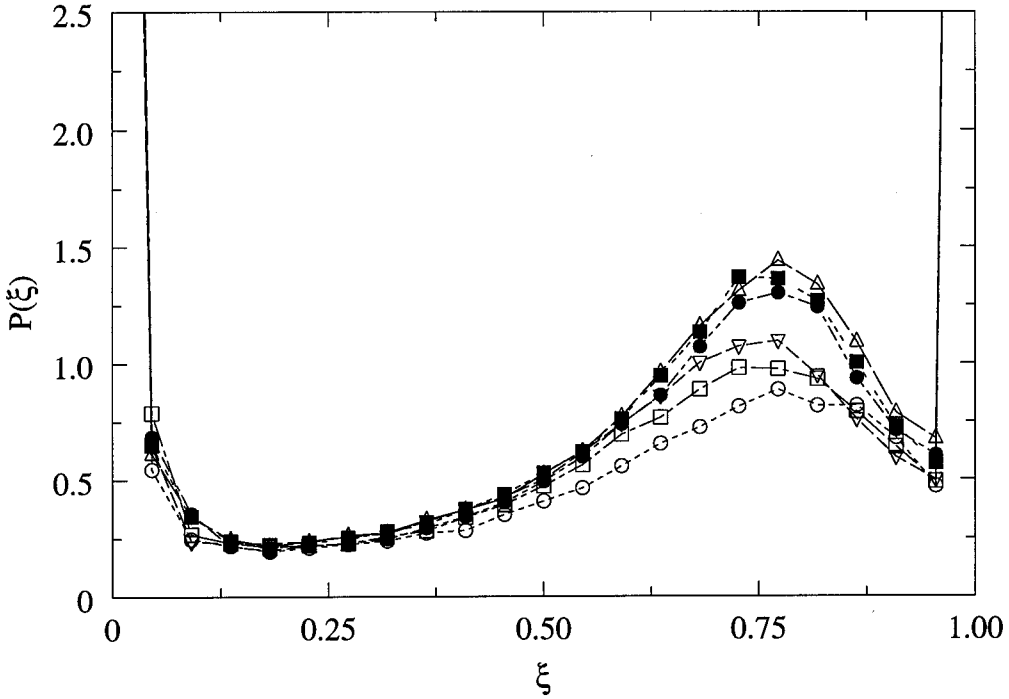

○ $x^* = 0.28$, □ $x^* = 0.31$, ▽ $x^* = 0.34$, ● $x^* = 0.37$, ■ $x^* = 0.41$, △ $x^* = 0.44$

Figure C.1. Streamwise evolution of the total pdf for the shear layer forced at $f = 2$ Hz, $A = 2°$.

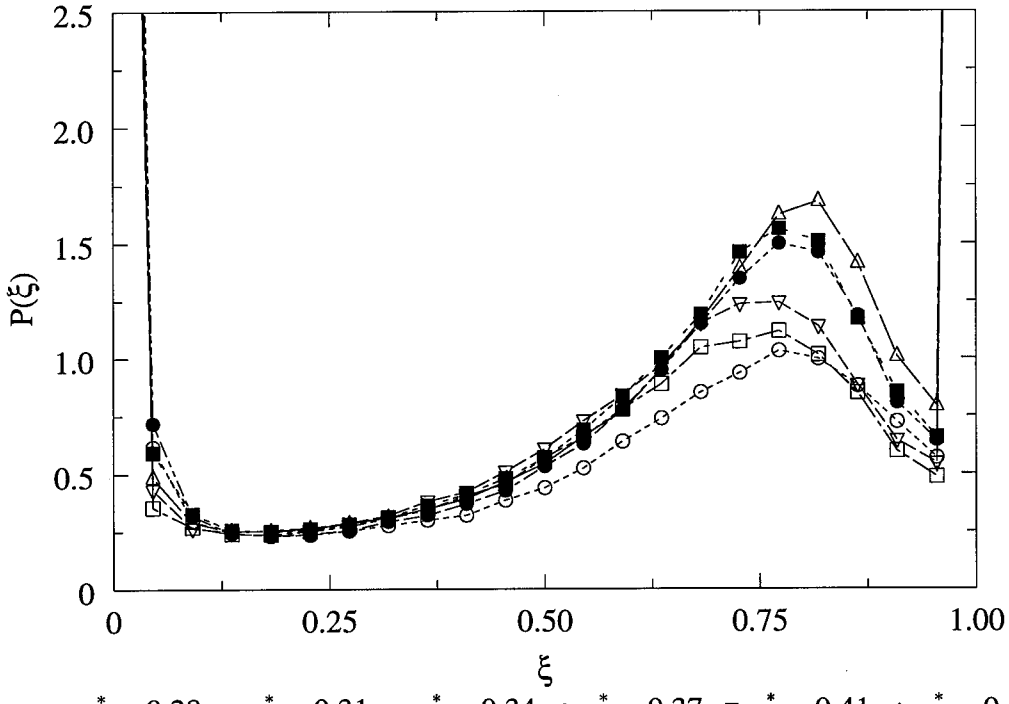

○ $x^* = 0.28$, □ $x^* = 0.31$, ▽ $x^* = 0.34$, ● $x^* = 0.37$, ■ $x^* = 0.41$, △ $x^* = 0.44$

Figure C.2. Streamwise evolution of the total pdf for the shear layer forced at $f = 2$ Hz, $A = 8°$.

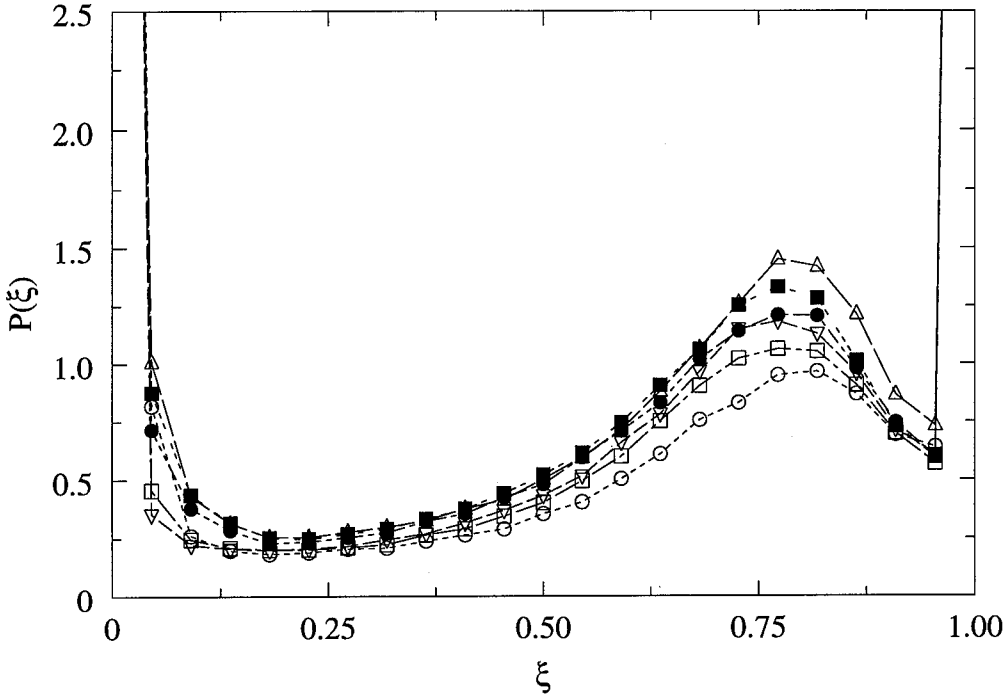

○ $x^* = 0.56$, □ $x^* = 0.62$, ▽ $x^* = 0.68$, ● $x^* = 0.75$, ■ $x^* = 0.82$, △ $x^* = 0.88$

Figure C.3. Streamwise evolution of the total pdf for the shear layer forced at $f = 4$ Hz, $A = 2°$.

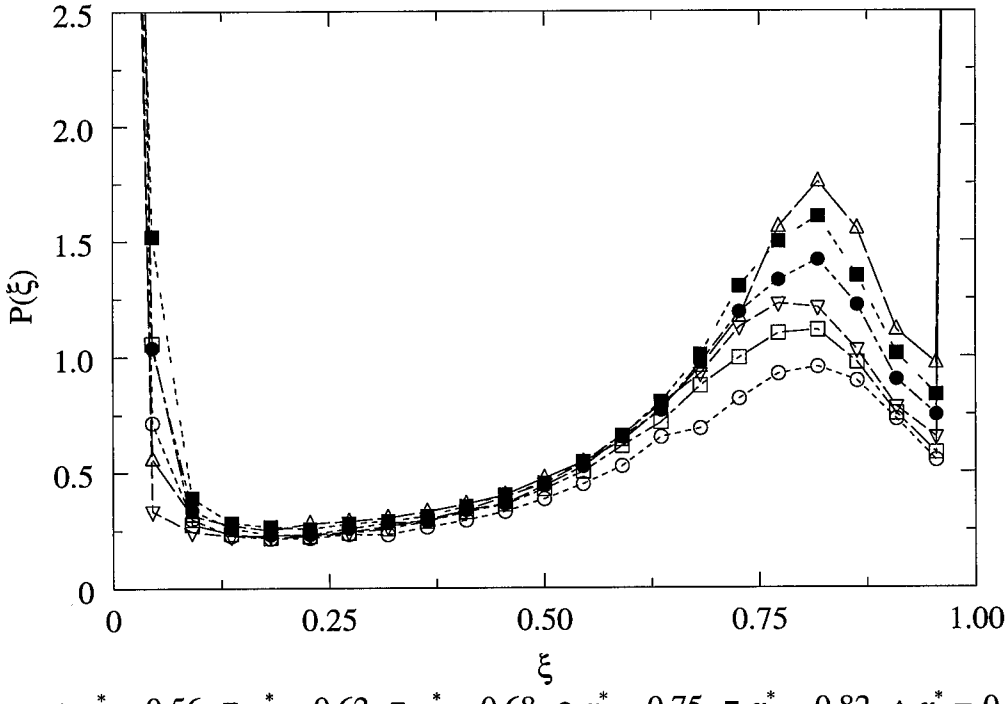

○ $x^* = 0.56$, □ $x^* = 0.62$, ▽ $x^* = 0.68$, ● $x^* = 0.75$, ■ $x^* = 0.82$, △ $x^* = 0.88$

Figure C.4. Streamwise evolution of the total pdf for the shear layer forced at $f = 4$ Hz, $A = 6°$.

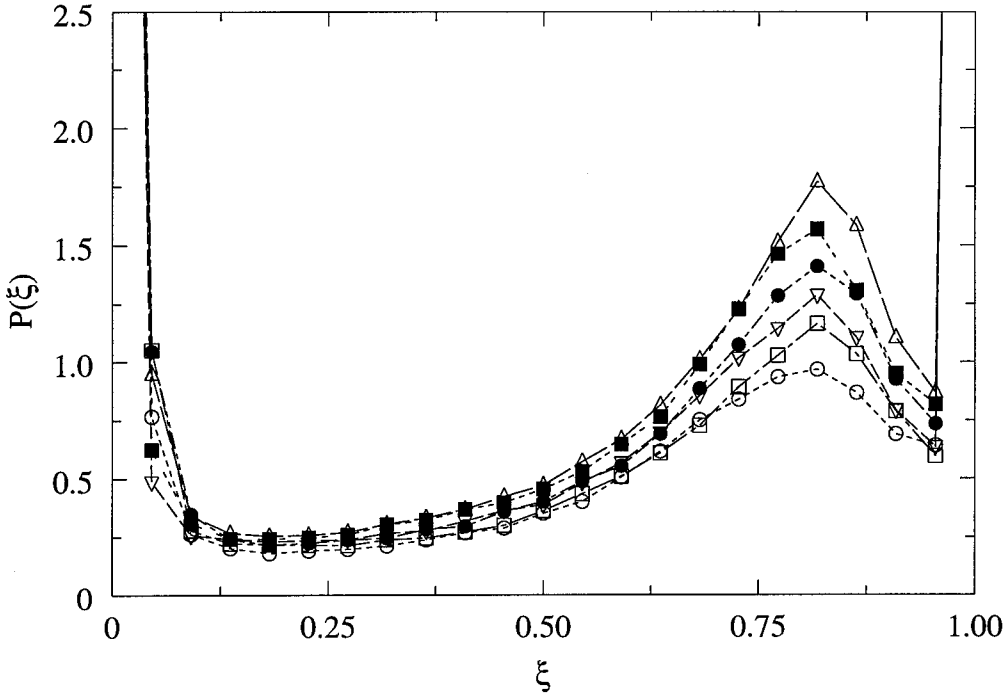

○ $x^* = 1.11$, □ $x^* = 1.24$, ▽ $x^* = 1.38$, ● $x^* = 1.51$, ■ $x^* = 1.64$, △ $x^* = 1.78$

Figure C.5. Streamwise evolution of the total pdf for the shear layer forced at $f = 8$ Hz, $A = 2°$.

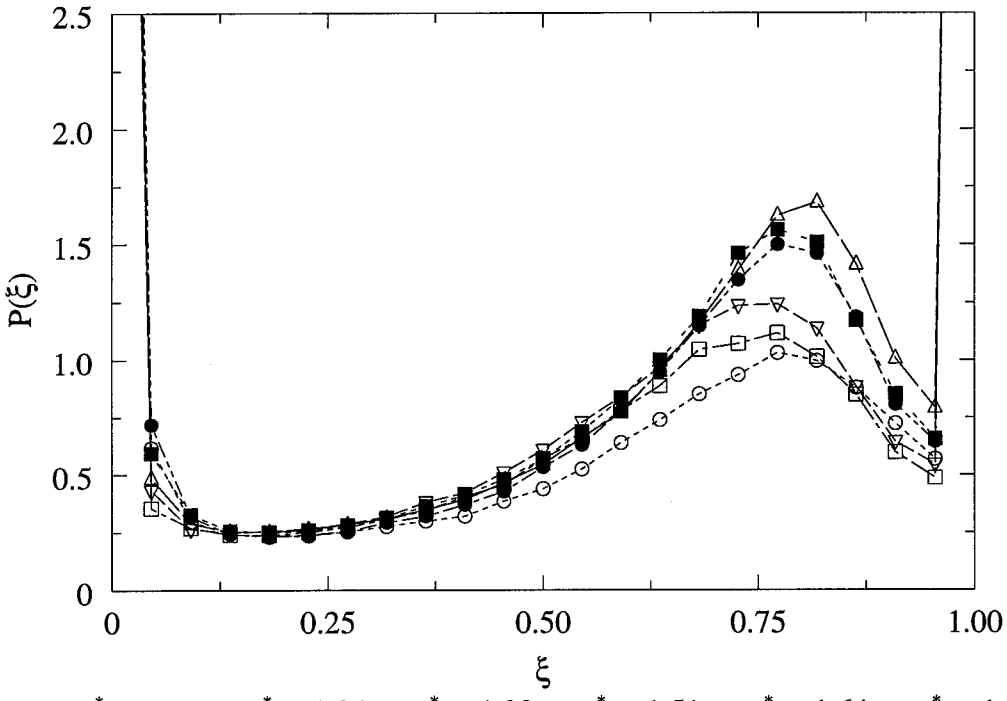

○ $x^* = 1.11$, □ $x^* = 1.24$, ▽ $x^* = 1.38$, ● $x^* = 1.51$, ■ $x^* = 1.64$, △ $x^* = 1.78$

Figure C.6. Streamwise evolution of the total pdf for the shear layer forced at $f = 8$ Hz, $A = 6°$.

APPENDIX D

Amplitude dependence of the total pdf

Amplitude dependence of the total pdf for the forced shear layers at the downstream locations not presented in Section 3.5.2 are shown in Figures D.1 - D.15.

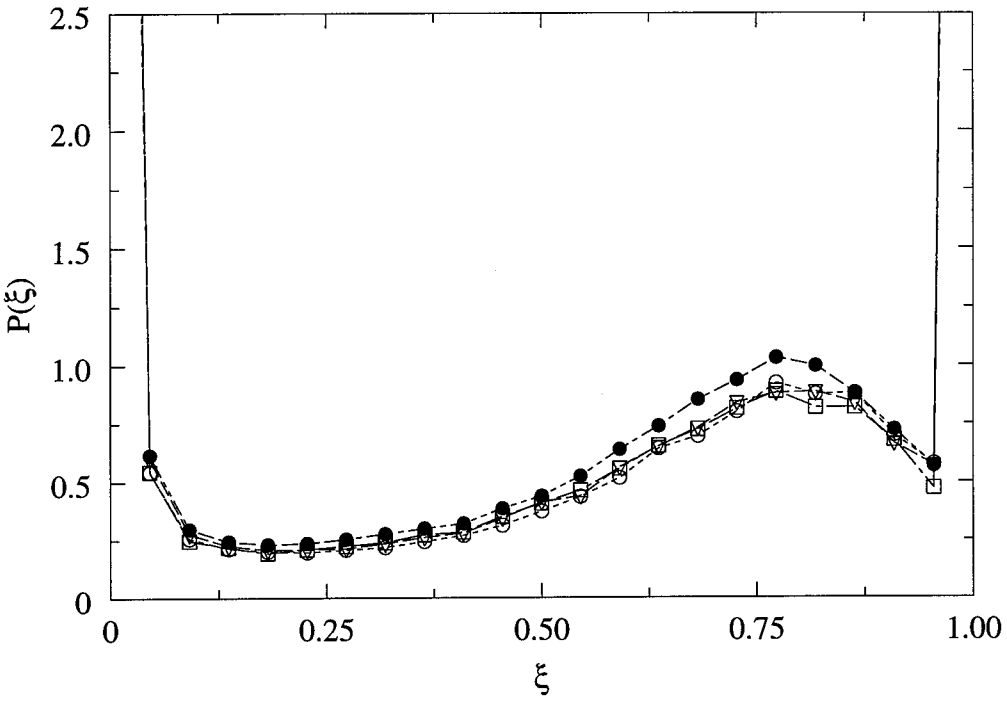

○ Unforced case, □ $A = 2°$, ▽ $A = 4°$, ● $A = 8°$

Figure D.1. Amplitude dependence of the total pdf for the shear layer forced at $f = 2$ Hz, at $x = 12.5$ cm ($x^* = 0.28$), compared to the unforced case.

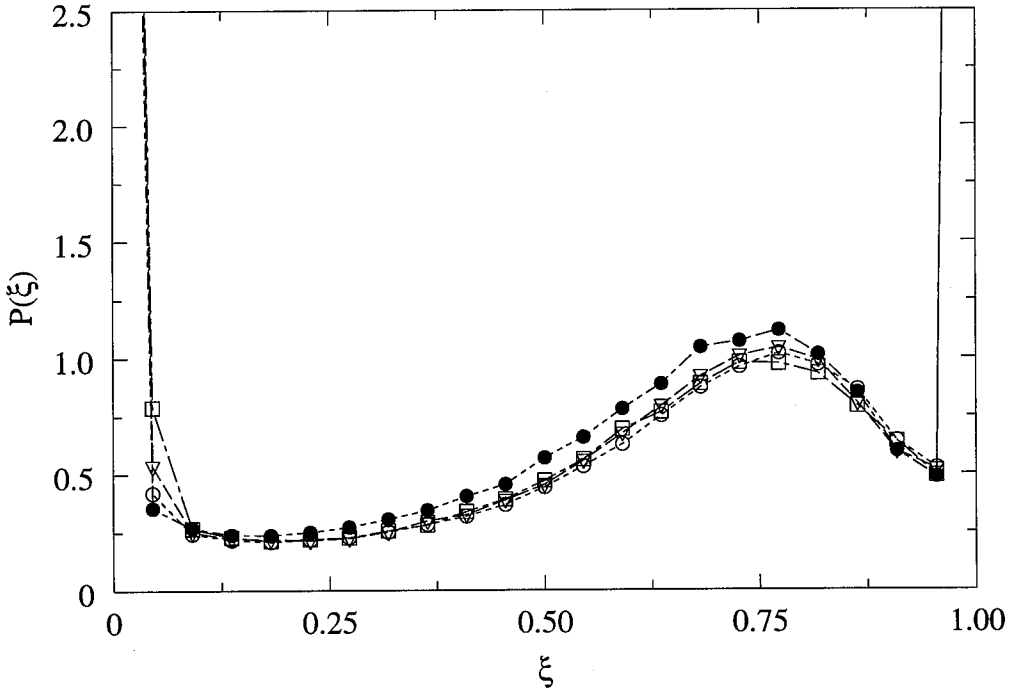

○ Unforced case, □ $A = 2°$, ▽ $A = 4°$, ● $A = 8°$

Figure D.2. Amplitude dependence of the total pdf for the shear layer forced at $f = 2$ Hz, at $x = 14.0$ cm ($x^* = 0.31$), compared to the unforced case.

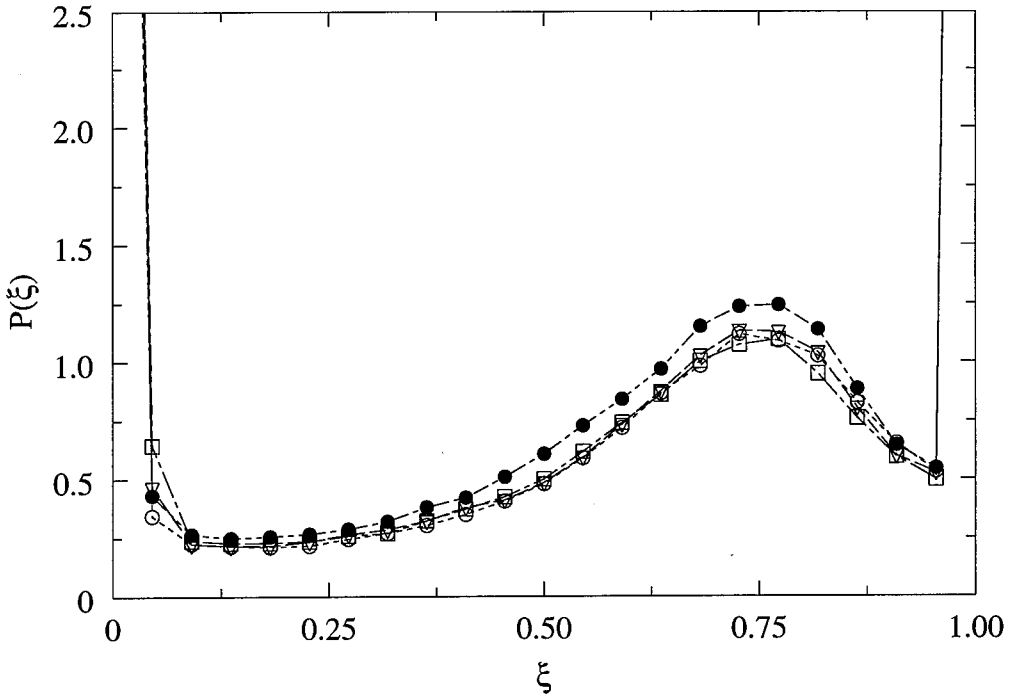

○ Unforced case, □ $A = 2°$, ▽ $A = 4°$, ● $A = 8°$

Figure D.3. Amplitude dependence of the total pdf for the shear layer forced at $f = 2$ Hz, at $x = 15.5$ cm ($x^* = 0.34$), compared to the unforced case.

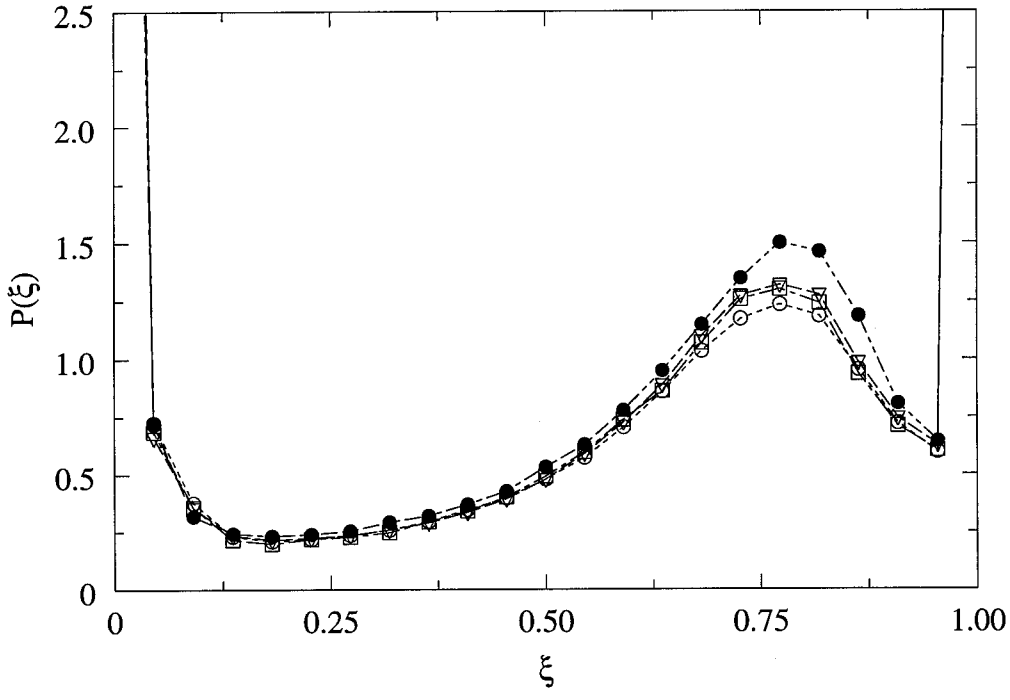

○ Unforced case, □ $A = 2°$, ▽ $A = 4°$, ● $A = 8°$

Figure D.4. Amplitude dependence of the total pdf for the shear layer forced at $f = 2$ Hz, at $x = 17.0$ cm ($x^* = 0.37$), compared to the unforced case.

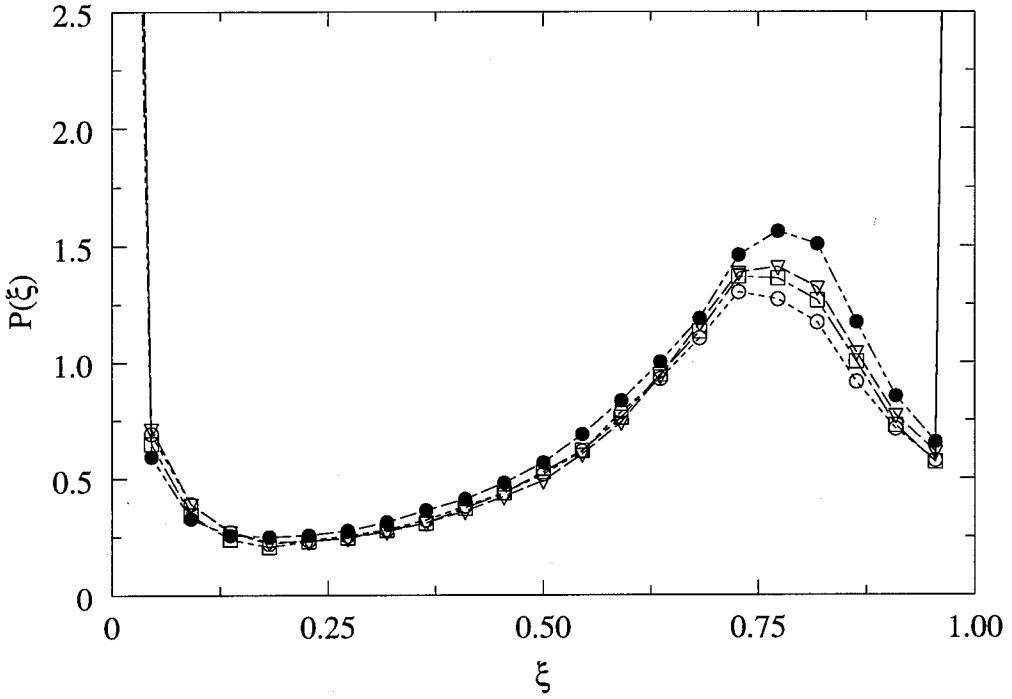

○ Unforced case, □ $A = 2°$, ▽ $A = 4°$, ● $A = 8°$

Figure D.5. Amplitude dependence of the total pdf for the shear layer forced at $f = 2$ Hz, at $x = 18.5$ cm ($x^* = 0.41$), compared to the unforced case.

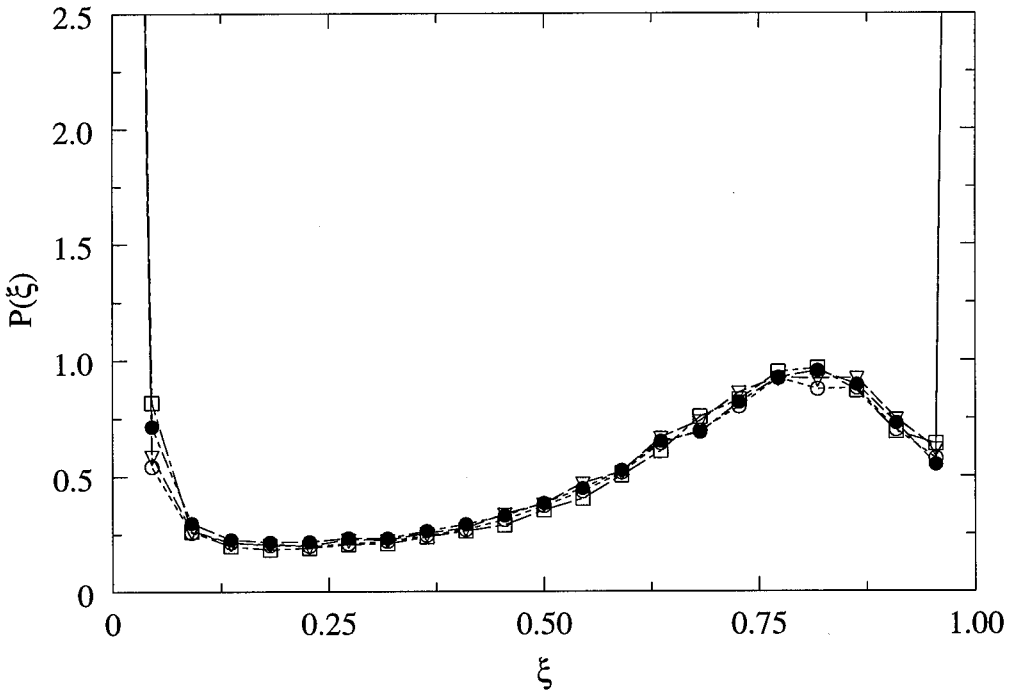

○ Unforced case, □ $A = 2°$, ▽ $A = 4°$, ● $A = 6°$

Figure D.6. Amplitude dependence of the total pdf for the shear layer forced at $f = 4$ Hz, at $x = 12.5$ cm ($x^* = 0.56$), compared to the unforced case.

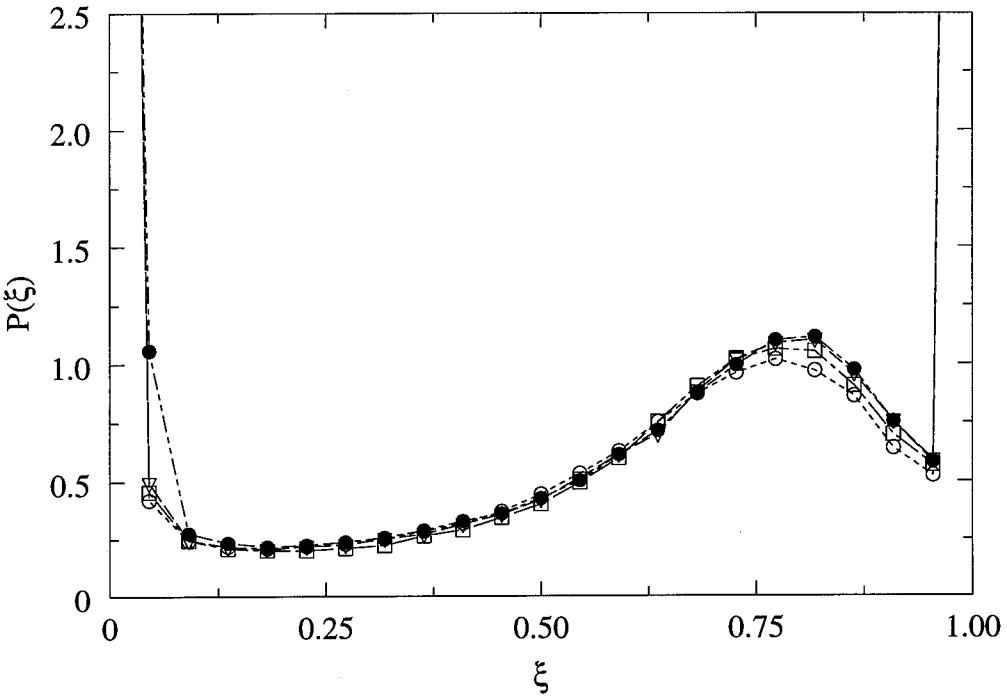

○ Unforced case, □ $A = 2°$, ▽ $A = 4°$, ● $A = 6°$

Figure D.7. Amplitude dependence of the total pdf for the shear layer forced at $f = 4$ Hz, at $x = 14.0$ cm ($x^* = 0.62$), compared to the unforced case.

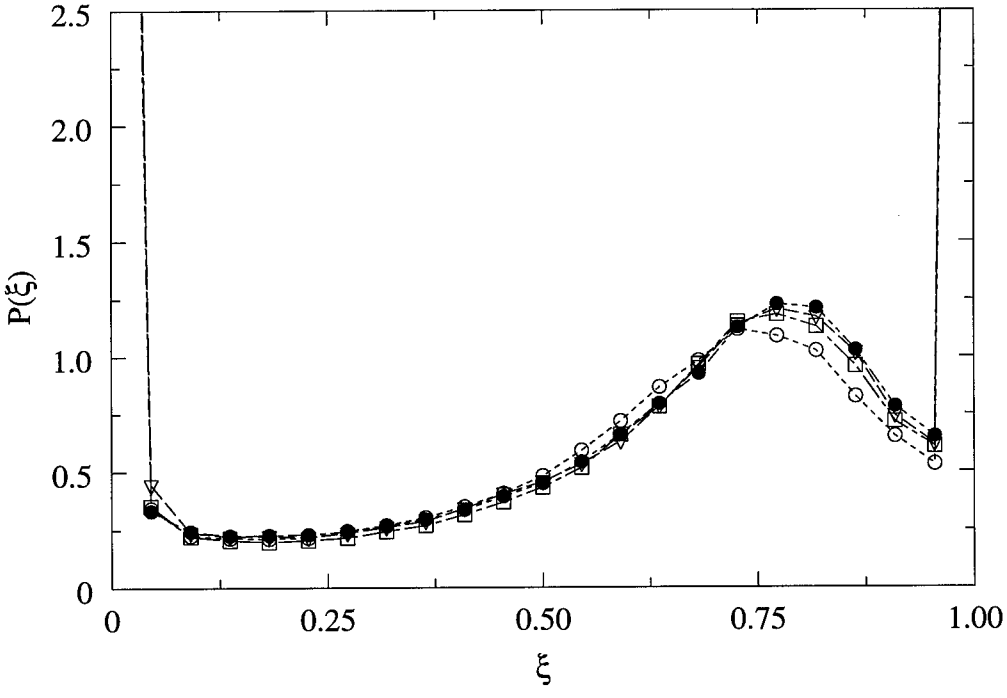

○ Unforced case, □ $A = 2°$, ▽ $A = 4°$, ● $A = 6°$

Figure D.8. Amplitude dependence of the total pdf for the shear layer forced at $f = 4$ Hz, at $x = 15.5$ cm ($x^* = 0.68$), compared to the unforced case.

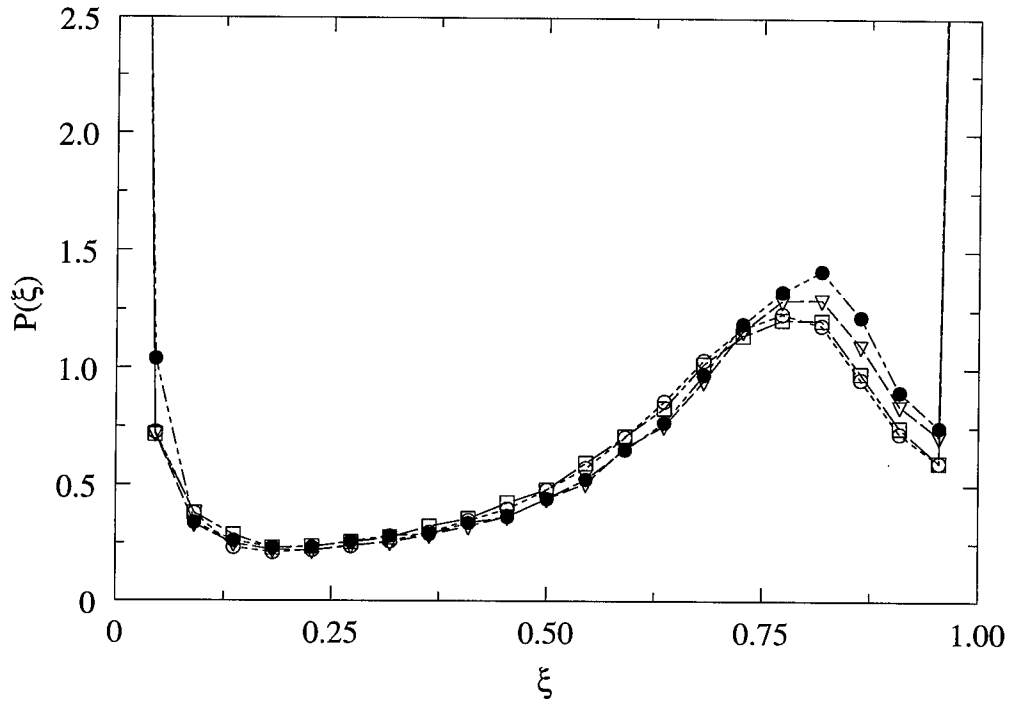

○ Unforced case, □ $A = 2°$, ▽ $A = 4°$, ● $A = 6°$

Figure D.9. Amplitude dependence of the total pdf for the shear layer forced at $f = 4$ Hz, at $x = 17.0$ cm ($x^* = 0.75$), compared to the unforced case.

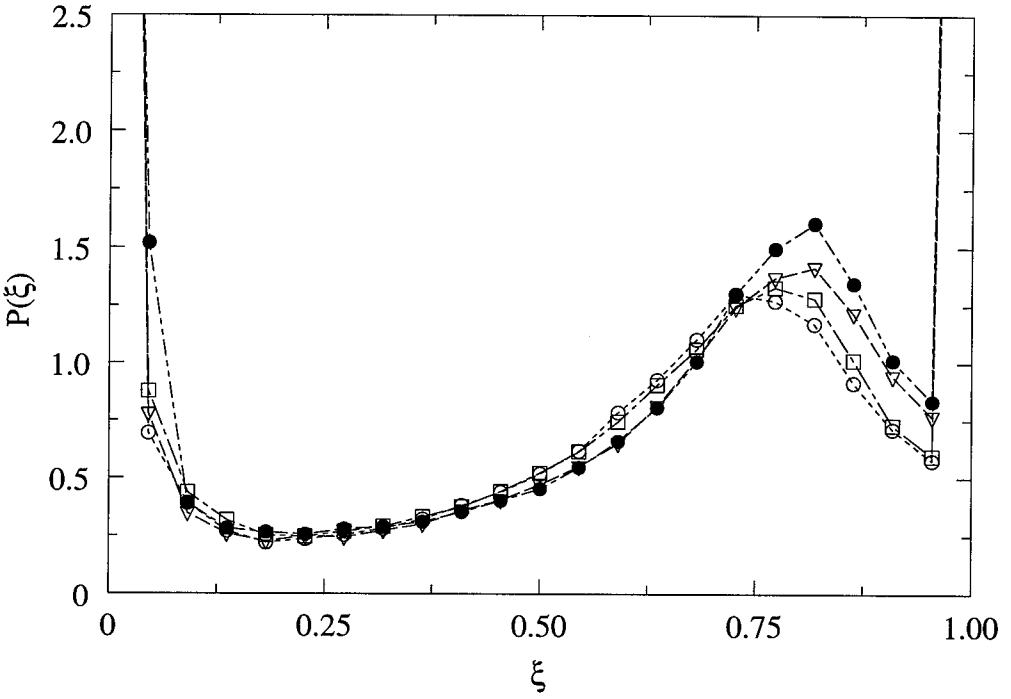

○ Unforced case, □ $A = 2°$, ▽ $A = 4°$, ● $A = 6°$

Figure D.10. Amplitude dependence of the total pdf for the shear layer forced at $f = 4$ Hz, at $x = 18.5$ cm ($x^* = 0.82$), compared to the unforced case.

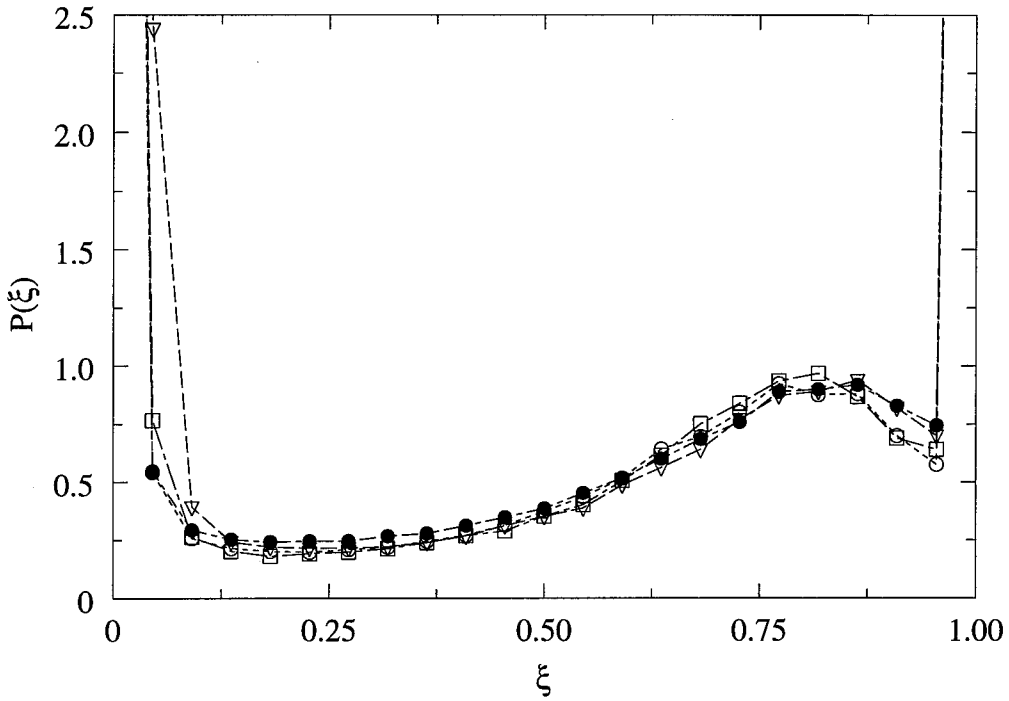

○ Unforced case, □ A = 2°, ▽ A = 4°, ● A = 6°

Figure D.11. Amplitude dependence of the total pdf for the shear layer forced at f = 8 Hz, at x = 12.5 cm (x^* = 1.11), compared to the unforced case.

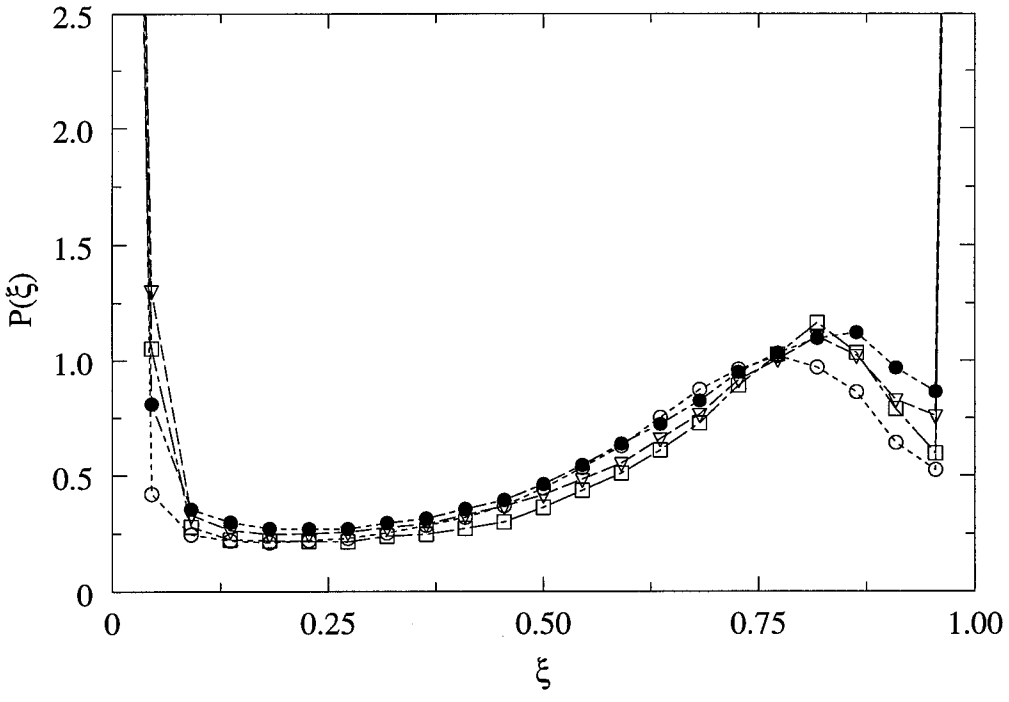

○ Unforced case, □ A = 2°, ▽ A = 4°, ● A = 6°

Figure D.12. Amplitude dependence of the total pdf for the shear layer forced at f = 8 Hz, at x = 14.0 cm (x^* = 1.24), compared to the unforced case.

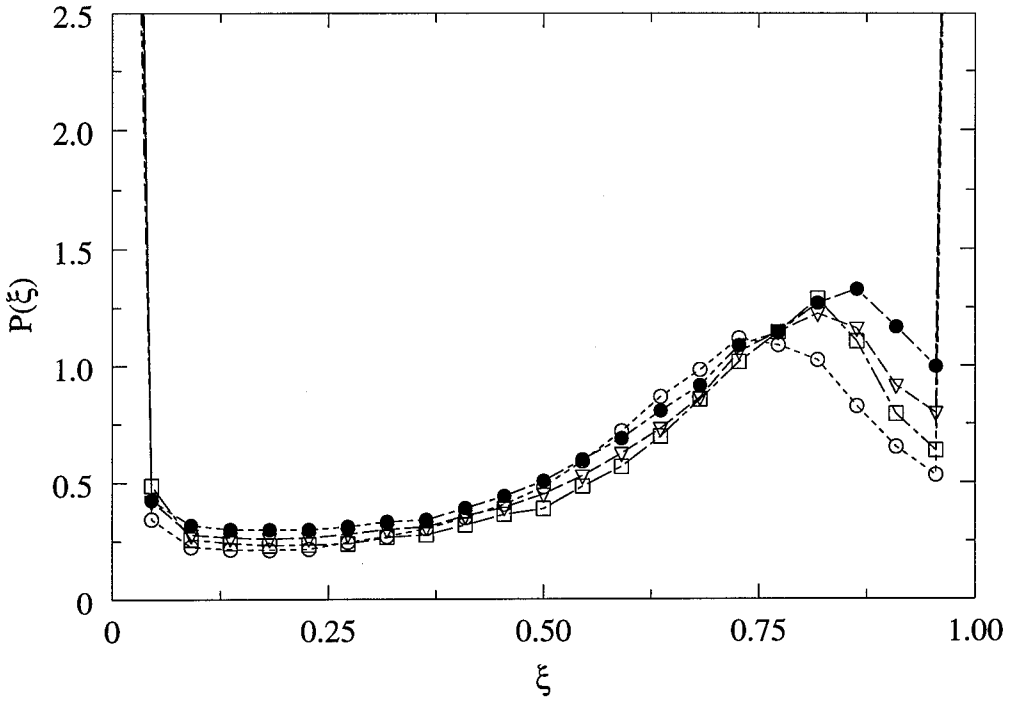

○ Unforced case, □ $A = 2°$, ▽ $A = 4°$, ● $A = 6°$

Figure D.13. Amplitude dependence of the total pdf for the shear layer forced at $f = 8$ Hz, at $x = 15.5$ cm ($x^* = 1.38$), compared to the unforced case.

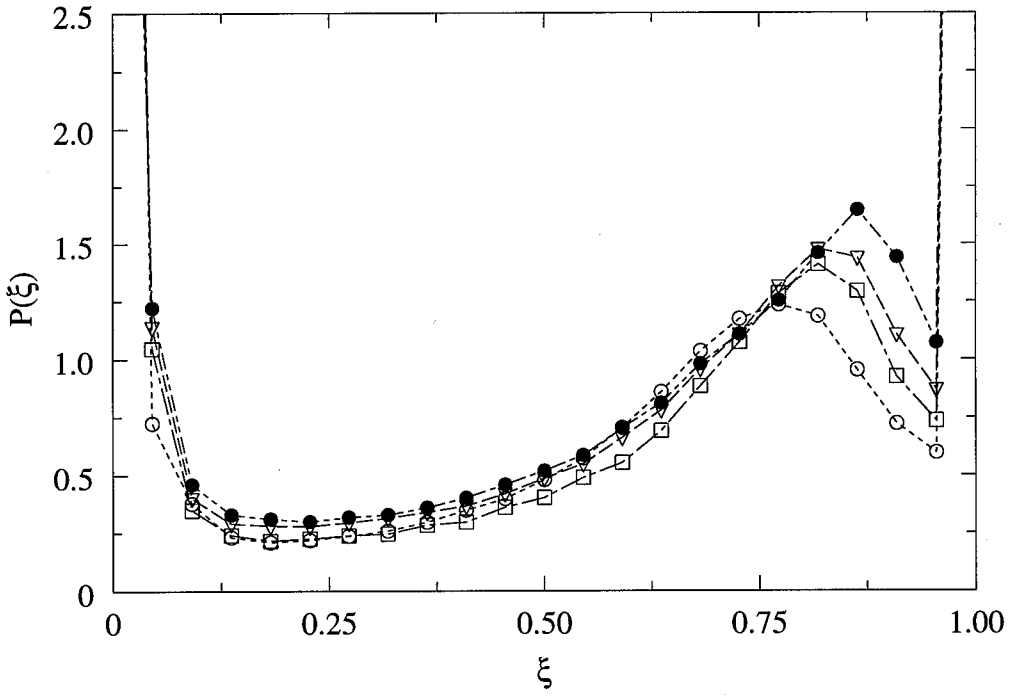

○ Unforced case, □ $A = 2°$, ▽ $A = 4°$, ● $A = 6°$

Figure D.14. Amplitude dependence of the total pdf for the shear layer forced at $f = 8$ Hz, at $x = 17.0$ cm ($x^* = 1.51$), compared to the unforced case.

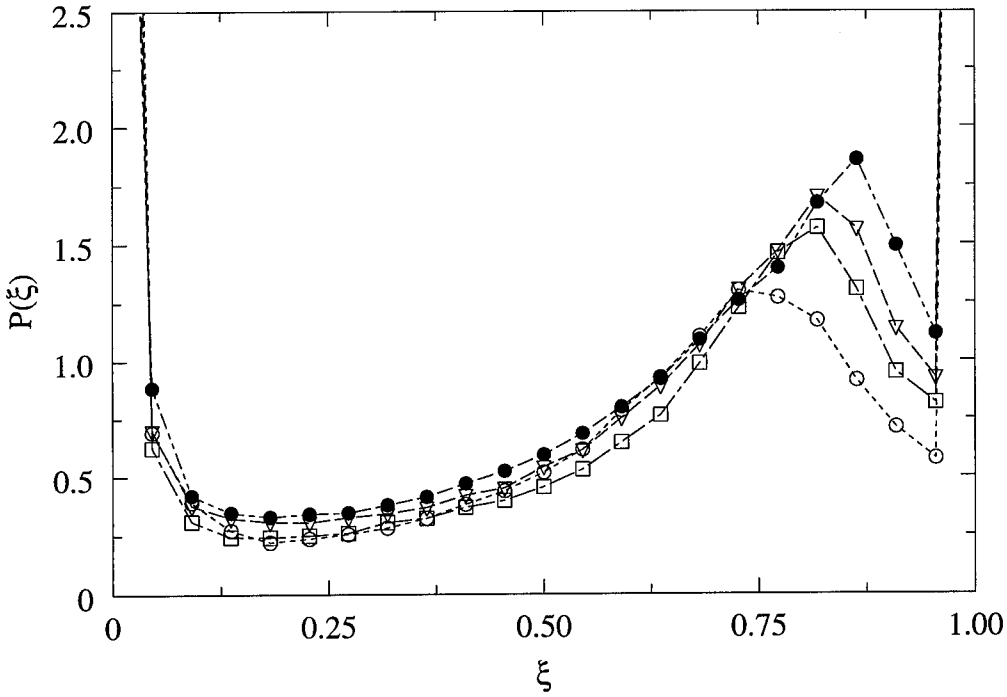

○ Unforced case, □ $A = 2°$, ▽ $A = 4°$, ● $A = 6°$

Figure D.15. Amplitude dependence of the total pdf for the shear layer forced at $f = 8$ Hz, at $x = 18.5$ cm ($x^* = 1.64$), compared to the unforced case.

REFERENCES

Breidenthal, R. E., " A chemically reacting turbulent shear layer," PhD. Thesis, California Institute of Technology, Pasadena, California, 1978.

Breidenthal, R. E., "Structure in turbulent mixing layers and wakes using a chemical reaction," *Journal of Fluid Mechanics*, Vol. 109, 1981, pp. 1-24.

Browand, F. K. and Ho, C. M., "The mixing layer: An example of quasi two-dimensional turbulence," *Journal de Mecanique Theorique et Appliquee Numero Special*," 1983.

Brown, G. L. and Roshko, A., "The effect of density difference on the turbulent mixing layer," Turbulent Shear Flows, AGARD-CP-93, 1971, pp. 1-12.

Brown, G. L. and Roshko, A., "On density effects and large structure in turbulent mixing layers," *Journal of Fluid Mechanics*, Vol. 64, 1974, pp. 775-816.

Dimotakis, P. E., "Two dimensional shear layer entrainment," *AIAA Journal*, Vol. 24, No. 11, 1986, pp. 127-144.

Dimotakis, P. E. and Brown, G. L., "The mixing layer at high Reynolds number: large-structure dynamics and entrainment," *Journal of Fluid Dynamics*, Vol. 78, 1976, pp. 535-560.

Fiedler, H. E., Dziomba, B., Mensing, P., and Roesgen, T., "Initiation, evolution, and global consequences of coherent structures in turbulent shear flows," *Lecture Notes in Physics*, Vol. 136, Springer-Verlag, Berlin, 1981, pp. 219-251.

Freymuth, P., "On transition in a separated laminar boundary layer," *Journal of Fluid Mechanics*, Vol. 25, 1966, pp. 683-704.

Ho, C. M. and Huang, L. S., "Subharmonics and vortex merging in mixing layers," *Journal of Fluid Mechanics*, Vol. 119, 1982, pp. 443-473.

Ho, C. M. and Huerre, P., "Perturbed free shear layers," *Annual Review of Fluid Mechanics*, Vol. 16, 1984, pp. 356-424.

Huang, L. S. and Ho, C. M., "Small-scale transition in a plane mixing layer," *Journal of Fluid Mechanics*, Vol. 210, 1990, pp. 475-500.

Karasso, P. S. and Mungal, M. G., "LIF measurements of mixing in turbulent shear layers," Sixth International Symposium on Applications of Laser Techniques to Fluid Mechanics, Lisbon, Portugal, 1992.

Konrad, J. H., "An experimental investigation of mixing in two-dimensional turbulent shear flows with applications to diffusion-limited chemical reactions," PhD Thesis, California Institute of Technology, Pasadena, California, 1976.

Koochesfahani, M. M., "Experiments on turbulent mixing and chemical reactions in a liquid mixing layer," PhD Thesis, California Institute of Technology, Pasadena, California, 1984.

Koochesfahani, M. M. and Dimotakis, P. E., "Laser induced fluorescence measurements of mixed fluid concentration in a liquid plane shear layer," *AIAA Journal*, Vol. 23, No. 11, 1985, pp. 1700-1707.

Koochesfahani, M. M. and Dimotakis, P. E., "Mixing and chemical reactions in a turbulent liquid mixing layer," *Journal of Fluid Mechanics*, Vol. 170, 1986, pp. 83-112.

Koochesfahani, M. M. and Dimotakis, P. E., "Effects of a downstream disturbance on the structure of a plane mixing layer," *AIAA Journal*, Vol. 27, No. 2, 1989, pp. 161-166.

Koochesfahani, M. M. and M^{ac}Kinnon, C. G., "Influence of forcing on the composition of mixed fluid in a two-stream shear layer," *Physics of Fluids A*, Vol. 3, No. 5, 1991, pp. 1135-1142.

M^{ac}Kinnon, C. G., "Influence of forcing on the composition of mixed fluid in a two-stream shear layer,", M. S. Thesis, Michigan State University, East Lansing, Michigan, 1991.

Miller, P. L. and Dimotakis, P. E., "Stochastic geometric properties of scalar interfaces in turbulent jets," *Physics of Fluids A*, Vol. 3, No. 1, 1991, pp. 168-177.

Oster, D. and Wygnanski, I., "The forced mixing layer between parallel streams," *Journal of Fluid Mechanics*, Vol. 123, 1982, pp. 91-130.

Roberts, F. A., "Effects of a periodic disturbance on structure and mixing in turbulent

shear layers and wakes," PhD Thesis, California Institute of Technology, Pasadena, California, 1985.

Roberts, F. A. and Roshko, A., "Effects of periodic forcing on mixing in turbulent shear layers and wakes," AIAA Paper 85-0570, 1985.

Wygnanski, I., Oster, D. and Fiedler, H., "A forced turbulent mixing layer: A challenge to the predictor," Turbulent Shear Flows 2: 2nd International Symposium on Turbulent Shear Flows, London, 1979, pp. 314-326.

Wygnanski, I., Oster, D., Fiedler, H. and Dziomba, B., "On the perseverance of a quasi-two-dimensional eddy-structure in a turbulent mixing layer," *Journal of Fluid Mechanics*, Vol. 92, 1979, pp. 1-16.

Zaman, K. B. M. Q. and Hussain, A. K. M. F., "Turbulence suppression in free shear flows by controlled excitation," *Journal of Fluid Mechanics*, Vol. 103, 1981, pp. 133-159.